August 2004 • NREL/SR-520-36610

Subcontractor Report

Implementation of a Comprehensive On-Line Closed-Loop Diagnostic System for Roll-to-Roll Amorphous Silicon Solar Cell Production

Phase I Annual Report
23 April 2003–31 August 2003

T. Ellison
Energy Conversion Devices, Inc.
Troy, Michigan

National Renewable Energy Laboratory
1617 Cole Boulevard, Golden, Colorado 80401-3393
303-275-3000 • www.nrel.gov

Operated for the U.S. Department of Energy
Office of Energy Efficiency and Renewable Energy
by Midwest Research Institute • Battelle

Contract No. DE-AC36-99-GO10337

August 2004 • NREL/SR-520-36610

Implementation of a Comprehensive On-Line Closed-Loop Diagnostic System for Roll-to-Roll Amorphous Silicon Solar Cell Production

Phase I Annual Report
23 April 2003–31 August 2003

T. Ellison
Energy Conversion Devices, Inc.
Troy, Michigan

NREL Technical Monitor: Richard Mitchell

Prepared under Subcontract No. ZDO-3-30628-11

National Renewable Energy Laboratory
1617 Cole Boulevard, Golden, Colorado 80401-3393
303-275-3000 • www.nrel.gov

Operated for the U.S. Department of Energy
Office of Energy Efficiency and Renewable Energy
by Midwest Research Institute • Battelle

Contract No. DE-AC36-99-GO10337

BACKGROUND and EXECUTIVE SUMMARY

ECD has developed and built 7 generations of roll-to-roll amorphous silicon PV production equipment. In the ECD/United Solar production process we deposit about a 1 μm-thick 12-layer coating consisting of a metal/oxide backreflector, a 9 layer a-Si/a-SiGe alloy triple junction solar cell, and top transparent conductive oxide coating onto 125 μm thick, 35.5 cm wide stainless steel webs in a series of three roll-to-roll deposition machines. Figure 1 shows a schematic of the United Solar 25 MW a-Si deposition machine; a photograph of the machine is shown in Fig. 2.

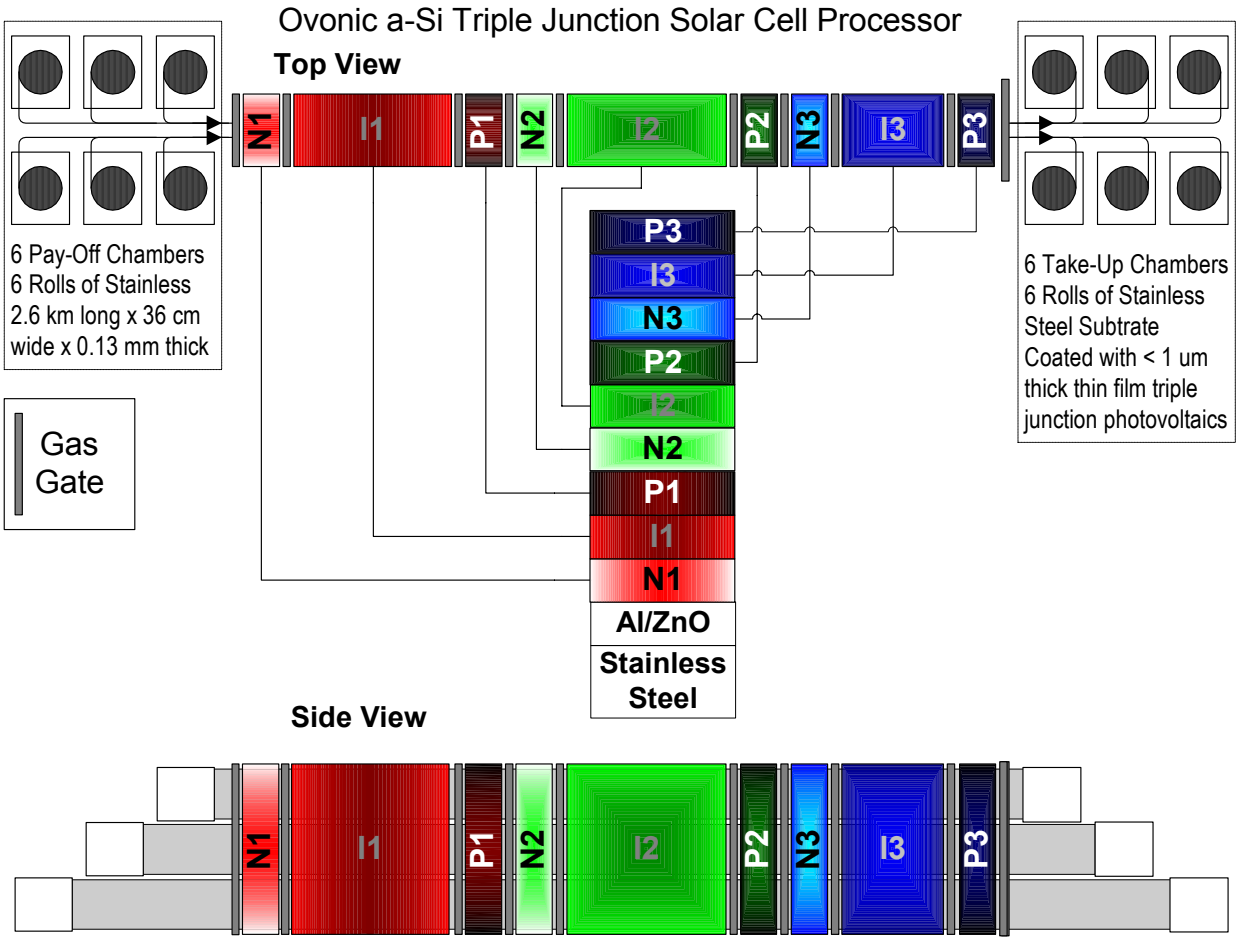

Fig. 1. Schematic of the United Solar 25 MW/yr a-Si deposition equipment.

All the developments of the PVMaT 5A program have been incorporated into this machine:

- A substrate heating and monitoring system, using durable NiChrome heater elements;
- Reactive sputtering for low-cost deposition of the Al/ZnO backreflector;
- A new PECVD cathode providing uniform deposition over large areas and reduced germane usage;

- "Pinch Valves" that allow the rolls of substrate to be installed and removed while keeping the deposition regions of the machine under vacuum; and
- Hardware for online diagnostic systems, including the non-contacting PV Capacitive Diagnostic (PVCD) system, which can measure the a Si solar cell electrical properties in-situ without an ITO top coating[4], and reflection spectrometers to measure the cell thickness;

"Included in the machine" might be an understatement: many of these technologies are essential to the machine. For example, the a-Si machine processes almost ½ MW of material in a single "batch". Offline Q/A-Q/C may not be available batch-cycle – such a machine would not be possible without the online diagnostic systems (e.g. PVCD and spectrometers) developed in the PVMat 5A program.

Fig. 2. Side view of the United Solar 30 MW/yr a Si processor.

In the PV Manufacturing R&D 6 program, ECD is building upon these accomplishments to enhance the operation of the present production machine, and lay the foundation for improvements in the next generation machine. The four major work areas undertaken by ECD and United Solar in the present PV Manufacturing R&D program are described below:

1. Development of closed loop thickness control systems for the ZnO, ITO layers, and a-Si component layer thicknesses (the last is an expansion of this program);
2. Continued development of the PVCD, including new systems to measure the J/V characteristics of components cells in the triple-junction device, and the initiation of online optimization using these devices;
3. The development of plasma monitoring systems to further optimize the i-layer deposition process, and for possible online implementation;

4. Yield improvement by investigating substrate chemical and plasma cleaning, and investigations into sources of reduced yield.

In the first two tasks we are using the tools we have developed in PVMaT 5A and PV Man R&D 6 to go beyond simple monitoring or Pass/Fail online QA/QC to closed loop control and online device optimization. The 4th task, if successful, will allow us to eliminate 1 of the 4 roll-to-roll front-end production machines and simplify the production process.

United Solar has been expanding its manufacturing capability at a rate of about 30%/yr – doubling capacity every 3 years, and increasing by a factor of 10 every decade. The PV Man R&D program is playing a key roll in this expansion – allowing ECD/United Solar to develop new technologies to enhance the present equipment and lay the foundation for the next generation machines.

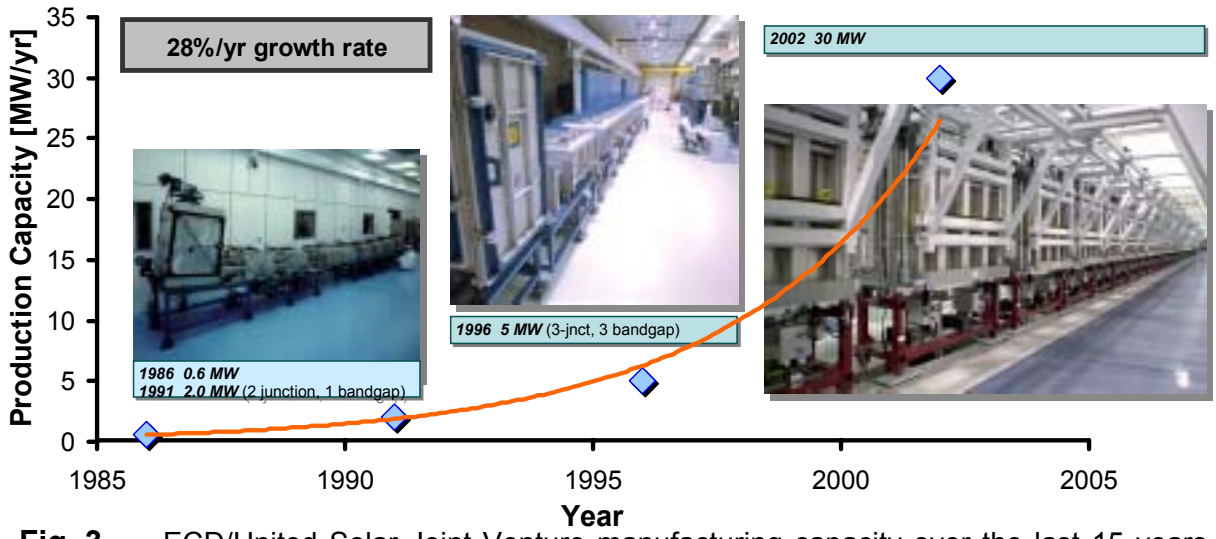

Fig. 3. ECD/United Solar Joint Venture manufacturing capacity over the last 15 years. During this time capacity has expanded at about 30%/year, with more rapid expansion in the last 5 years.

As of August 2003, ECD has completed the Phase I work for the first two Tasks, and will complete the Phase I work for the second two tasks within the next two months. In the following report we summarize the Phase I work in each of these tasks.

We have involved United Solar production personnel in each of these Tasks. This is important for two reasons:

- Firstly, the collaboration of ECD and United Solar personnel keep the projects responsive to the developing needs at United Solar;
- Most of the tasks affect operations and consequently need the support of United Solar production and QA/QC managers.

In the process we have developed a good working relationship between the production personnel, whose mantra is “change nothing”, and the R&D personnel, who mantra is “change everything”.

CONTENTS

TASK 1: Develop Closed-Loop Control of Film Thickness

-- **Jeff Karn (ECD)**, Rujiang Liu and Jon Call (United Solar), Dave Dodge (Focus Software)

Milestones

Complete	**M-1.0.1**	**Complete testing of 1st generation a-Si reflection spectrometer in production equipment.**
Complete	**M-1.1.1**	**Complete conceptual design of 1st generation ITO and ZnO closed-loop thickness-control systems.**
Complete	**M-1.2.1**	**Complete installation of 2nd generation a-Si reflection spectrometer in production equipment.**
Complete	**M-1.3.1**	**Complete fabrication of 1st generation closed-loop thickness-control systems for ITO and ZnO.**
Complete	**M-1.4.1**	**Complete the Phase I portion of the effort under Task 1.**

Deliverables

Complete	**D-1.0.1**	**Report summarizing the testing of the 1st generation a-Si reflection spectrometer in the production equipment.**
Complete	**D-1.2.1**	**Report summarizing closed-loop thickness-control systems fabricated for the ITO and ZnO film thickness**
Complete	**D-1.3.1**	**ECD/United Solar confidential datalog display from a complete production roll of material demonstrating a-Si spectrometer thickness measurements**

1.1 Introduction

To monitor the thickness of deposited films the three deposition machines at United Solar Systems Corporation (United Solar) have been configured with reflection spectrometers. On the ZnO Machine two spectrometers are used to measure the thickness of the [aluminum] deposition and the thickness of the [aluminum + ZnO] deposition. On the a-Si Machine two *1st Generation* spectrometers are used to measure the state of the input material (ie back-reflector only) and the final thickness [bottom + middle + top]. A newly added *2nd Generation* spectrometer measures the thickness of the [bottom + middle] layer. Lastly, the ITO Machine has been configured with six spectrometers that provide transverse thickness uniformity measurements across multiple webs. The layout of all spectrometers on their respective machines is summarized in Figure 1.1. All systems provide real-time data to operators and, in the case of the ZnO and ITO Machines, are the primary metric for machine setup and optimization. A prototype closed-loop control system has been fabricated for the ZnO Machine and is undergoing off-line testing.

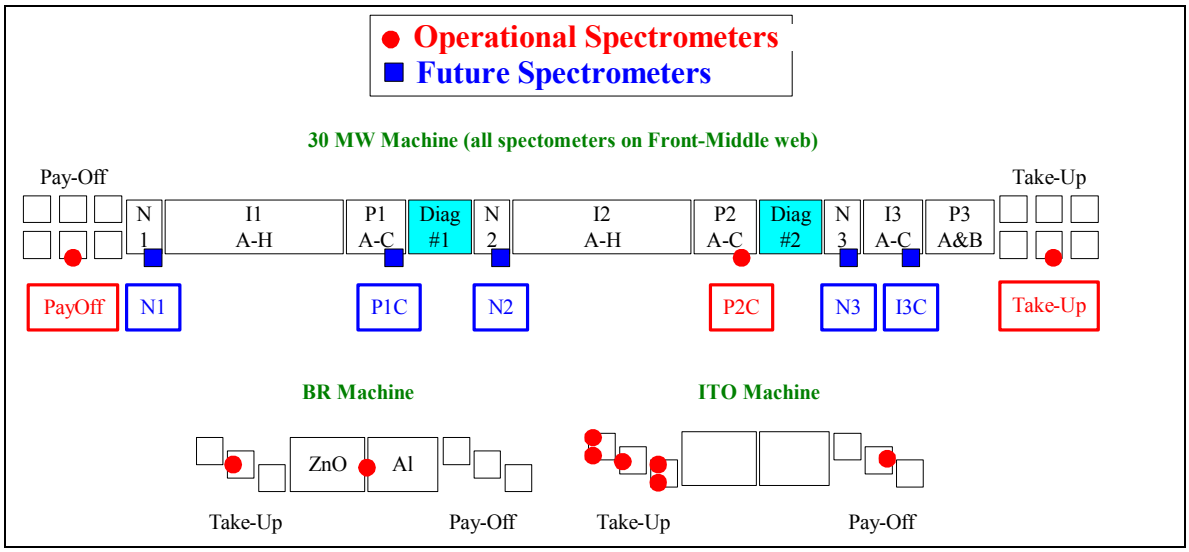

Fig. 1.1. Present and Future Spectrometer Installation Locations

1.2 1st Generation a-Si Spectrometer

1.2.1 Overview

Two *1st Generation* spectrometers were installed on the a-Si Machine. One device is located in the Pay-Off Chamber and measures the thickness of the back-reflector layer as the material enters the machine. The second device is located in the Take-Up Chamber and measures the overall thickness of the triple cell on the exiting material. The Take-Up spectrometer became operational in April 2002 and the Pay-Off spectrometer in August 2002. During this time period both devices provided valuable thickness information during the critical commissioning of the 30MW Machine. The hardware and software for both devices are identical and constitute the 1st generation a-Si reflection spectrometer.

1.2.2 Spectrometer Hardware

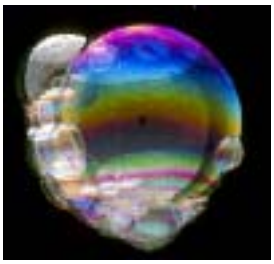

The thickness of PV layers can be measured and monitored using commercial spectrometer systems. These systems are based on the interference spectrum produced when white light reflects off of a thin film. This is the same concept that produces the colors seen in an oil slick on top of water or in soap bubbles.

The United Solar spectrometer systems are built with a combination of commercially available optical components and custom machined mounting hardware. A rack-mount system manufactured by Ocean Optics contains the light source and multiple S2000 spectrometer channels for digitization of the reflected light. The S2000 units are temperature regulated and provide a spectral resolution of 0.3 nm.. Each rack unit is equipped with an extra channel that monitors the stability of the light

source. The system is configured for operation between 400 and 1000 nm wavelengths. Fiber optics split the light source and transport the incident and reflected light the 25 meters between the rack electronics and the subject material. At the chamber a pair of Insulator Seal ultra-high vacuum fiber optic feedthroughs provide the interface between air and vacuum. Inside the vacuum chamber the incident and reflected fibers share a common collimating lens for focusing the light to and from the reflection surface. The reflected light is sent back to the spectrometer where it is digitized. The wavelengths of the extrema in the interference pattern are proportional to the thickness of the film. A schematic layout is shown in Figure 1.2. Plotted in Figure 1.3 are two sample interference patterns with the obvious wavelength shift due to a thickness change from a missing deposition cathode.

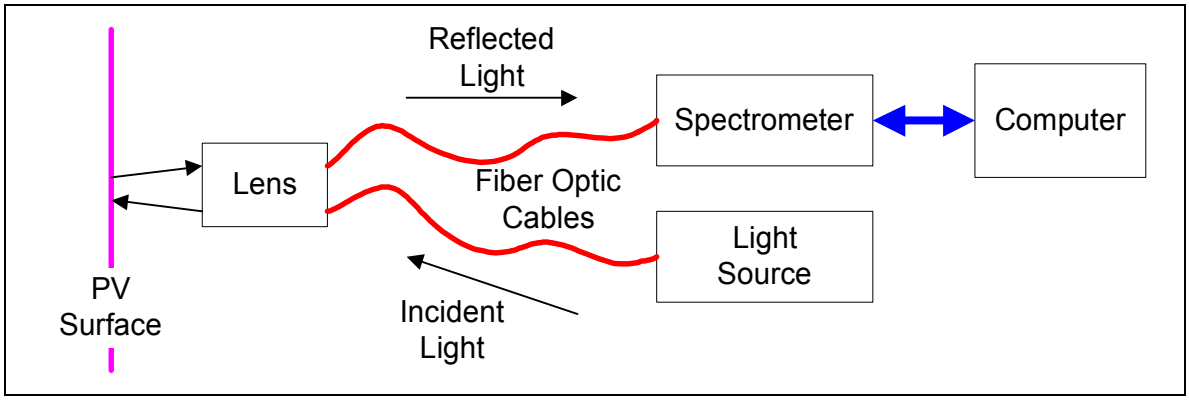

Fig. 1.2. Schematic Diagram of Spectrometer System

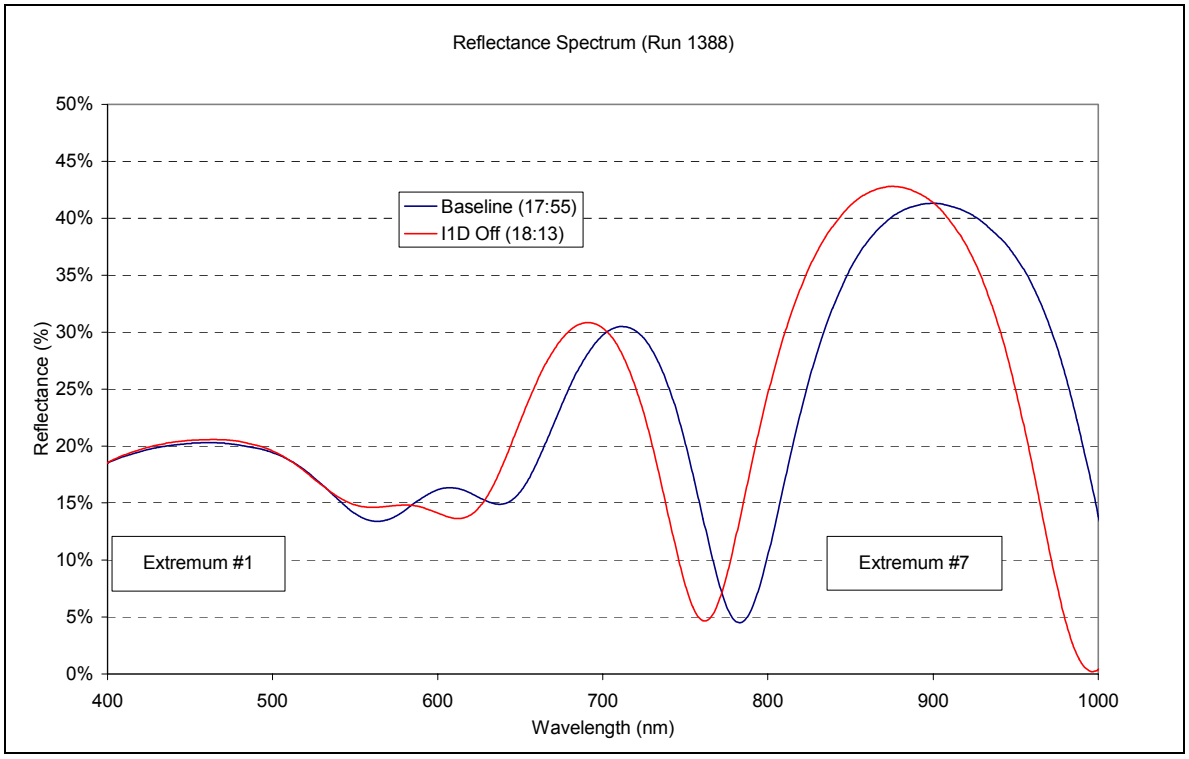

Fig. 1.3. Change in Interference Pattern from Loss of Plasma RF

For maximum signal strength the incident light must be perpendicular to the material being sampled. To permit optimization of this alignment a mechanical mount with three degrees of freedom was designed by the ECD Machine Division. Also critical in minimizing signal noise is the stability of the substrate as it passes under the spectrometer lens. To minimize vibrations the lens, and its alignment hardware, were located to measure the substrate as it passes around a ten inch roller. This has proven to produce a very stable signal with negligible effects from the precession of the roller. The alignment system has also met full expectations in its ability to maximize signal strength. The hardware assembly is shown in Figure 1.4 with the spectrometer lens (in black) centered vertically on the roller (with blue a-Si material in-situ.)

Fig. 1.4. Take-Up Chamber Spectrometer Mount

1.2.3 Spectrometer Software

Three separate software utilities have been developed to support spectrometer operations: a data acquisition utility, a run-time operator display utility, and an off-line expert analysis utility. All software was developed under the National Instrument's LabView environment.

1.2.3.a Data Acquisition Utility

The data acquisition (DAQ) utility provides all aspects of instrument configuration, data collection, data pre-processing, data archiving, and various complexities of data display. The Ocean Optics spectrometer electronics communicate with LabView via USB. Spectrometer settings including integration time, averaging, and trigger rate are set from an *expert panel* (Figure 1.5.) The *expert panel* also contains controls and graphs for performing system calibrations and for saving the calibration constants and spectra.

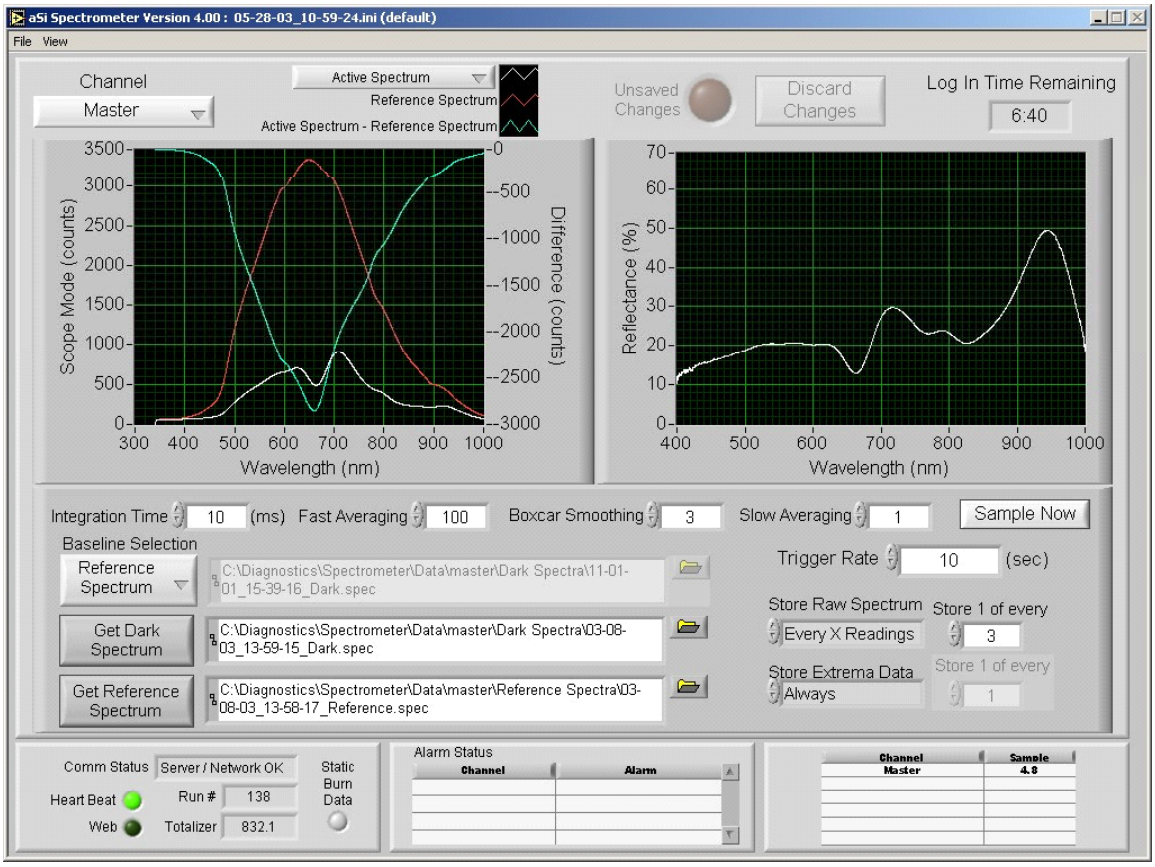

Fig. 1.5. Data Acquisition Utility – Expert Panel

Upon collection of an interference spectrum, analysis is performed to identify the extrema of interest and verify the integrity of the data. Developing these algorithms has proven to be quite challenging and has undergone several iterations. The complexity arises from the extreme variation in spectra (i.e. large thickness dynamic range) during the commissioning of the 30MW Machine. Although these routines are a work in progress, the present version of the extrema tracking is successful over a reasonable range of thickness changes. Shown in Figure 1.6 is the *details panel* that displays the active interference spectra and the result of the found extrema. Tolerance bands can be set on several features of the located extrema and used to generate warning and alarms to the operators.

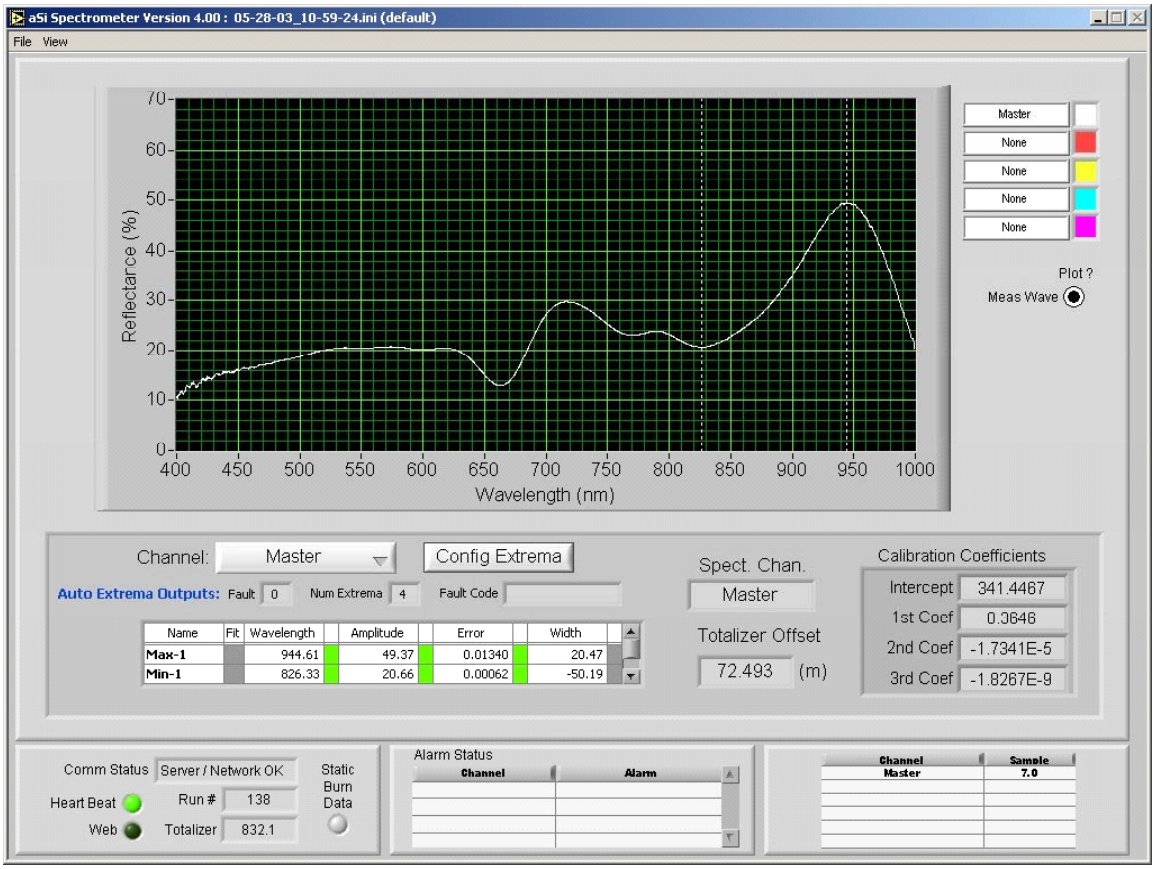

Fig. 1.6. Data Acquisition Utility – Details Panel

Another important role of the DAQ utility is to communicate with the PLC-based machine control system. This allows synchronization of collected data to actual web meter marks and allows the DAQ software to only acquire data when the machine is in operation. In addition, thickness data measured by the spectrometer can be sent to the machine controls for archiving in the historian database. This ability to correlate thickness data to machine settings is a necessity for future closed-loop control.

1.2.3.b Run-time Operator Display Utility

The Operator Display Utility allows for run-time trend plotting of spectrometer thickness data. This utility also plots data from the PVCD diagnostic and can display affected regions of a run from pre-programmed machine experiments. The x-axis of the display can be switched between *meters* of material for location-specific analysis and date/time for time-specific analysis. The range of the x-axis can be expanded to include past runs for long-term trend analysis. A typical control room view of the display is shown in Figure 1.7. In this figure spectrometer thickness data are plotted in the bottom graph and results from the PVCD diagnostic on the top and middle graphs. Data from the various diagnostics are shifted to account for their different locations along the machine.

Fig. 1.7. Run-time Operator Display Utility

1.2.3.c Off-line Expert Analysis Utility

As mentioned earlier, the development of the extrema tracking algorithms was a complex and iterative process. To ease this developmental process, and to minimize operational down-time due to software changes, an off-line spectra viewing utility was required. This utility reads in the interference spectra saved by the DAQ utility and allows the playback of these data through various developmental algorithms. A sample screen display is shown in Figure 1.8. In this display, the top graph is plotting the wavelength of two extrema through a section of a run. The cursor can be dragged, or the data played, and the spectrum for the current frame will be displayed on the lower graph. This has proven to be a valuable tool for the development of spectrum analysis software for the 30MW Machine, as well as, spectrometers on the BR and ITO deposition machines.

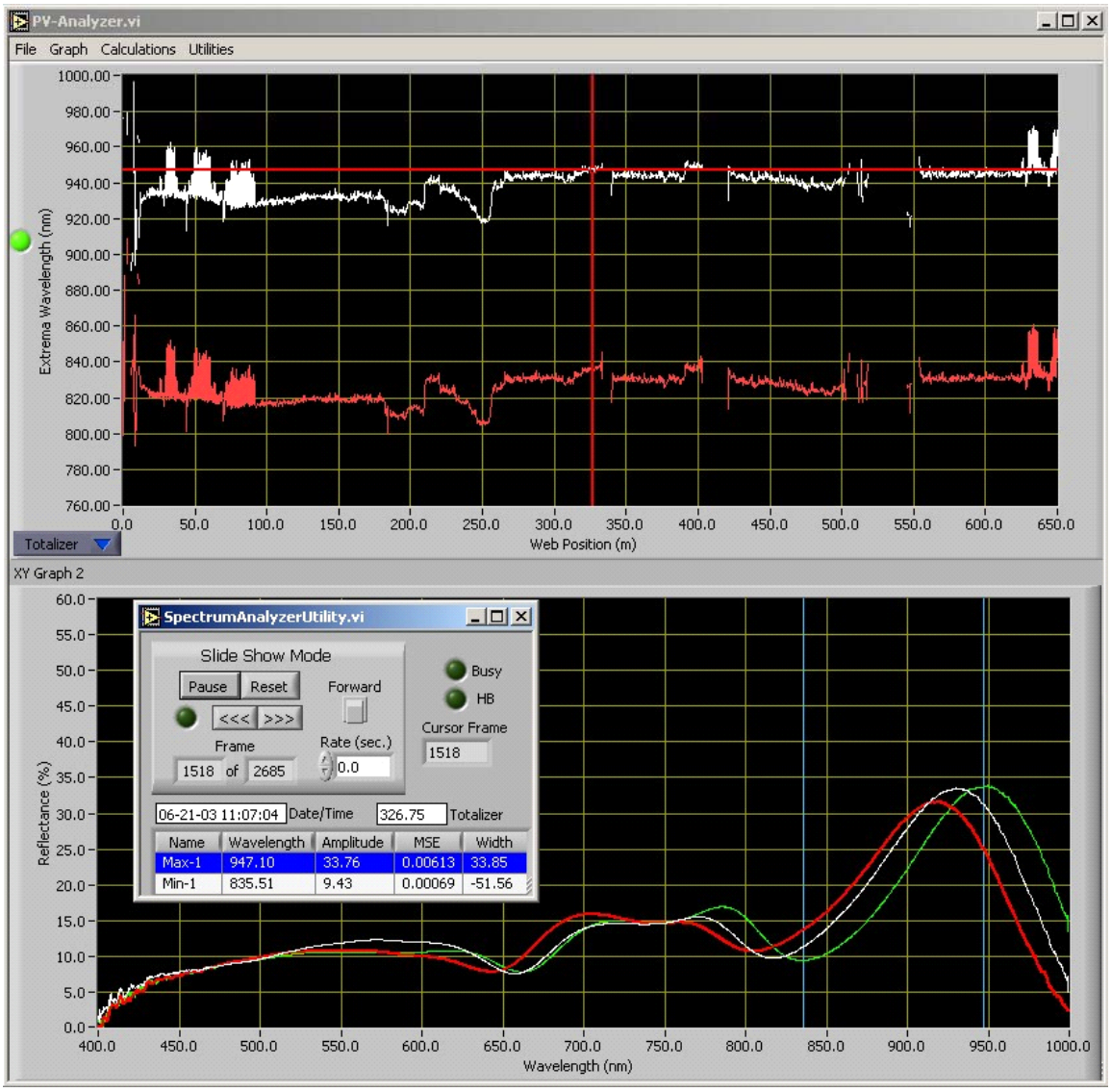

Fig. 1.8. Off-line Expert Analysis Utility

1.2.4 Run-Time Operations

As mentioned earlier, during the commissioning of the 30MW Machine the wide variation in deposition thickness caused a wide range of reflection spectra. As the machine transitioned to a production mode these spectra have stabilized and their typical shapes are plotted in Figure 1.9. In this figure, the main extrema of interest are identified by the vertical dashed lines. The primary extrema of interest are the ~600 nm maximum in the Pay-off curve and the ~850 nm minimum of the Take-Up curve. These two extrema are trend plotted on the Operator Display Utility.

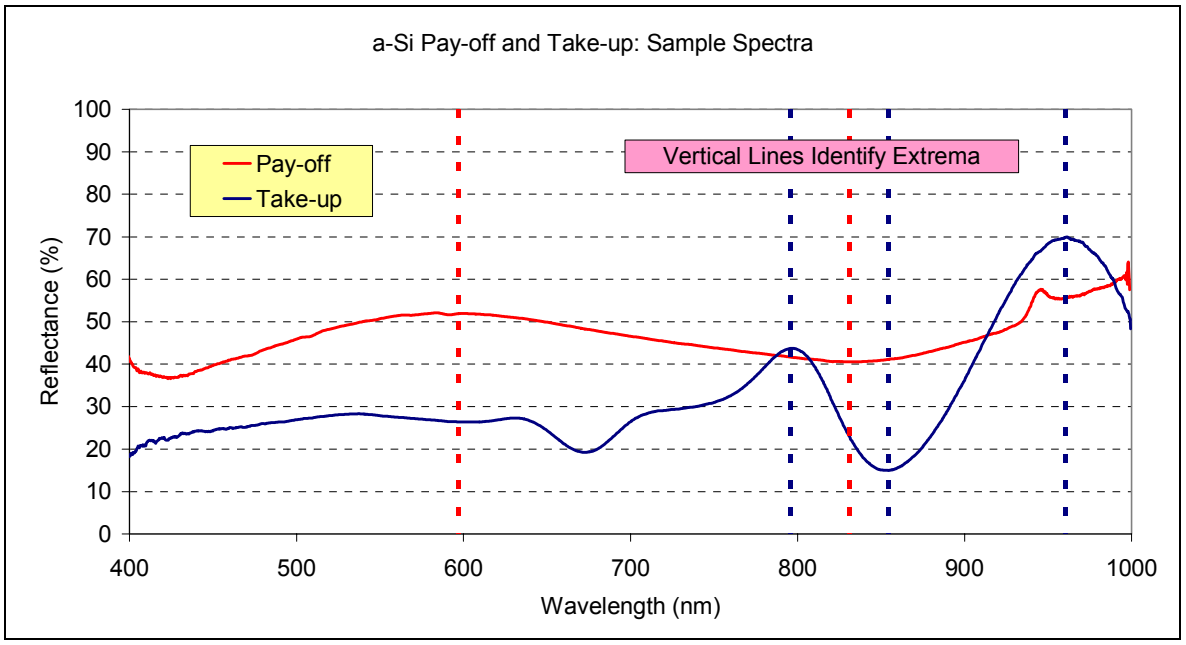

Fig. 1.9. Typical Reflection Spectra for Production PV Material

Shown in Figure 1.10 are a series of events plotted with the Operator Display Utility. In the top two graphs the PVCD shows large drops in the PV voltage and current. The bottom graph plots the spectrometer Pay-off thickness in red and the Take-up thickness in blue. The coinciding drops in the Pay-off thickness identify the source of these events as being defects in the material (ie in the back-reflector coating) entering the machine. The spectrometers and the PVCDs, while measuring different cell properties, provide a valuable redundancy check.

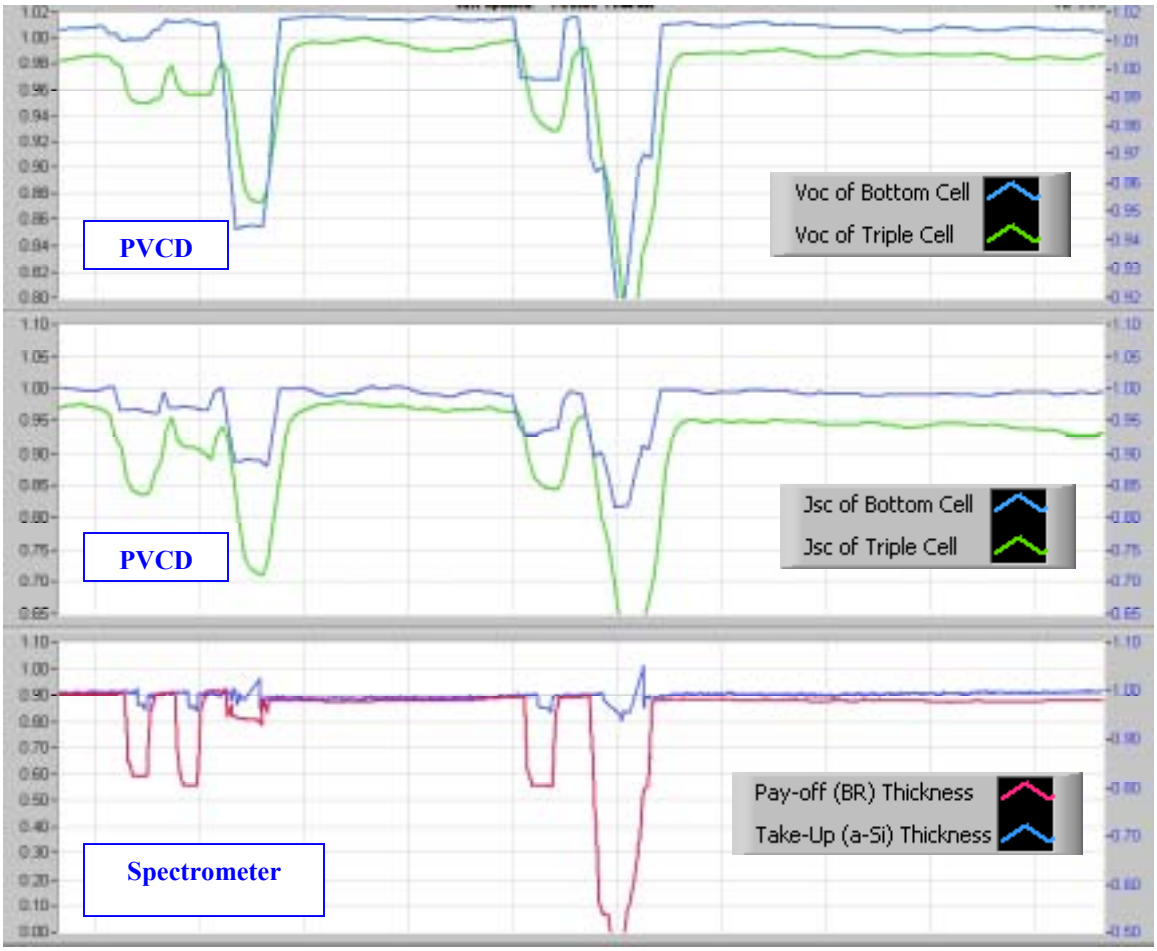

Fig. 1.10. Operator Display Showing Event Traceable to Input Material

1.2.5 Cathode Thickness Profile Measurements

In addition to its *traditional* role, an exciting new application of the Take-Up spectrometer has been developed. When the web is stopped for a brief period (~ minutes) the deposition under a cathode is increased while the material between cathodes remains at the nominal thickness. When the web is restarted and advances past the Take-Up spectrometer the changes in thickness are measured. These data provide a complete longitudinal deposition profile for every cathode in the machine. Profiles from a one minute web stoppage are plotted in Figure 1.11 (with cathode edges plotted in dark gray vertical bars.) The baseline thickness (from between cathodes) has been subtracted so the vertical axis plots the relative change in thickness. The negative thickness (etching) of certain P-cathodes is also seen.

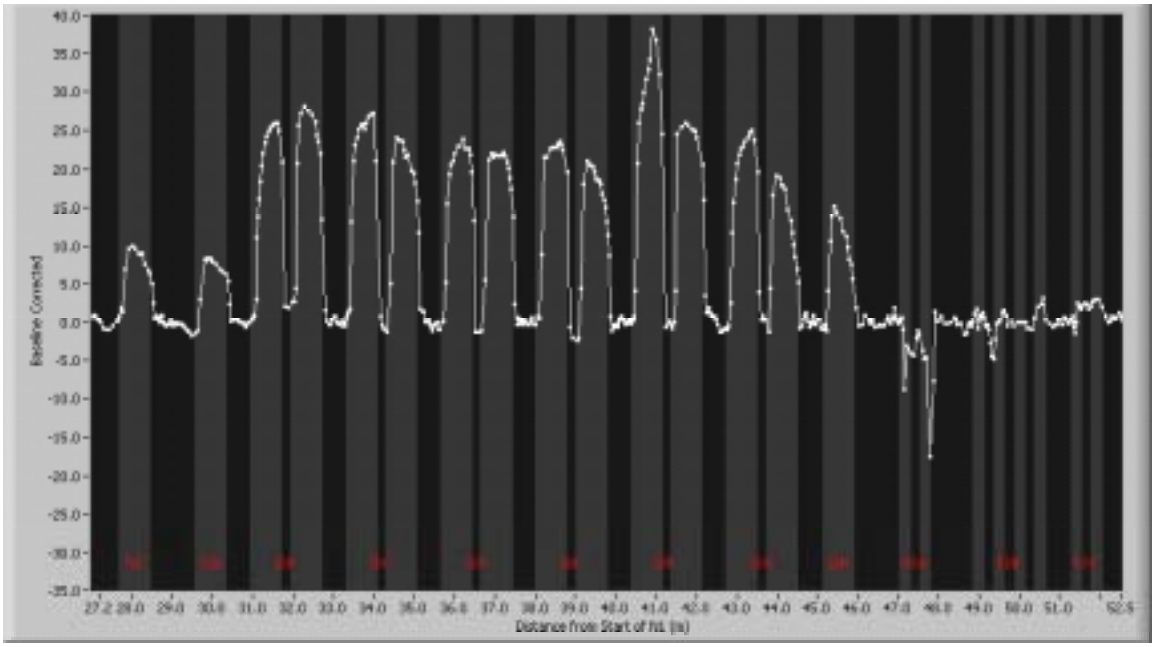

Fig. 1.11. Cathode Deposition Thickness Profiles

The usefulness of this tool to identify problematic cathodes has led to the development of an automated measurement system. To optimize the process experiments were performed varying the length of the web stoppage. It was determined that a one minute stop provided a measurable thickness change but did not compromise the integrity of the PV material. Automatic one minute stops were programmed into the machine control system to produce several data sets per run. To improve measurement resolution the spectrometer data acquisition software was modified to automatically increase its collection rate to around two seconds (~ 2 cm. of web travel.)

A LabView-based interface was developed to synchronize profiles to their respective cathodes, correct for variations in the baseline thickness, and integrate along each cathode. The interface also allows the operator to quickly zoom in and out of regions of interest and compare profiles from multiple data sets. Plotted in Figure 1.12 are the profiles of four sample cathodes from twenty data sets. The spread in the variation for a given cathode is around 20% with some clear outliers. Also, obvious in the left-most cathode are two events where the cathode was turned off and operating at half- power.

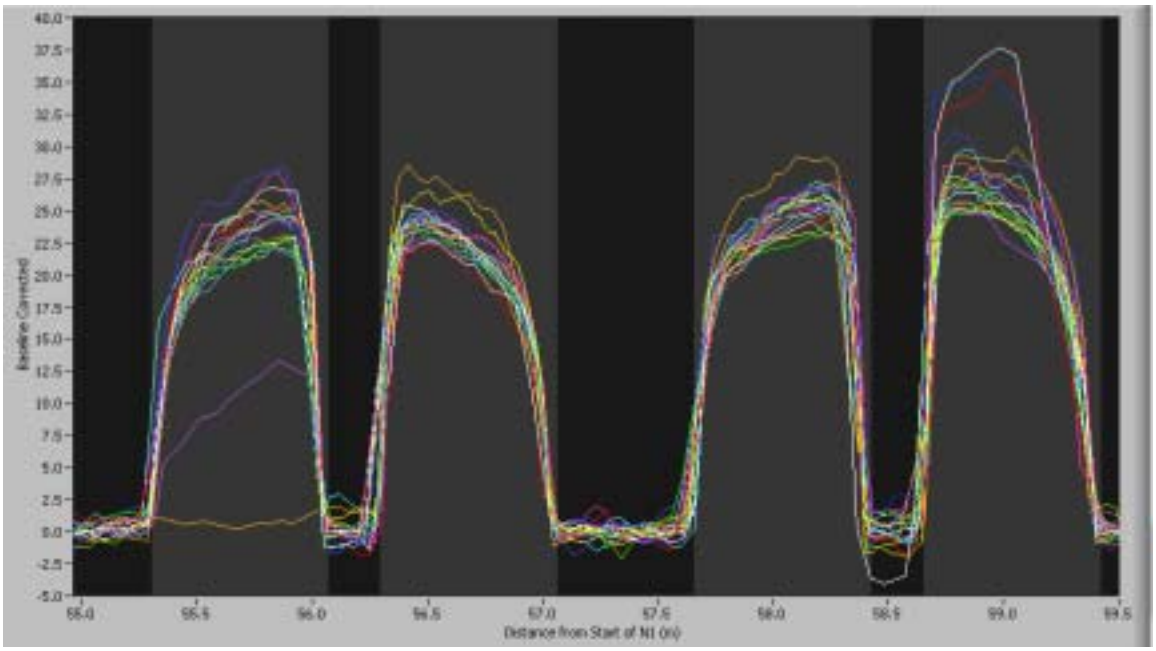

Fig. 1.12. Cathode Profile Variation Over Multiple Runs

Although the profiles plotted in Figure 1.12 provide a powerful graphical tool, a more quantitative approach is to integrate over the length of the cathode. While the integral for a single cathode can identify major problems, the typical variation may not always impact the ultimate performance of the device. What may be of primary interest are the integrals over groups of cathodes (egs N, I, or P layers, as well as, bottom, middle, and top cell.) By tracking these regions and establishing pass/fail criteria the operator can be alerted to potential problems. Individual cathodes can then be studied to further localize a discrepancy. Plotted in Figure 1.13 are the integrals over each of the three cells (ie bottom, middle, top.) The establishment of a baseline and the criteria for defining non-conforming material continues to be studied.

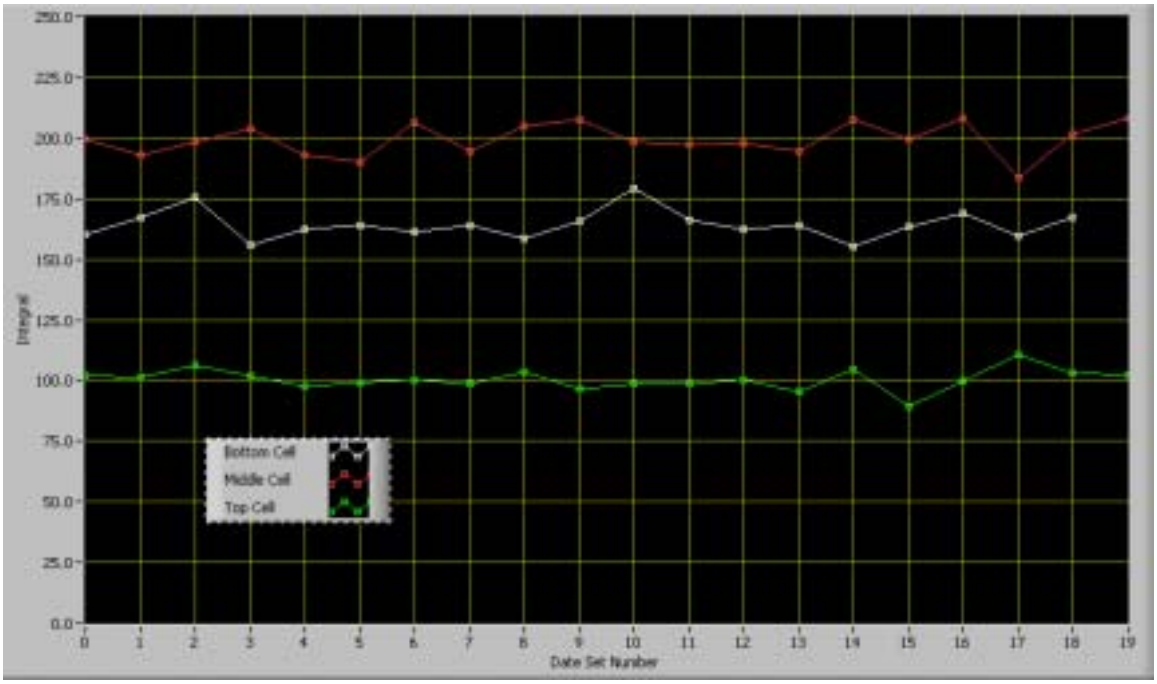

Fig. 1.13. Cell Integrated Deposition

1.2.6 Reliability and Accuracy Experience

With over a year of experience operating the Ocean Optics spectrometers there have been no hardware failures. The accuracy of each system is routinely verified during machine operation down-times. For this check, a standard sample of PV material is placed under the detection lens and the extrema wavelengths recorded. These standard wavelengths have been consistent over time, and consistent for multiple spectrometer systems, at the 2 nm level. No recalibration of any CCDs has been required.

Small drifts in the dark current have been observed that result in second order errors on extrema at the low or high end of the spectrum. These drifts are easily corrected by turning the light source off and measuring the dark current. At present, this is a manual process but software is under development to make this automated and routine.

Also of interest is the spectral stability of the light source. In all systems an extra channels has been installed for monitoring of the light source. At present this has only been used as an alarm for light source failure. Future analysis is required to quantify any variation, and if required, make corrections to all affected channels.

1.3 2nd Generation a-Si Spectrometer

1.3.1 Overview

As described in the previous section, a pair of *1st Generation* spectrometers in the a-Si Machine measures the film thicknesses of the material entering and exiting the deposition chambers. While measurement of the composite device can provide pass/fail information, it provides minimal insight as to where along the deposition process a problem resides. To provide this information a series of additional spectrometers (refer back to Figure 1.1) are planned for installation among the deposition chambers. These installations require a new and challenging design due to space limitations and the more hostile environment of the deposition chambers. A prototype *2nd Generation* spectrometer has been installed at the end of the second layer (in the P2C Chamber) and testing is in progress.

1.3.2 Design Considerations

One of the primary goals of the 2nd generation spectrometer design was to produce a common set of hardware that would be compatible at all planned (and un-planned) locations. To achieve a flexible design, the spectrometers would have to be mounted through existing flanges on the deposition chambers. This required the following design considerations:

- capable of withstanding temperatures over 300 C (plus the thermal cycling during machine start-up)
- compatible with UHV requirements
- must avoid a-Si deposition on spectrometer optics
- moving web must be free from vibration or angular changes with respect to the spectrometer detection lens
- location of detection lens would be inside a long narrow region formed by the front and rear webs. A location that is hidden from visual inspection as well as from any sort of hands-on adjustment.

The approach taken was to install a quartz-tube that passed through the chamber between two concentric flanges on the top and bottom chamber walls. Similar *visual inspection tubes* had been designed for other applications so the engineering expertise for the vacuum seal already existed. The center of the tube is at atmosphere and houses the spectrometer detection lens and its adjustment hardware. To dampen vibrations of the web a small vespel-tipped finger applies a gentle pressure on the back-side of the passing substrate.

To maximize the reflected signal the lens must be aligned perpendicular to the passing web. Thus, the alignment system must provide angular adjustments in pitch and yaw. The adjustment-end of the assembly is shown in Figure 1.14. The dial in the center adjusts the lens pitch over a $\pm 7°$ range. The micrometer knob adjusts the lens yaw over a $\pm 5°$ range. The viewing-end of the assembly is shown in Figure 1.15. A 90° mirror is

used to transition from the vertical running fiber to the required horizontal incident/reflection path.

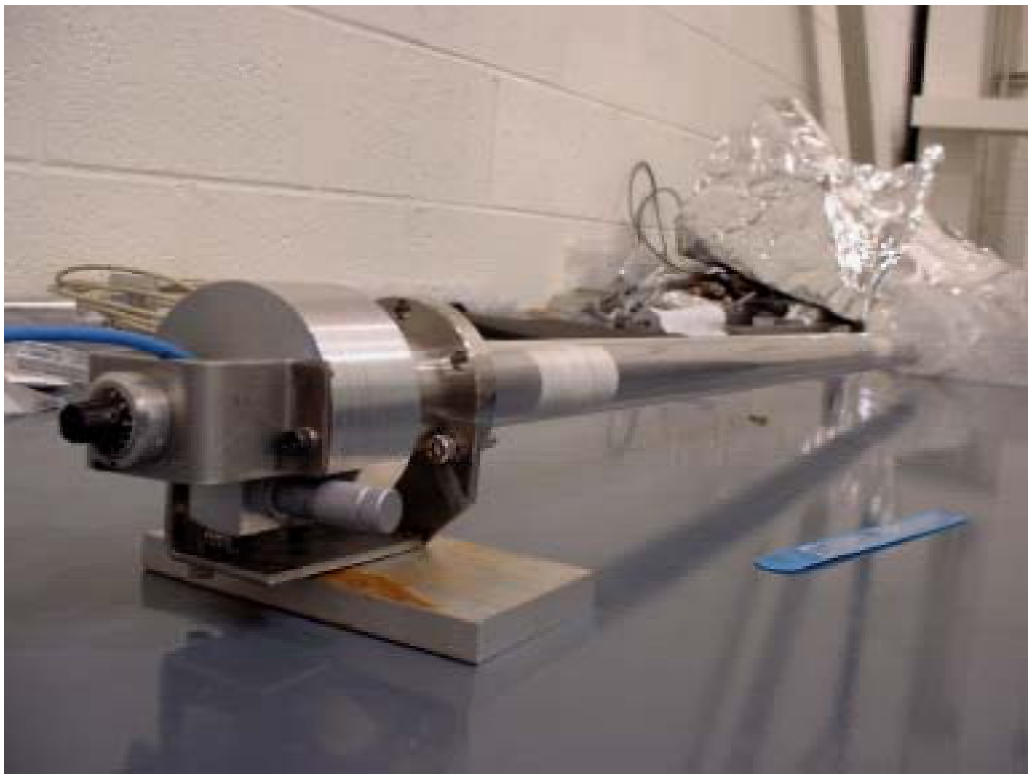

Fig. 1.14. Adjustment end of spectrometer assembly

Fig. 1.15. Viewing end of spectrometer assembly

1.3.3 Preliminary Testing

The design and prototyping was split into two separate tasks: the quartz tube vacuum assembly and the spectrometer lens alignment assembly. The quartz tube assembly was the simplest and has been successfully installed and tested. After six months of machine operations a negligible amount of deposition has been found on its outside surfaces. In addition, the integrity and durability of the two vacuum seals has been verified.

The spectrometer alignment assembly has only recently been installed in the machine and commissioning results have been encouraging. Thickness measurements from a production run are plotted in Figure 1.16. In this plot the thickness from the new P2C spectrometer (measuring the double layer) can be compared to the thickness of the triple layer (as measured with the Take-Up spectrometer.) As noted in the plot, this section of the run saw several events: a one minute static burn experiment, several glitches in the BR, and the result of repairs to I3 following a tuner failure. Analysis of the burn data is plotted in Figure 1.17. The scaling difference in the burn data between the spectrometers is due to the overall thickness difference between the double and triple layer. The agreement of these preliminary data is encouraging and the new P2C spectrometer will continue to be studied and optimized.

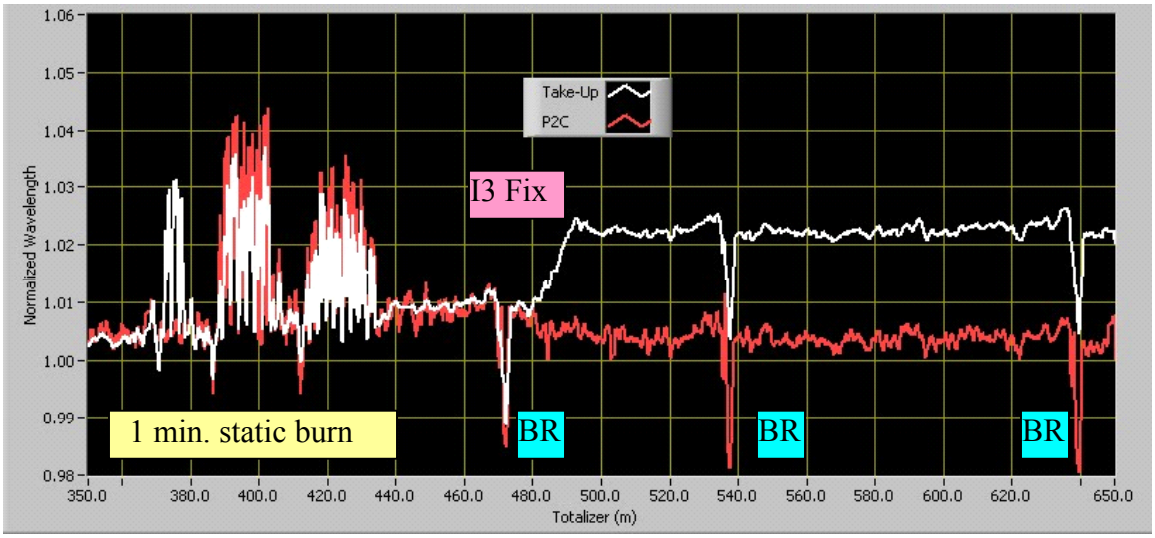

Figure 1.16: Thickness of Double Cell (P2C) and Triple Cell (Take-Up)

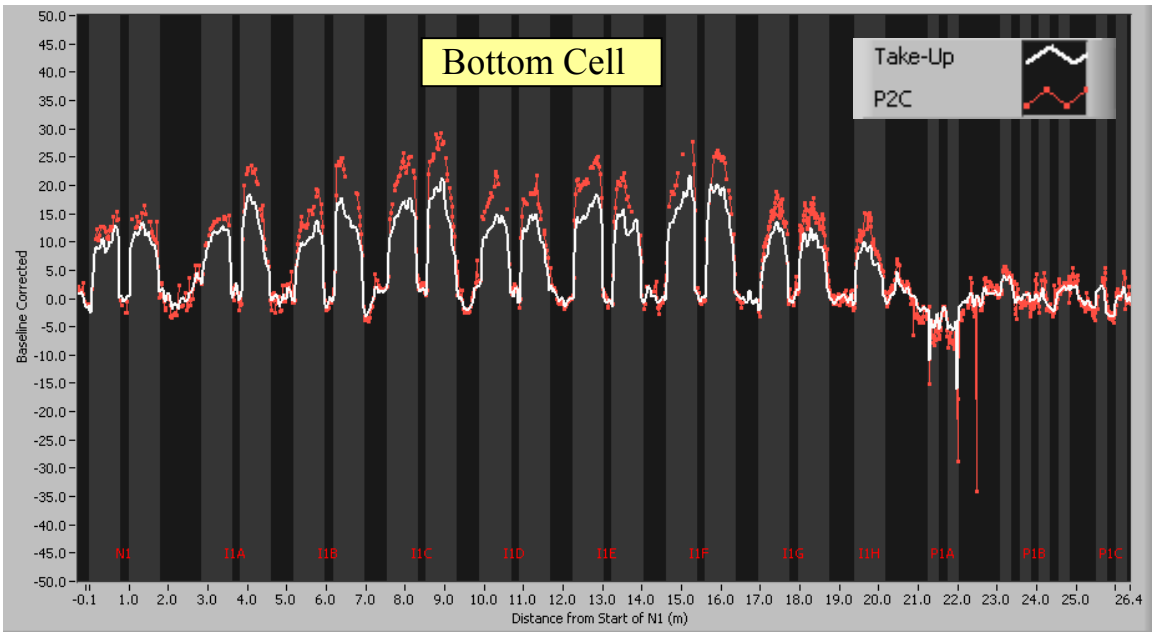

Fig. 1.17. Bottom Cell Static Burn

1.4 ZnO Closed-Loop Thickness Control

1.4.1 Overview

As described above, spectrometers have provided valuable information to the machine operators during the commissioning of the ZnO, a-Si, and ITO Machines. While this thickness information was provided at run-time to the operator, it still required interpretation and corrective action by the operator using the appropriate control set points. To optimize this process and improve the machine performance a closed-loop thickness control system has been developed.

The control software for this system is presently undergoing off-line testing and a *1st Generation* system is scheduled for installation on the ZnO Deposition Machine. The ZnO Machine was chosen since it is the most understood of the three machines. The thickness control system on the ITO Machine has grown from one spectrometer to six spectrometers as uniformity and color issues continue to be characterized. The thickness control system on the a-Si Machine is presently being upgraded from three spectrometers to eight spectrometers to quantify individual layer contributions. The multi-spectrometer nature of the ITO and a-Si thickness systems will be an added challenge to closed-loop control. In comparison, the ZnO machine with its one spectrometer offers a more advantageous starting point for the development of a closed loop thickness control program.

1.4.2 Thickness Monitoring and ZnO Deposition Control Points

A screen shot of a typical ZnO reflection spectrum is shown in Figure 1.18. The maximum around 587 nm (ZnO_{max}) and the minimum around 780 nm are tracked by the spectrometer software and an alarm condition generated if either drift out of specification.

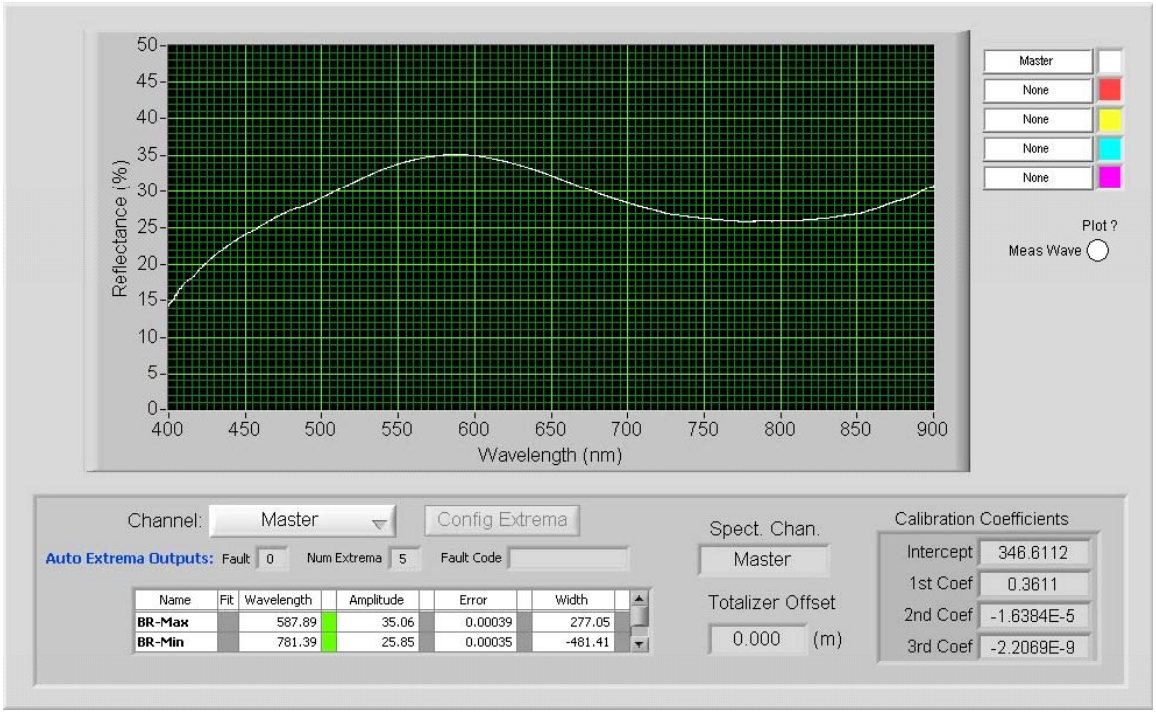

Fig. 1.18. Typical ZnO Reflection Spectrum

The thickness of the ZnO layer can be controlled by changing the intensity of the plasma. The ZnO Machine has six plasma emission monitors (PEMs) at various locations in the deposition chamber. These devices use a PID controller to regulate the oxygen flow and maintain the plasma intensity to a given set point. The six PEMs are collectively calibrated (using off-line measurements) to produce uniform deposition. However, it has been observed that while the uniformity remains constant, the overall ZnO thickness will vary over time. The change in thickness can be corrected by scaling all six PEMs accordingly. The present operational procedure for the ZnO Machine requires the operator to monitor ZnO thickness with the spectrometer and make required corrections using the PEMs. Plotted in Figure 1.19 is the variation in ZnO_{max} through a production run. The saw-tooth pattern is produced as the thickness drifts beyond the established tolerance and the operator makes a corrective PEM change.

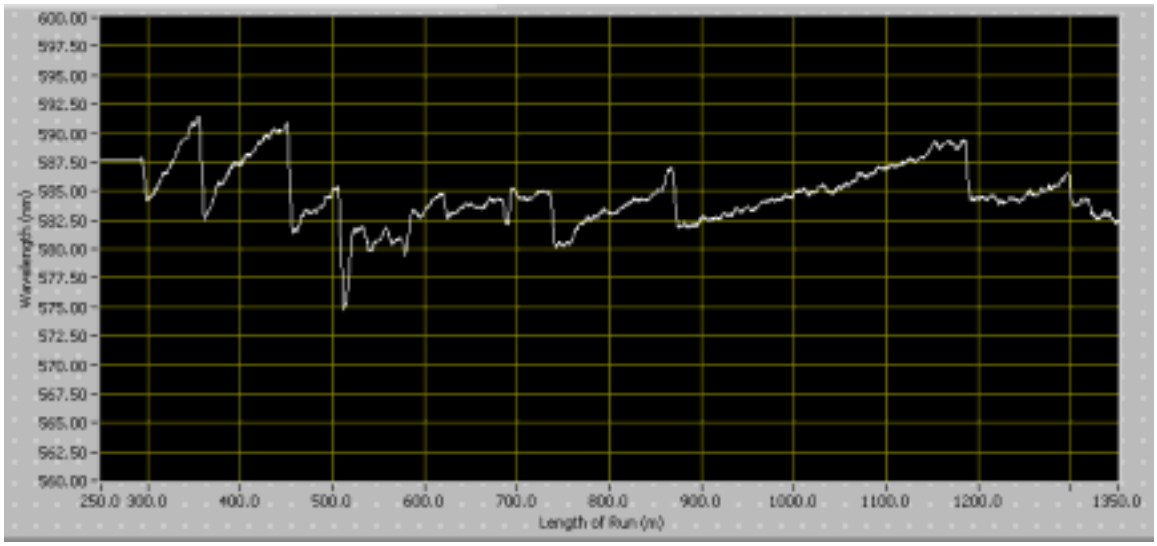

Fig. 1.19. Variation in ZnO_{max} Through a Production Run

To quantify the change in thickness due to a PEM change an experiment was performed that stepped the PEM settings to ± 9% and ± 18% of nominal. The reflection spectra from the spectrometer are plotted in Figure 1.20 and the resulting shift in ZnO_{max} plotted in Figure 1.21.

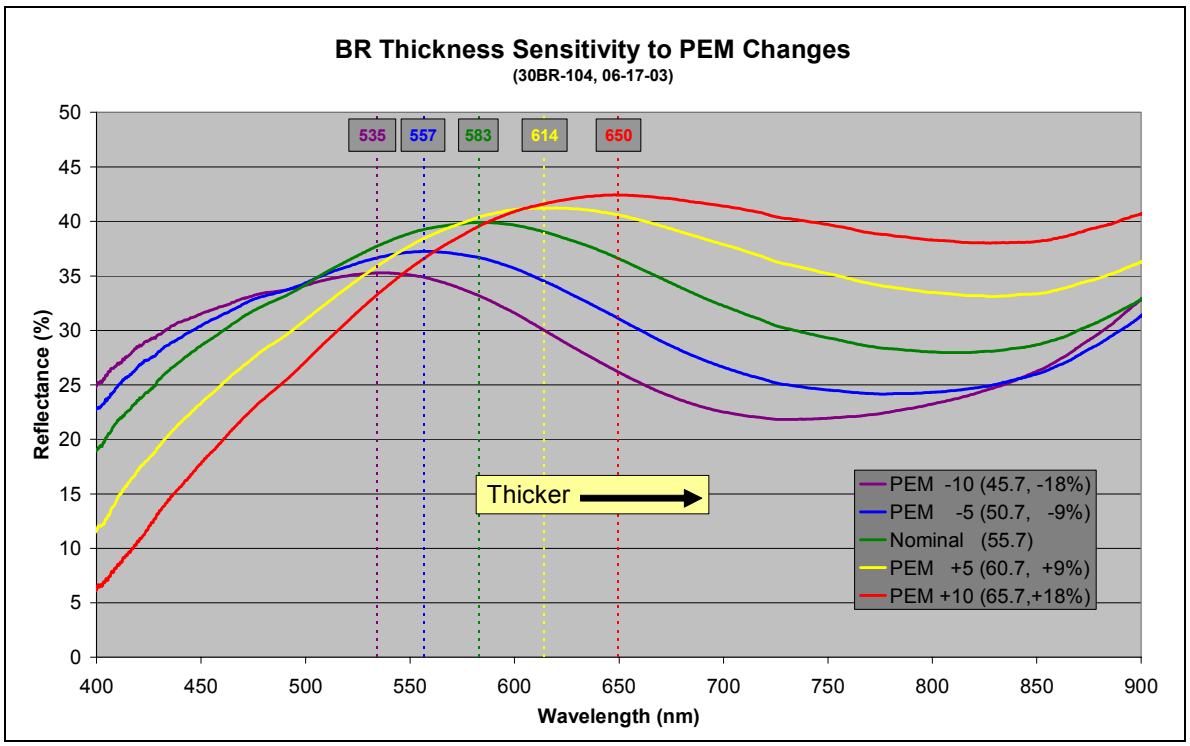

Fig. 1.20. Shift in the Reflection Spectrum from PEM Change

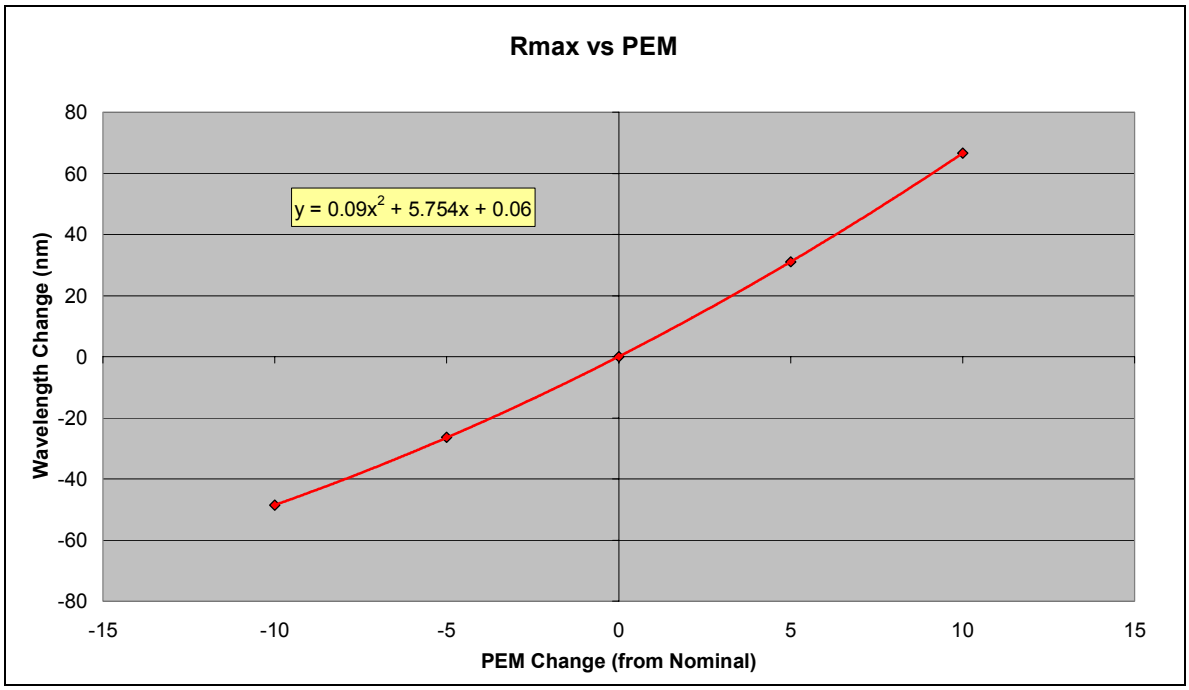

Fig. 1.21. Shift in ZnO_{max} from PEM Change

1.4.3 Closed-Loop Control Software

Shown in Figure 1.22 is a schematic of the principal feedback system components and their respective computers. To assure a reliable and fail-safe system the closed loop control algorithms will reside on the *Controls PC*. In consideration of the large time delay between the plasma target (actuator) and the thickness measurement (monitor,) a simple feedback control strategy was chosen for this *1st Generation* system. This method applies an increment to the machine control set-points that is proportional to the required correction. The system will then delay by the amount of time required for the spectrometer to measure the effective change. For the ZnO Machine this corresponds to an elapsed time of six minutes. The controller parameters were determined according to the experimental data shown in Figure 1.21. An expert control panel (Figure 1.23) controls all aspects of the feedback algorithm and provides charts and readbacks for monitoring system performance. The flow chart in Figure 1.24 summarizes the closed-loop control and exception handling. The need for a more advanced control method (egs Predictive Control,) driven by a need for faster correction, will be assessed as the system is commissioned.

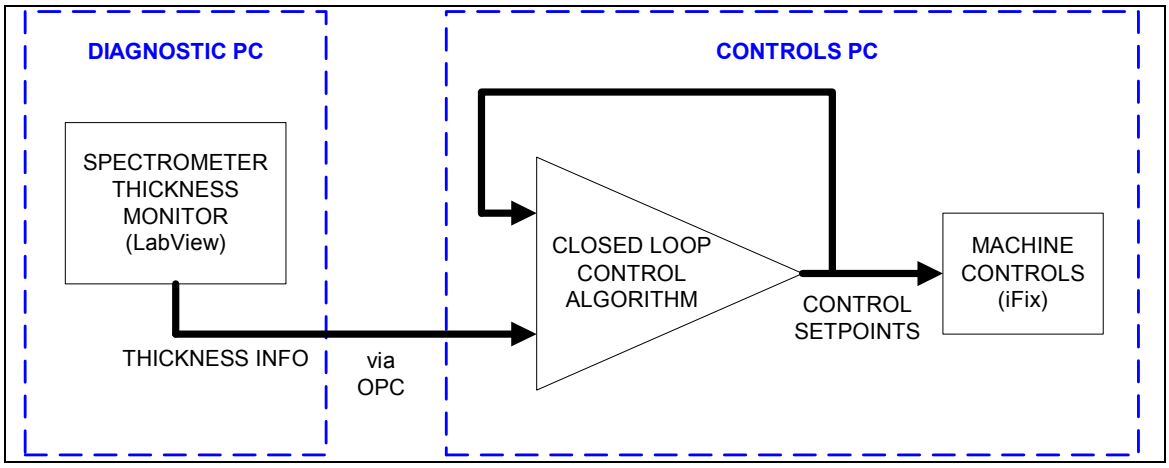

Fig. 1.22. Schematic of Main Algorithms and Their Resident Computers

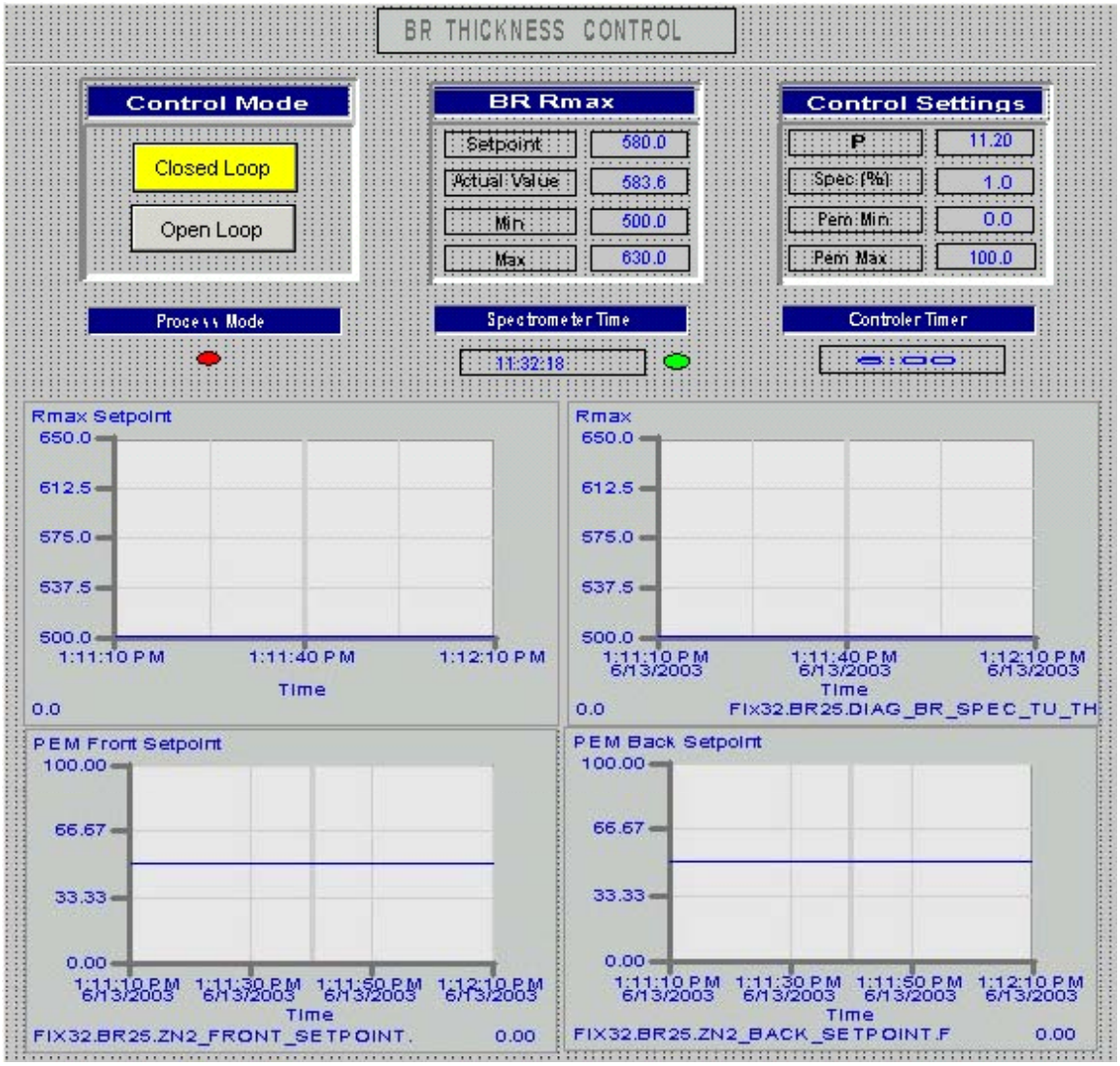

Fig. 1.23. Expert Control Screen

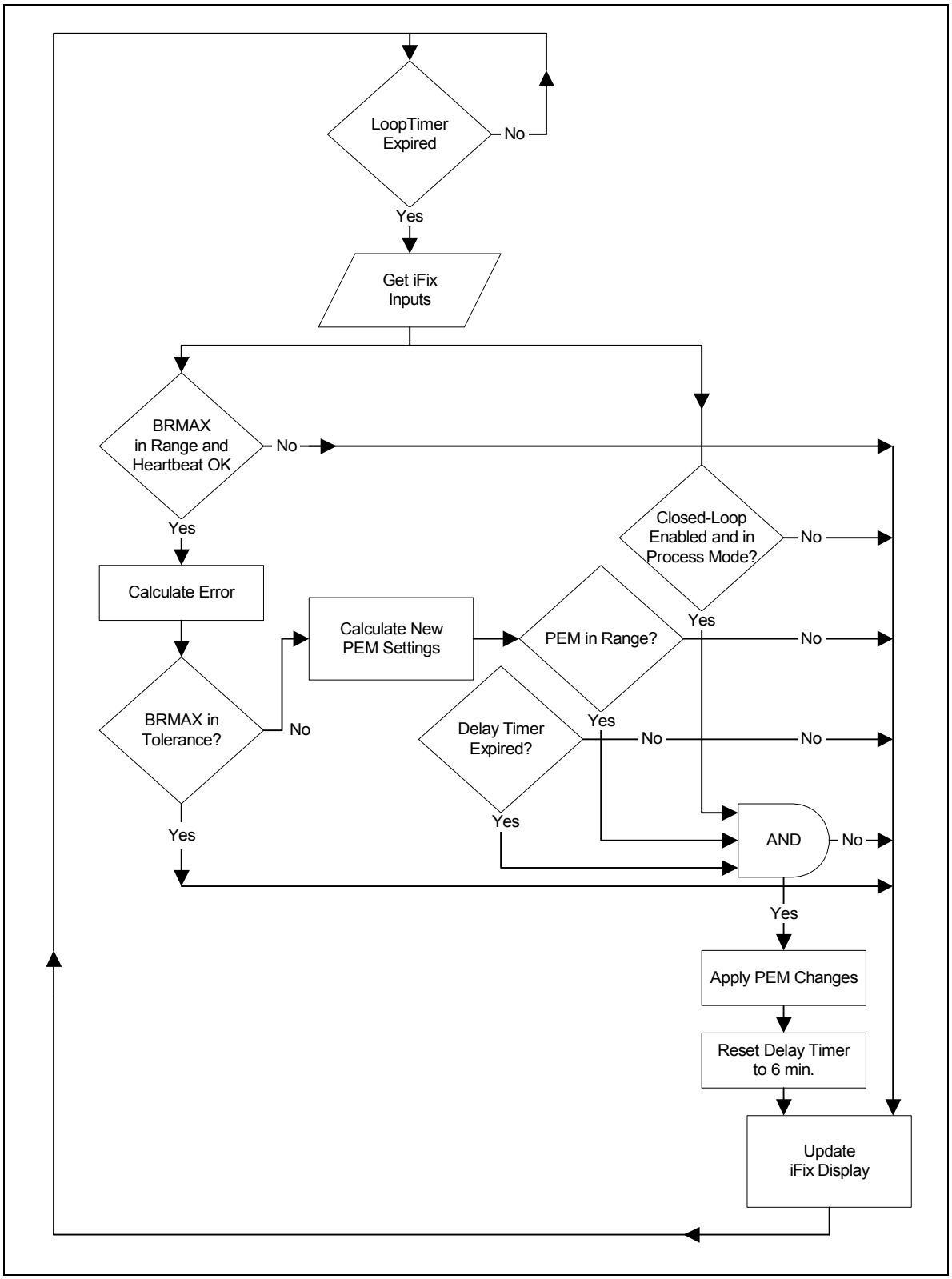

Fig. 1.24. Schematic of Closed-Loop Process and Exception Handling

TASK 2: PV Capacitive Diagnostic Design and Fabrication for Bottom and Middle Cells

– Tim Ellison, Rob Kopf and Wayne Messing (ECD); Dave Dodge (Focus Software)

Milestones

Complete	**m-1.0.2**	**Complete initial bench testing of component cell PVCD.**
Complete	**m-1.0.3**	**Complete bench testing of component high intensity LED light source and light source power supply.**
Complete	**m-1.1.2**	**Complete preliminary testing of component cell PVCD in production machine.**
Complete	**m-1.3.2**	**Complete installation of retrofitted component cell PV Capacitive Diagnostic in production equipment.**
Complete	**m-1.4.2**	**Complete the Phase I portion of the effort under Task 2.**

Deliverables

Complete	**D-1.0.1**	**Report summarizing bench testing of high intensity LED light source and light source power supply**
Complete	**D-1.1.1**	**Report summarizing design and installation of component cell PV Capacitive Diagnostic in production equipment.**

2.1 Background

In the PVMaT 5A program we developed the PV Capacitive Diagnostic[1]. This device has proven its capability to make precise in-line measurements[2,3] of the PV device open circuit voltage, V_{OC}, and short circuit current divided by cell capacity, J_{SC}/C. The device works on material before both before and after application of the top ITO coating, and has become an essential online diagnostic for production QA.

2.2 Motivation

As in the Task 1 discussion of the thickness monitors in the a-Si machine, while a single monitor at the end of the machine in the Take-Up (TU) Chamber can alert the operator to a change, it cannot point to the location in the machine where the change or problem occurred. The same is true for the PV Capacitive Diagnostic (PVCD):

- Although the PVCD in the TU Chamber can alert the operator to a change in open-circuit voltage, V_{OC}, of the triple-junction device, it often cannot tell the operator in which of the three cells the voltage reduction occurred.
- While the TU Chamber PVCD can measure the top (last-deposited) cell short-circuit current divided by cell capacity (J_{SC}/C), it provides less clear information on the bottom cell J_{SC}/C, and almost no clear information on the middle cell J_{SC}/C.

---

[1] Tim Ellison, “Non-contacting PV Capacitive Diagnostic (PVCD) System for real-time in-situ analysis, QA/QC, and optimization”, *Proc. 28th IEEE Photovoltaic Specialists Conference* (Anchorage Alaska, 15 – 22 Sept 2000).

[2] Greg DeMaggio et al., “Development of Online Diagnostic Systems for Roll-to-Roll a-Si Production: ECD’s PV Manufacturing R&D Program”, Proceedings of the 2003 NCPV Review Meeting (Denver, 24 – 26 March 2003).

[3] Masat Izu and Tim Ellison, “Roll-to-roll manufacturing of amorphous silicon alloy solar cells with in-situ cell performance diagnostics” in Solar Energy Materials and Solar Cells, Elsevier Science B.V., Amsterdam.

In this program we are designing and implementing a Component Cell PVCD that can be inserted in the machine after the bottom and middle cells of the triple-junction device. This will allow unambiguous measurements of the V_{OC} and J_{SC}/C for each component cell in the device. This is a significant breakthrough:

- Even in offline QA/QC testing, we only obtain a V_{OC} for the complete device; this online device will provide us with information on the V_{OC} for each of the component cells. This will change the language that we use – if one says that the V_{OC} has changed, in the future one will ask, "which V_{OC}?".
- Online troubleshooting will become much easier – rather than saying we have a problem, we will be able to locate the problem in a specific cell. Additional information from the PVCD and from the Second Generation spectrometers being developed may help us locate the problem with better precision.
- Finally, with reliable voltage, current [and thickness] measurements of each component cell in the triple-junction device, we can seriously embark on a significant continuous online optimization program.

2.3 Component Cell PVCD Design

2.3.1 Design Challenges

There were a number of challenges associated with the Component Cell PVCD that did not need to be addressed when designing the Take-Up chamber PVCD's. These include:

- Space is a premium for the component cell PVCDs: there is a 6" access port through which the complete device must be inserted; the device must be positioned between two webs a few inches apart. In contrast, the Take-up chamber PVCD has a 10" heater to discharge the web, followed by a 10" pre-cooler, and followed by a 10" pusher plate and PVCD. The tight spacing for this device is shown in Fig. 2.1.
- The position of the sensor, once inserted, must remain stable with respect to the position of the web, to within 0.002" to maintain 0.5% accuracy. There are no capstan rollers in this location to stabilize the web position.
- Once inserted, between the webs, the system cannot be easily viewed, serviced, or calibrated.
- Whereas the PVCD in the TU chambers did not need to be compatible with UHV techniques, the Component Cell PVCD must be UHV compatible, including all cabling, the LED light source, photo-detectors, etc.
- Whereas the TU chamber PVCDs are far removed from EMI sources, the Component Cell PVCD is adjacent to high power plasmas, high current heaters, ionizing U.V. radiation and the resulting conducting gases. It was not clear before testing – and indeed, for some time after initial installation and testing, whether such a device could work in this environment.

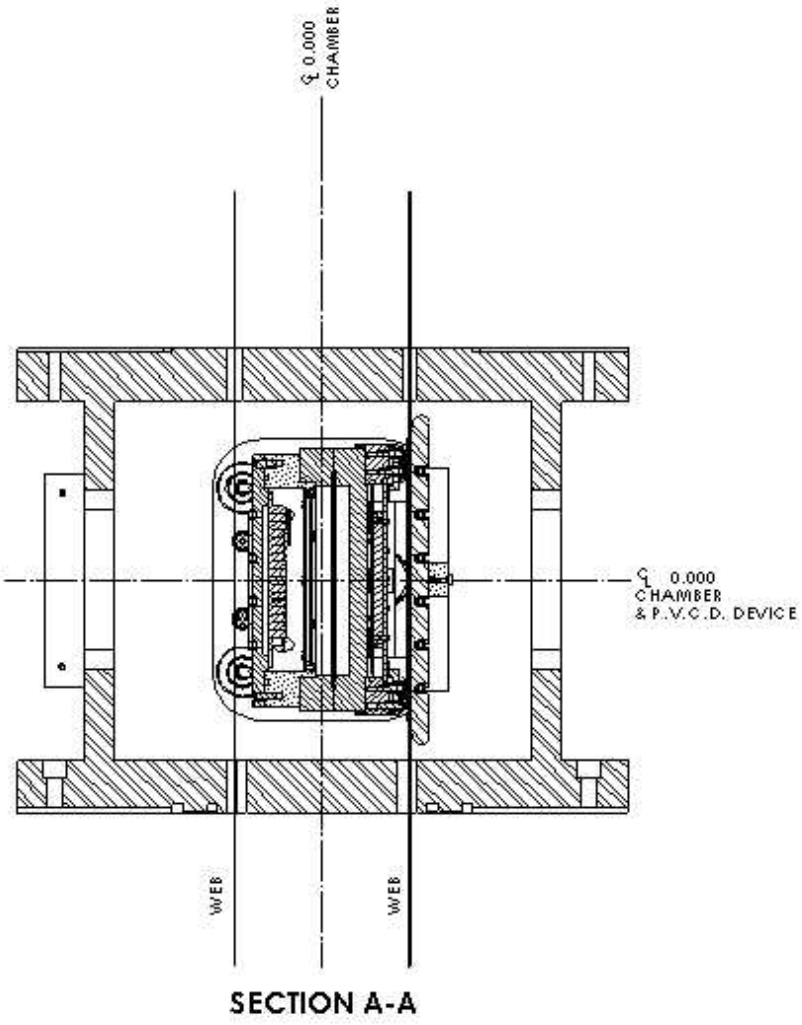

Fig. 2.1. Top section view of the Component Cell PVCD installed in the production machine. Physical space was a significant design constraint. There is only a few inches between the two webs.

Expanding upon the last bullet, the PVCD sensor amplifiers are quite sensitive, with typical charge-to-voltage gains of about 1 mV/1000 electrons, and current-to-voltage gains of about 100 mV/[fA = 10^{-9} μA]. Even the type of cable attached to the amplifier input can change the low frequency noise level due to charges moving in the cable by 3 orders of magnitude as shown in Fig. 2.2. A bad cable alone can saturate the amplifier. This noise is roughly proportional to the cable length. Adding to the challenge of the Component Cell PVCD we found that that all cables compatible with UHV [e.g., TFE dielectrics] were the worst from a charge-noise standpoint; making matters still worse, the cable length for the Component Cell PVCD is an order of magnitude longer than that used for the TU chamber PVCD's. We are continuing testing of UHV-compatible cables for "charge noise".

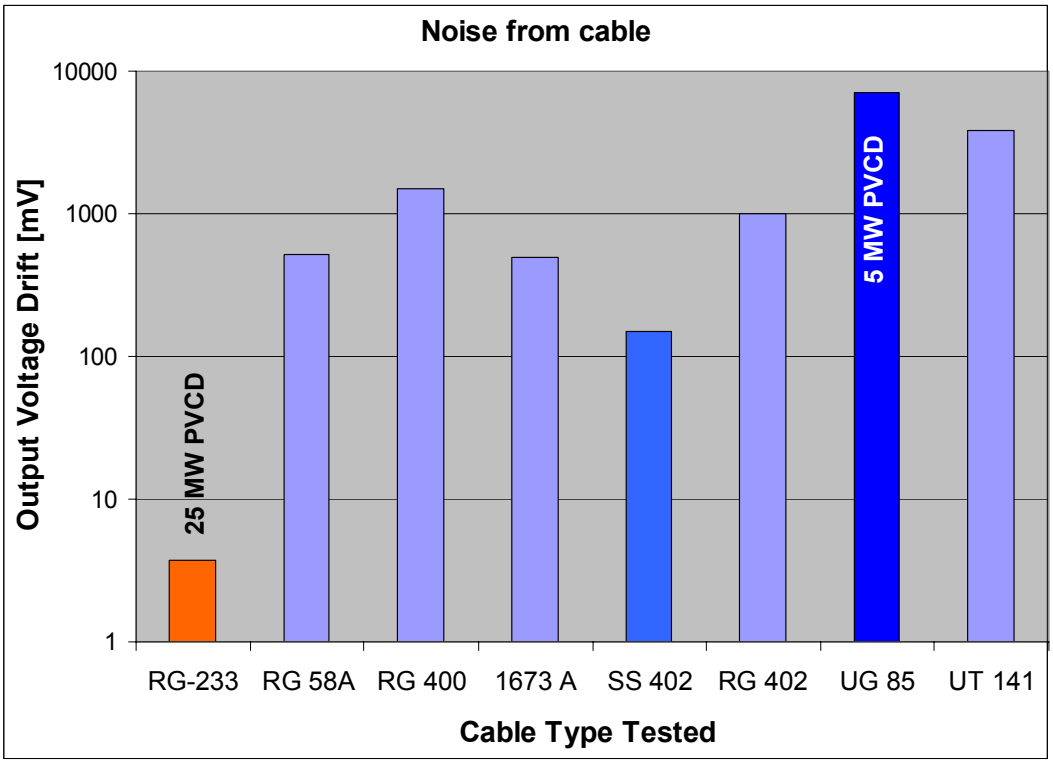

Fig. 2.2. Measured low frequency noise arising from charge disturbances inside of various coaxial cables evaluated for the Component Cell PVCD. The RG-233 was used in the TU chamber PVCDs for the 25 MW production equipment, but could not be used in the Component Cell PVCD's because it was not UHV-compatible.

2.3.2 Shutter Assembly

We designed a shutter assembly that moves between the PVCD sensor head and the web to address a number of the design challenges:

- A grounded shutter moving between the shutter and the PVCD sensor head can be used to measure the residual voltage on the web. This system solves the problem of not having space to install a web heater and pre-cooler to discharge the web. This solution, however, also has its own design challenge: any insulator in the assembly, or close to the PVCD sensor head, quickly develops static charges and resulting voltages orders of magnitude larger than the voltage the system is attempting to measure, and consequently dominate the measurement. By careful design, we were able to make this system work.
- The shutter can also be used to check the system calibration by applying a small voltage to it. Again there is an associated design challenge: since the shutter is so close to the PVCD sensor head, its position when moved into place must be repeatable to within 0.002" to provide 1% repeatability.

2.3.3 Completed Component Cell PVCD Design and Assembly

Renderings of the Component Cell PVCD are shown Figs. 2.3 – 2.5; a photograph of the assembly prior to installation is shown in Fig. 6. The system was first dirty-assembled for bench testing, retrofitting, and optimization. After an iterative process of retro-fitting, refinement, and optimization, the system disassembled, cleaned, re-assembled, leak-checked, and re-tested prior to installation.

Fig. 2.3. Component Cell PVCD assembly showing the sensor head, and web temperature and position stabilizing “pusher plate”.

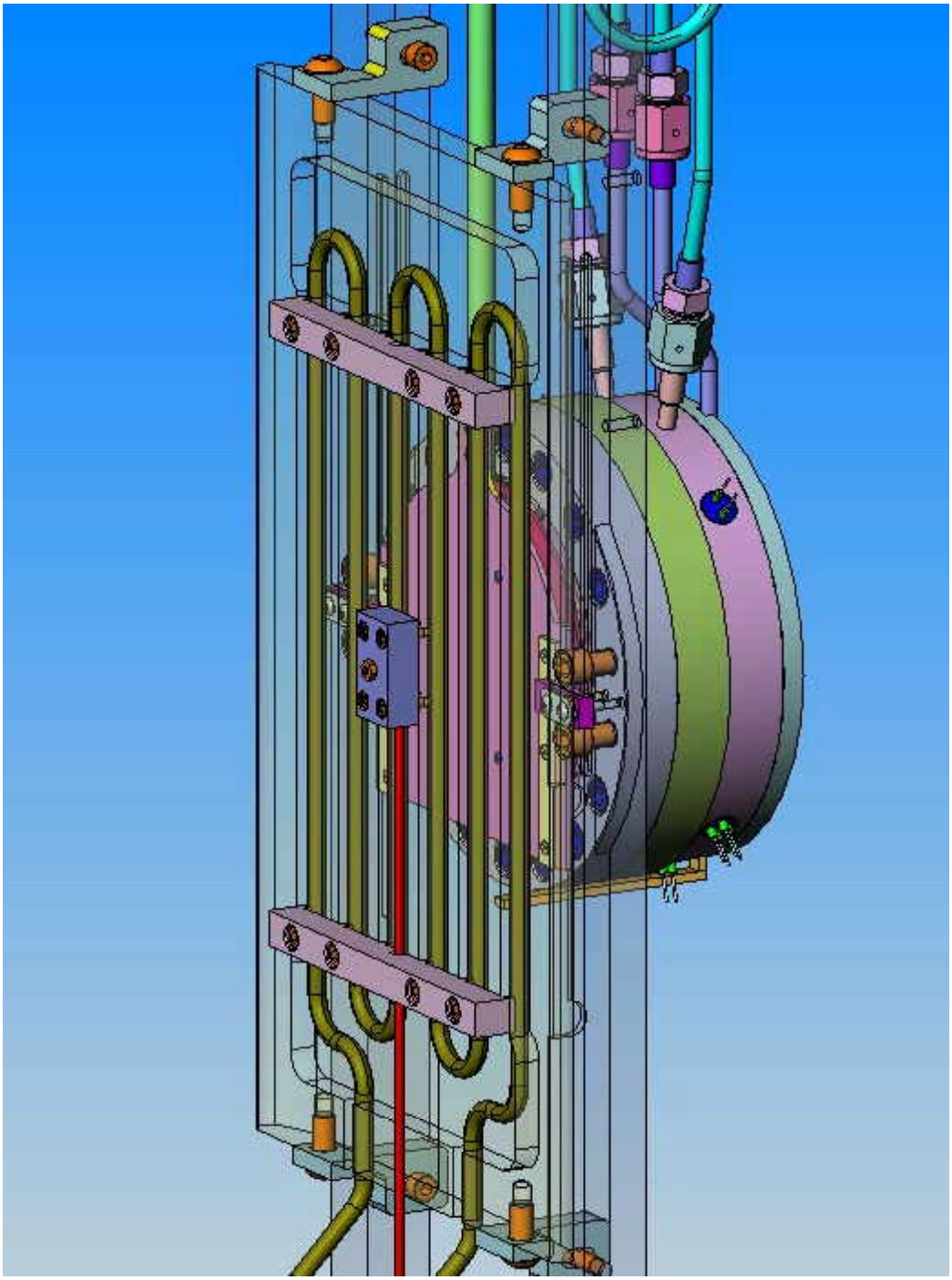

Fig. 2.4. Close-up view of the PVCD sensor head, shutter, and transparent view of the “pusher plate”.

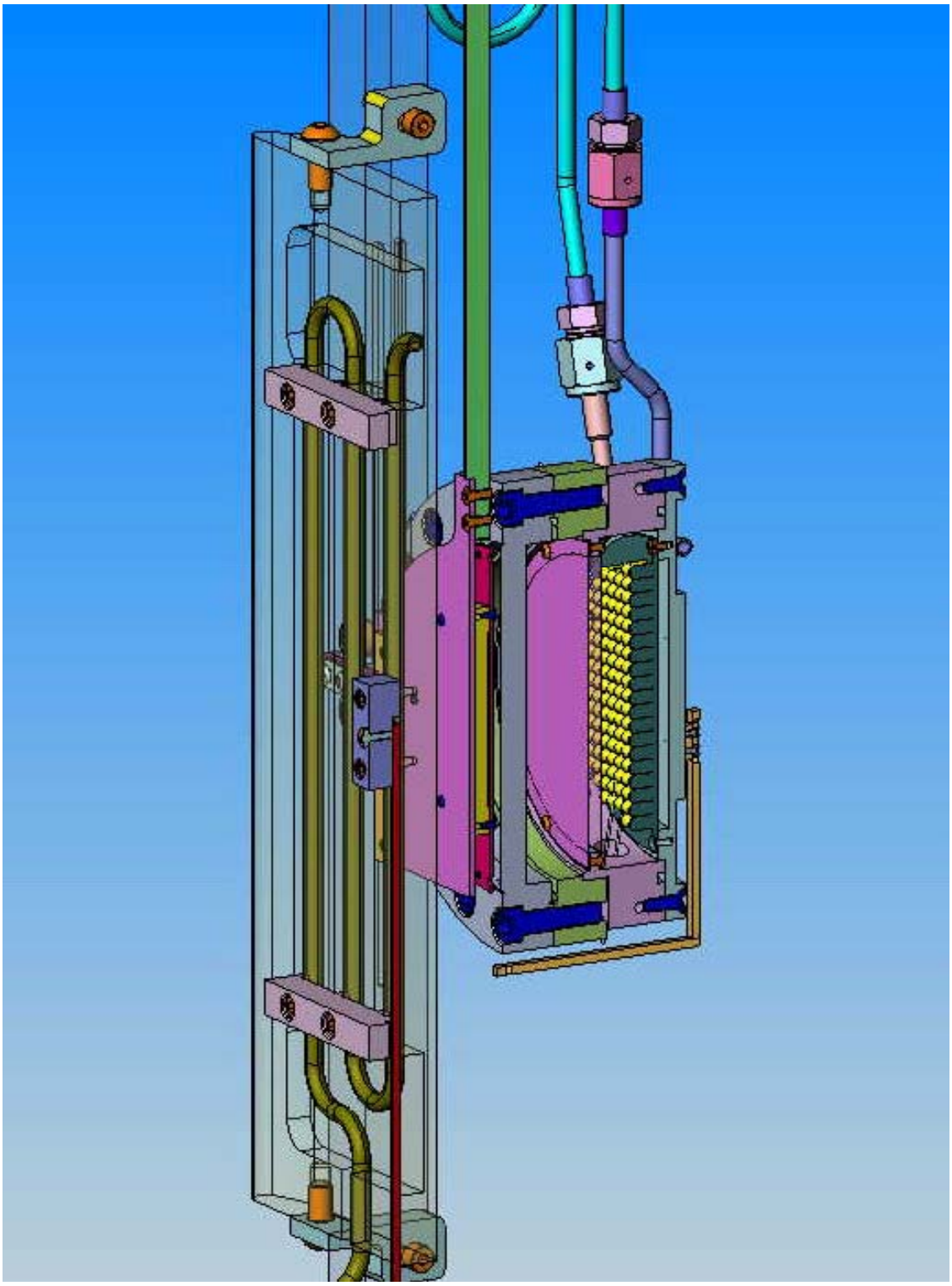

Fig. 2.5. Close-up view section view of the PVCD sensor head, shutter, and transparent view of the “pusher plate”.

Fig. 2.6. Photograph of the First Generation Component Cell PVCD after bench testing, being prepared for installation. The PVCD sensor and LED Solid State Light Source are located in the round vacuum chamber at the bottom of the picture. Shown is the backside of the sensor.

2.4 Component Cell Light Source Design and Testing

The PVCD is an *in-situ* non-contacting device. As such, it is a.c.-coupled to the web and requires a time-varying voltage or electric field. We obtain this changing voltage by pulsing a light source onto a discharged PV web, causing the PV material to charge up to its open circuit voltage. Consequently a bright, uniform, repeatable pulsed light source is required. We use LED's, which are inexpensive, available in a wide range of wavelengths, compact – easily packaged into the PVCD device, bright, and stable.

Off hand one might conclude that the ideal light source might have the AM 1.5 spectrum and intensity and meet or exceed the ASTM Class A specifications. The present source, pulsed, can achieve a photon flux of about $1/5^{th}$ that of the AM 1.5 spectrum, and uses only 4 wavelengths of LED's (the ASTM standard for the AM 1.5 spectrum has 6 wavelength bins].

So, while we are far from meeting Class A specifications and envision continual improvements eventually leading to a solid state Class A simulator, the present source works well:

- With experience we have established that V_{OC} measurements made with a photon flux density of about 15% of AM 1.5 correlate, to the percent level with the V_{OC} measured at AM 1.5 intensities. Once could envision almost perfect agreement by fitting the measured V_{OC} as a function of intensity and extrapolating to AM 1.5 intensities. While the PVCD hardware and software is capable of this measurement, we have not observed any significant gains from this added complexity.
- There are technical reasons why light levels far lower than the AM 1.5 level are actually *desirable* and advantageous for many measurements.
- While the present light source does not have the AM 1.5 spectrum, many online diagnostic measurements do not require such a spectrum. In some cases, different spectra are actually *desirable*. For example, the LED wavelengths chosen for the present source, when pulsed individually, allow probing individual cells in a multi-junction device with high selectivity, something an AM 1.5 source would not allow.

While we have completed the development of the solid-state (LED) light source (SSLS) and light source power supply for the Component Cell PVCD, in other program we have continued this development work. The present SSLS has a photon flux, when pulsed at 200 mA, of about 20% of the AM 1.5 spectrum. Another two factors of two would get our SSLS up to AM 1.5 photon flux-densities. The photon flux from diodes has been increasing over the last 3.5 decades at an exponential rate of about a factor of 2 every two years. We consequently think it is possible, by pulsing diodes further beyond their specified range and using the best state-of-the-art diodes, to obtain AM 1.5 flux densities and possibly fabricate a Class A pulsed simulator within the next few years. If improvement in ECD's SSLS technology would be shown to significantly improve the capabilities of the PVCD's, we shall consider retrofitting the PVCD's with new light sources in the future.

The SSLS has two principle parts: a computer-controlled pulsed current-source, and the LED array.

2.4.1 LED Array

2.4.1.a LED Array Layout. The LED array, shown in Fig. 2.7, has over 200 LEDs arranged on a custom-design printed circuit board that fits inside of the component cell PVCD. In this array, each of the 4 different waveleng th LEDs are arranged in a number of parallel strings of series-connected diodes. Typically there is about 5 diodes/series string. The diodes of each wavelength are on separate circuits allowing for independent control. The measured light uniformity, measured 6 cm from the source, is shown in Fig. 2.8.

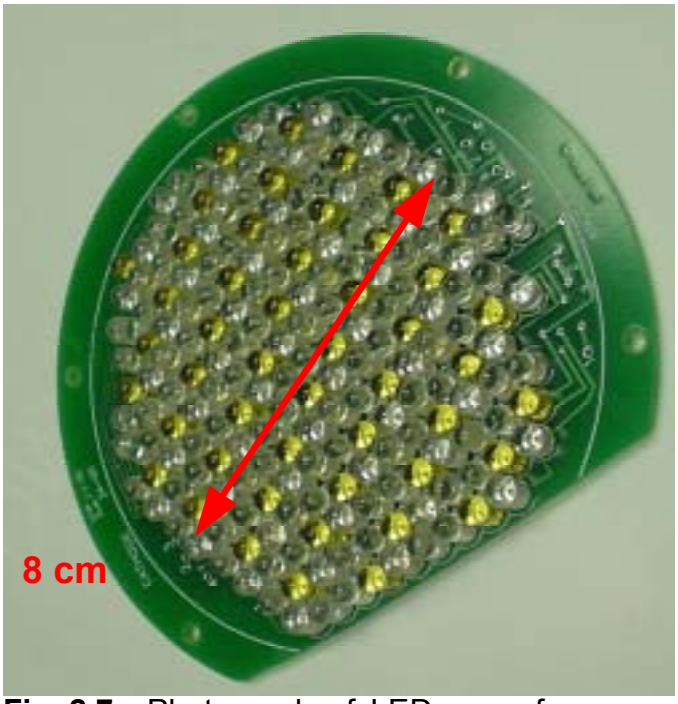

Fig. 2.7. Photograph of LED array for the solid state light source.

Fig. 2.8. Measured light uniformity. The diodes typically have a 30° cone angle. We find, at 6 cm from the source, that the light is relatively uniform out to 2 cm from the edge of the light source. The systematic decrease in intensity from 0 to 14 cm is probably a result of the measurement technique, rather than a property of the light source.

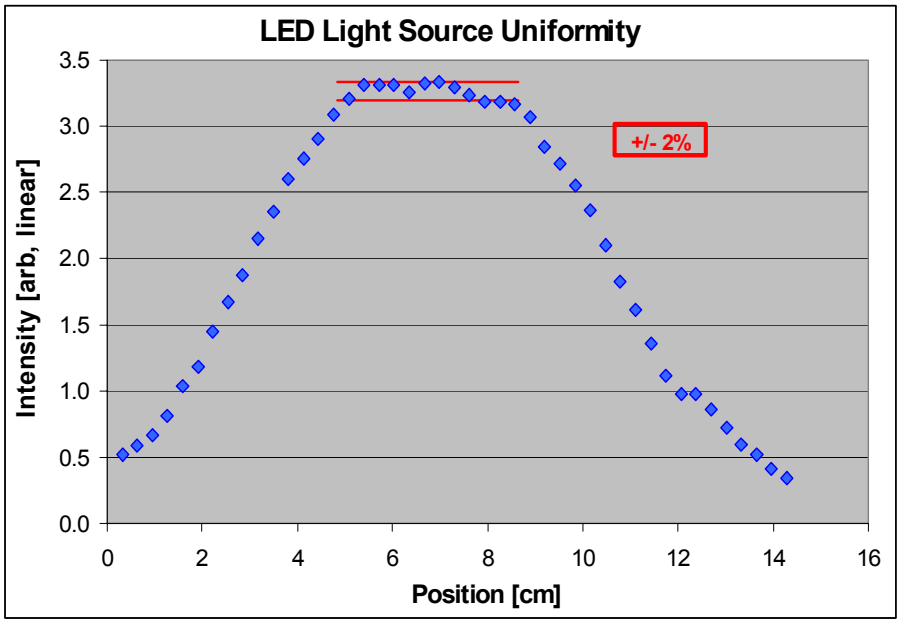

2.4.1b. LED Array Spectrum. Figure 2.9 shows the spectral power of the present SSLS when pulsed at 200 mA. The spectral distribution is measured with a spectral radiometer while operating the SSLS continuously at 10 – 20 mA. These data are scaled to higher pulsed currents by measuring the total flux with a photo-diode as a function LED current over the range from 1 to 200 mA. While the diodes are typically rated for 20 mA, we have found that we can pulse them with currents of 200 mA for short time periods without destroying them. The computer-controlled SSLS has programmed limitations on the pulse length as a function of LED current for currents above 20 mA. This current/pulse-length relation was based upon an electrical/thermal theoretical model. It may be that this model is too conservative and higher pulsed currents and/or pulse lengths can be used.

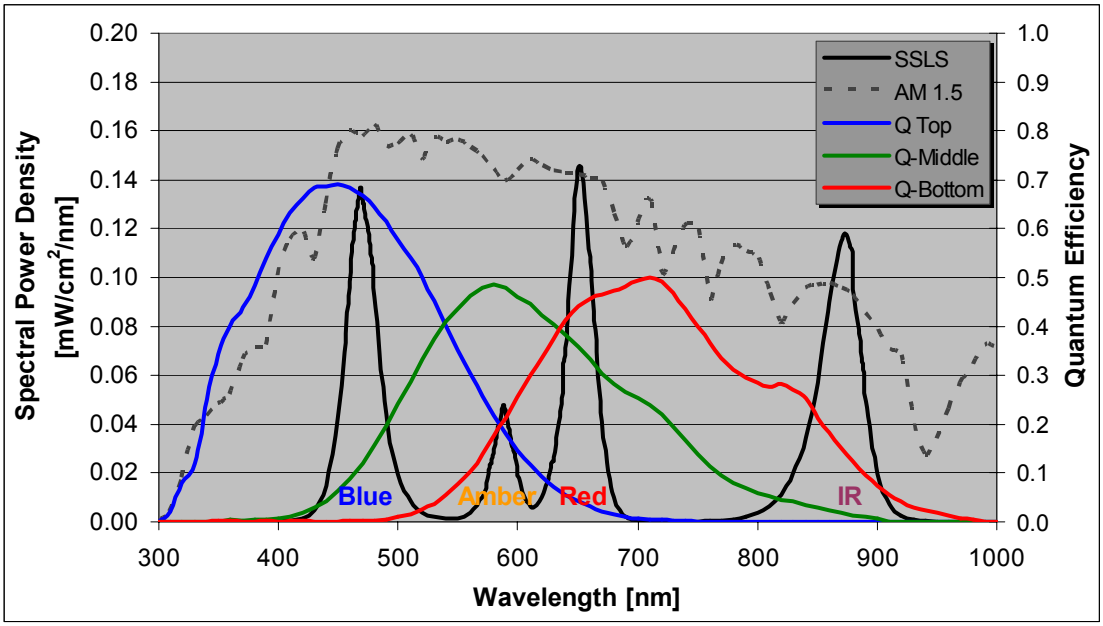

Fig. 2.9. PVCD solid state light source (SSLS) spectral power density [for 200 mA light pulse] along with the AM 1.5 spectrum and typical quantum efficiency curves for United Solar's triple junction device. The integrated number of photons is about 20% that of the AM 1.5 spectrum.

The SSLS has 4 types of LED's, each driven by a separate power supply, corresponding to the 4 peaks seen in the LED curves in Fig. 2.9. Figure 2.10 shows how the light from these 4 wavelengths is absorbed in each of the three cells in a typical United Solar triple junction device [blue curve: top cell; green curve: middle cell; and red curve: bottom cell]. Table 2.1 shows the "selectivity" of the different diodes when illuminating a triple-junction cell. Both the Blue and IR LEDs have high selectivity in measuring mainly the top and bottom cells respectively. This in principle would allow a single PVCD looking at the complete device to measure both the top and bottom cell J_{SC}/C when illuminating a triple junction cell.

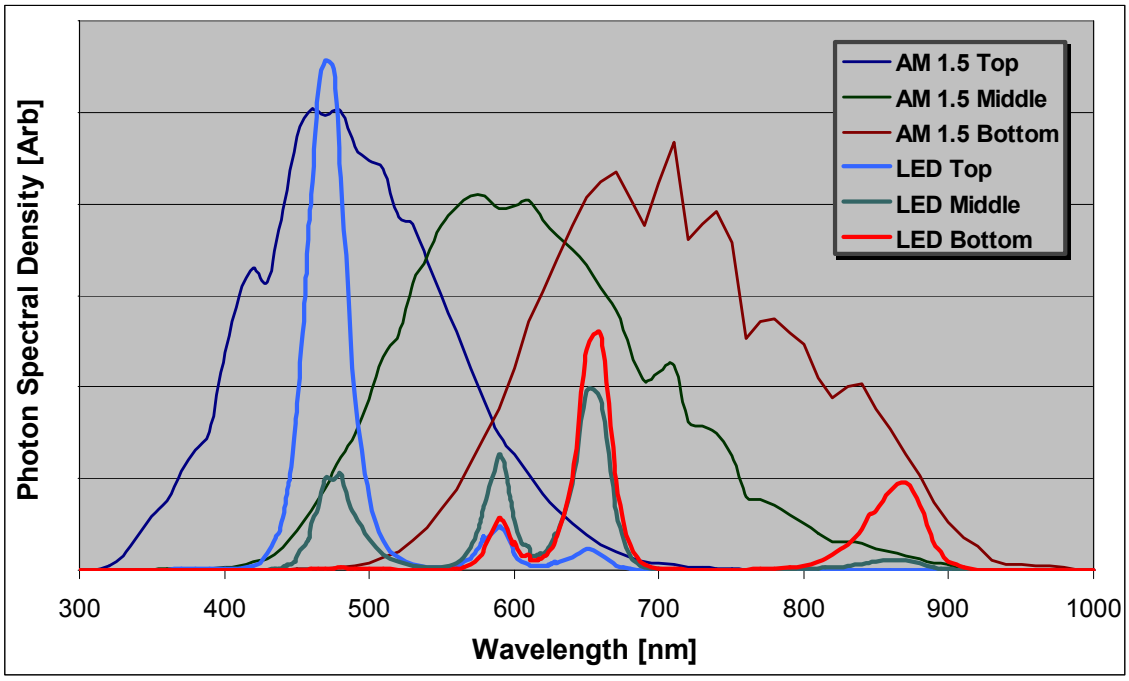

Fig. 2.10. Absorption of light from the SSLS in each of the cells when shining on a typical triple-junction device.

Table 2.1. Solid state light source nominal wavelengths and relative absorption in each of the three component cell.

LED	Wavelength [nm]	Absorption Top	Middle	Bottom
Blue	474	1.00	0.19	0.01
Amber	588	0.41	1.00	0.42
Red	652	0.09	0.78	1.00
IR	860	0.00	0.13	1.00

Given this high degree of selectivity, one might then ask, why component cell PVCD's? There are several reasons. A few are:

- Despite this degree of selectivity, a single PVCD cannot provide component cell V_{OC} measurements. While in principle, a crude estimate might be possible, the data would be unreliable, and we have not been able to demonstrate this ability. With Component Cell PVCDs, sub-percent-precision measurement of the V_{OC} for each component cell is possible.
- The selectivity of the light sources is limited – as can be seen in Table I, it is not possible to obtain high selectivity to measure the J_{SC}/C of the middle cell. One might argue that, in principle, middle cell measurements might be obtained by combining "non-selective" middle cell measurements with highly-selective measurements of the top and bottom cells. Again, such a measurement would not be highly accurate or reliable, and has not been demonstrated.

- Measurements of cells below the top of the stack are not as reliable or accurate as measurements of cells on top of the stack: to probe cells at the bottom of the stack with high selectivity one needs to use very long wavelength IR light which not only penetrates to the bottom of the stack, but also reflects off of the backreflector creating an interference in the reflection spectrum. Consequently, small changes in the total stack thickness can strongly affect the absorption of light leading to unreliable measurements, or again, another required level of corrections. Furthermore, long wavelength light in this regime is looking at the tail-end of the cell Quantum Efficiency curve, and is not necessarily representative of the cell.

2.4.1c. LED Temperature Effects. While in principle one can monitor the LED light source intensity as a function of time, and correct data to take into account the changing light intensity, analysis is far simpler if the light amplitude can be kept constant. The first order effect of LEDs is a change in forward resistance as a function of temperature. We compensate for this effect by using a current, rather than voltage, power supply. A second order effect is the change in LED light output at constant current with change in LED temperature. These temperature effects take place on different time scales.

Short time scale temperature effects are observed in the Al-In-Ga-P LEDs which provide amber and red wavelengths. These diodes heat up on the time scale of a few ms during high intensity pulses well beyond their rating. The diode temperature cannot be controlled or stabilized on this time scale. This leads to a reduction in light output on the same time scale as shown in Fig. 2.11. This effect is not observed with shorter [e.g. Blue] and longer [e.g. IR] wavelength LEDs.

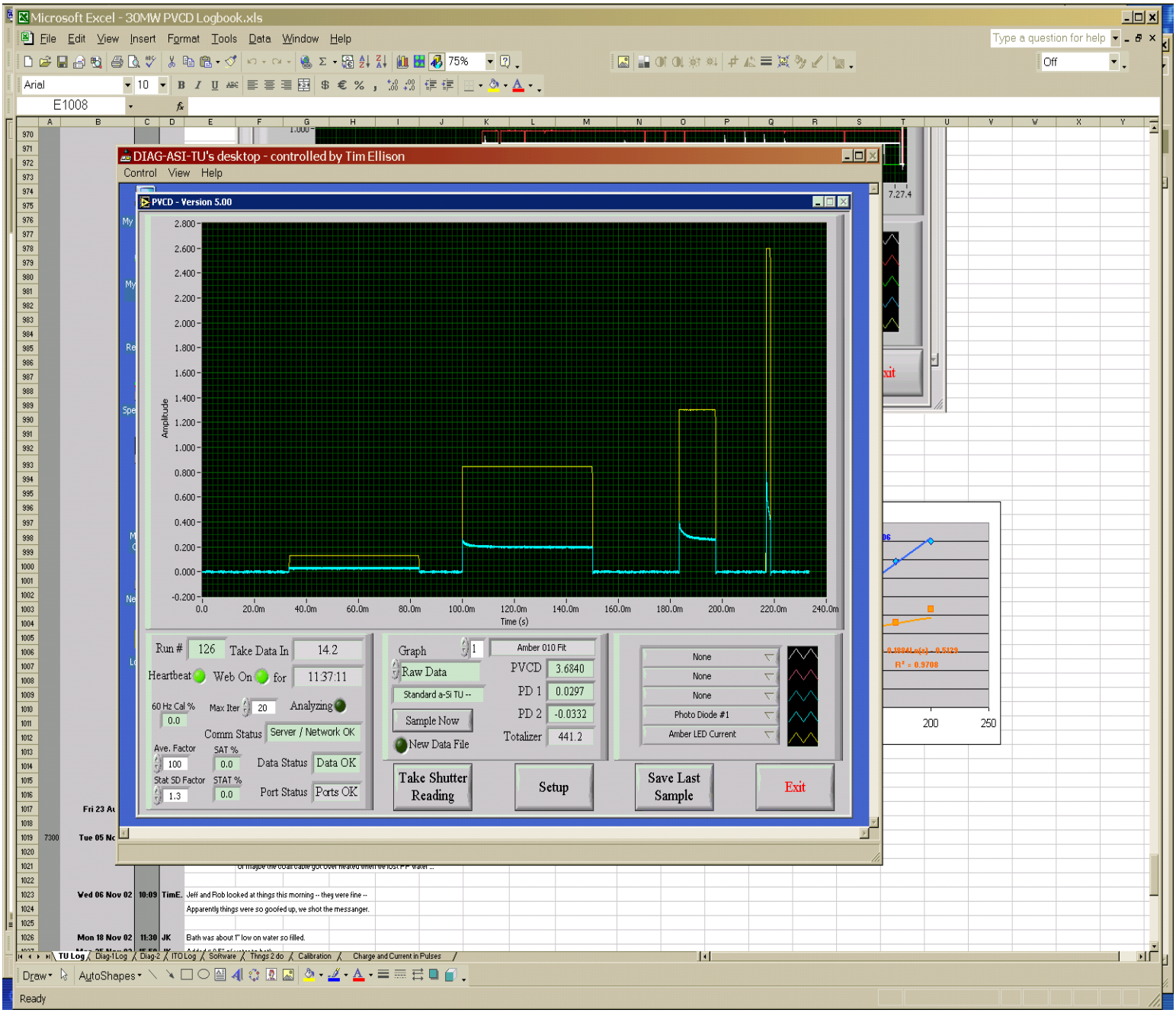

Fig. 2.11. Current and light output of an Al-In-Ga-P Amber diode demonstrating short term temperature effects. [Amber Curve: diode current, 215 mA FS; Blue: photo detector output]. The diode is pulsed at 10, 65, 100, and 200 mA. At currents above 50 mA the LED light output decreases with time for constant current. The effect increases with increasing current.

As shown in Fig. 2.12, the *initial* LED light output is indeed proportional to current, as expected. However, as shown in Fig. 2.11, at high currents the light output for constant current decays to a lower quiescent value. This lower value only increases approximately logarithmically with the LED currents as shown in Fig. 2.12.

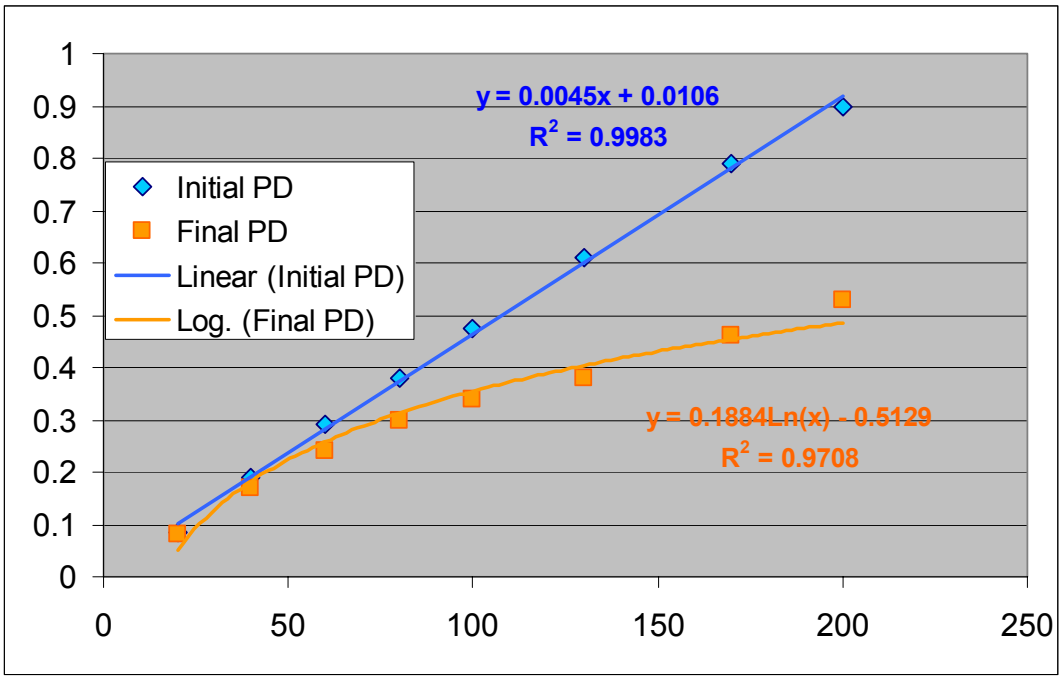

Fig. 2.12. Initial and quiescent light output from an Amber Al-In-Ga-P LED as a function of current. The higher currents final values appear to fall above the logarithmic model – this is expected because at higher currents we limit the pulse length and the diodes do not have time to reach their limiting output. If this final light output is a function of the junction temperature, keeping the diodes on till an equilibrium light output is reached would then probably eliminate any diode-protection effect of the reduced pulse length at high currents.

Long time scale temperature effects are also observed, where slowly, over a long period of time, the light output of the LEDs change as the ambient temperature slowly changes. These data are still being investigated, as they are also affect by the temperature coefficient of the photo-diodes used to measure the LED light output.

2.4.2 Pulsed Current Source

The resistance of LED's is highly temperature-dependent. We quickly found that a voltage supply would not work and designed a 4-channel computer-controlled current feedback power supply.

The pulsed current-feedback power supply can source up to 15 A at 50 V. Each of the 4 independent diode strings is independently controlled: diode strings can be pulsed individually, or in combinations. The computer control for this power supply allows one to program both the pulse width [from 10 μs to continuous] as well as diode current [< 1

to 400 mA – 20 times the rated diode current]. The computer control incorporates an algorithm for limiting the pulse width [when current is specified] and current [when the pulse width is specified] to protect the diode array.

During bench testing of the completed Component Cell PVCD we found that the ratio of currents for the four different diode types changed as a function of LED current when they were pulsed simultaneously. The problem was traced to interference in the current-monitoring circuits from small voltage drops in the current return wires. The power supplies were then retrofitted with lower impedance conductors, and the problem eliminated.

2.4.3 Future Work

Work on solid state pulsed light source has led to ongoing work to extend the SSLS capabilities to exceed the specifications for a Class A solar simulator [see Table 2.2] in another program. Below we outline the areas of development in this program:

Light Emitting Diodes

- Identify and test diodes that can output at least 5 times the photon flux of the present diodes.
- Systematically destructively test diodes to find their current/pulse width limitations.
- Document temperature coefficients of diodes.
- Identify diodes for use in each 100 nm wavelength bin of the ASTM Class A specification.
- Go further and identify diodes for 50, 25, and 10 nm wavelength bins.

SSLS Power Supply

- Increase the number of channels to accommodate 25 or 10 nm wavelength bins.
- Move from current feedback control to light output control. Assess feasibility of control to compensate for short time scale LED temperature effects.
- Incorporate temperature control for LED's and light output measurement circuits.
- Incorporate programming to change between AM 0 and AM 1.5 spectra.

Measurement and Calibration

The largest task might be developing new methods to calibrate such a light source. Since the wavelength distribution of each diode will be well known, perhaps the use of a highly accurate pyranometer for measurements with each diode type individually driven might be used.

Table 2.2. ASTM Spectral Distribution of Irradiance Performance Requirements

Percent of Total Irradiance Between 400 and 1100 nm of AM 1.5 Curve Within Various Wavelength Intervals		
Wavelength Interval [nm]	Percent of AM 1.5 Curve [normalized for 400 to 1100 nm interval]	
	Direct	Global
400 – 500	15.6	18.5
500 – 600	19.9	20.1
600 – 700	17.4	18.3
700 – 800	15.9	14.8
800 – 900	13.3	12.2
900 – 1000	17.9	16.1

2.5 Component Cell PVCD Installation

The First Generation Component Cell PVCD was installed in October 2002. Figure 2.13 shows the PVCD installed in the machine. The installation process was difficult:

- Due to other equipment that had been installed adjacent to the "Diagnostic Chamber", we found that is was impossible to install the assembled PVCD. Consequently, we devised a plan involving a partial disassembly of the system, and subsequent *in-situ* reassembly – akin to building a ship in a bottle!
- In the process of carrying out this plan the PVCD was damaged, specifically, a number of the fragile electrical feed-throughs were broken. We had fortunately installed spare feed-throughs on the device and were able to disassemble and re-wire the PVCD. We then attempted installation a couple of days later, and again we damaged the device, this time requiring significant re-work.
- A couple of weeks later the retro-fitted system was successfully installed. In the process we lost one of the four light LED light sources (the blue light) -- the least important light for bottom cell measurements. We decided that the benefits of this light source were not worth the risks of another removal and re-installation.

Fig. 2.13. First Component Cell PVCD after installation in the 25 MW production equipment. The green strap at the top of the PVCD assembly is attached to the overhead crane; notice the interference with the I-beam, around which this strap is bent. In the open Diagnostic Chamber one sees 3 of the six stainless steel webs (somewhat damaged from the installation process).

Figure 2.14 shows a view of the partially-reassembled PVCD looking up from an access port in the bottom of the "diagnostic" chamber. One again sees the severe spatial constraints faced in this design.

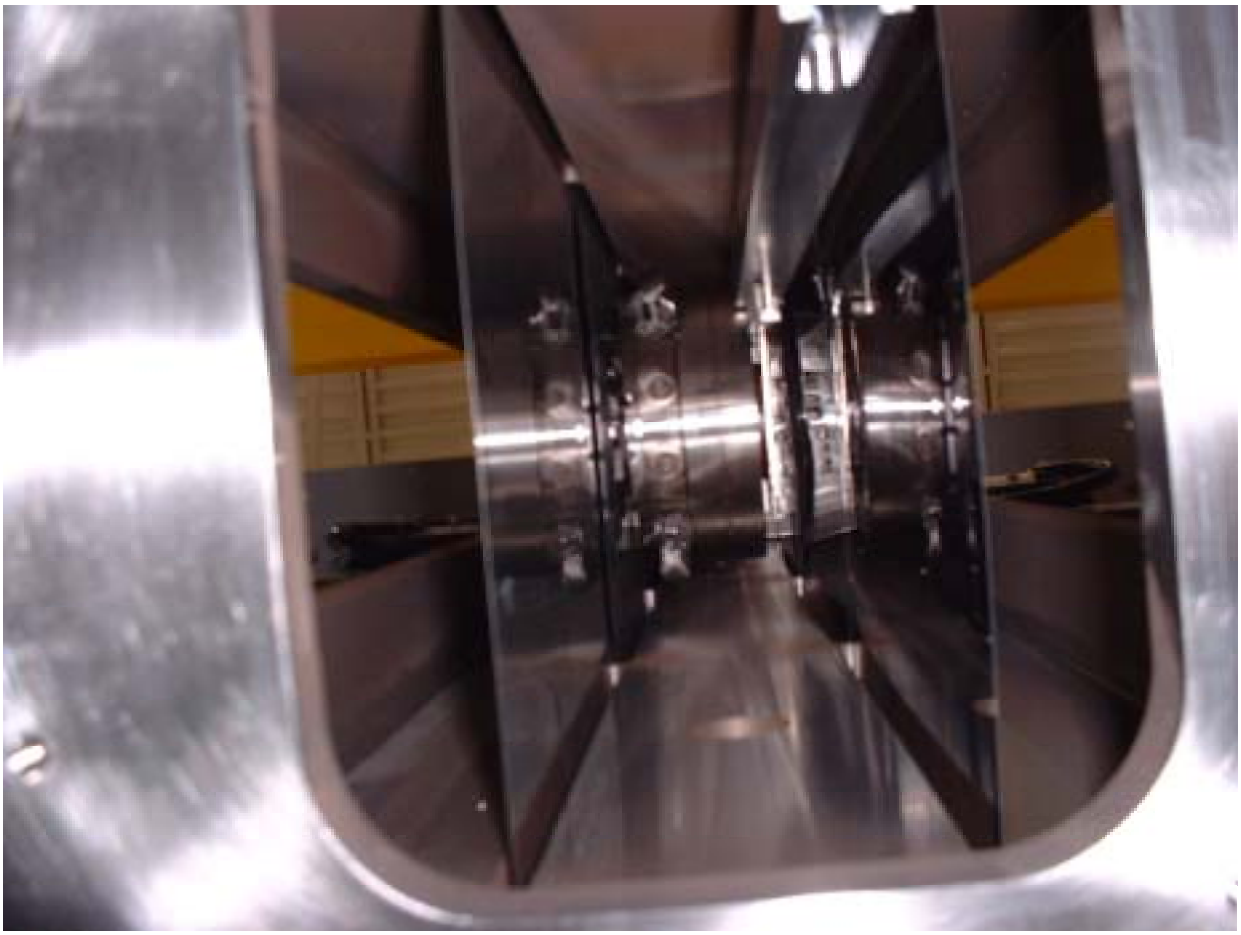

Fig. 2.14 . A view of the first Component Cell PVCD after installation in the 25 MW production equipment looking up from an access port in the bottom of the "diagnostic" chamber. The almost-vertical mirror-like pieces on either side of the PVCD sensor head are the stainless steel substrate.

2.5.1. Design Improvements for the Next Generation System

This experience led us to a number of design changes that will be incorporated into the next generation design. These changes include:

- "Notching" the flanges on the large I-beams spanning the top of the production machine and supporting the doors of the deposition chamber thereby allowing the complete assembly to be lowered into position by the crane;
- Re-designing the electrical connections to make them more robust;
- Optimizing the coatings on the "Pusher Plate" to eliminate wear and reduce backside web scratching;
- Identifying improved cabling to reduce the amplifier noise.

2.6. First Operation and Optimization of the Component Cell PVCD

2.6.1 Initial Operation and Optimization

The First Generation Component Cell PVCD was installed after the last deposition chamber for the bottom cell. With the machine idle – the heaters and plasmas off – the system worked splendidly, providing us with an excellent signal with negligible noise, as shown in Fig. 2.15. However, when the deposition chamber heaters and plasmas were turned on, the noise from low frequency currents flowing through the gas completely saturated the PVCD amplifier. Modifications made to the PVCD amplifier that reduced the low frequency gain allowed us to keep the amplifier out of saturation – most of the time – and achieve a S/N ratio of about 0.5, as shown in Fig 2.16.

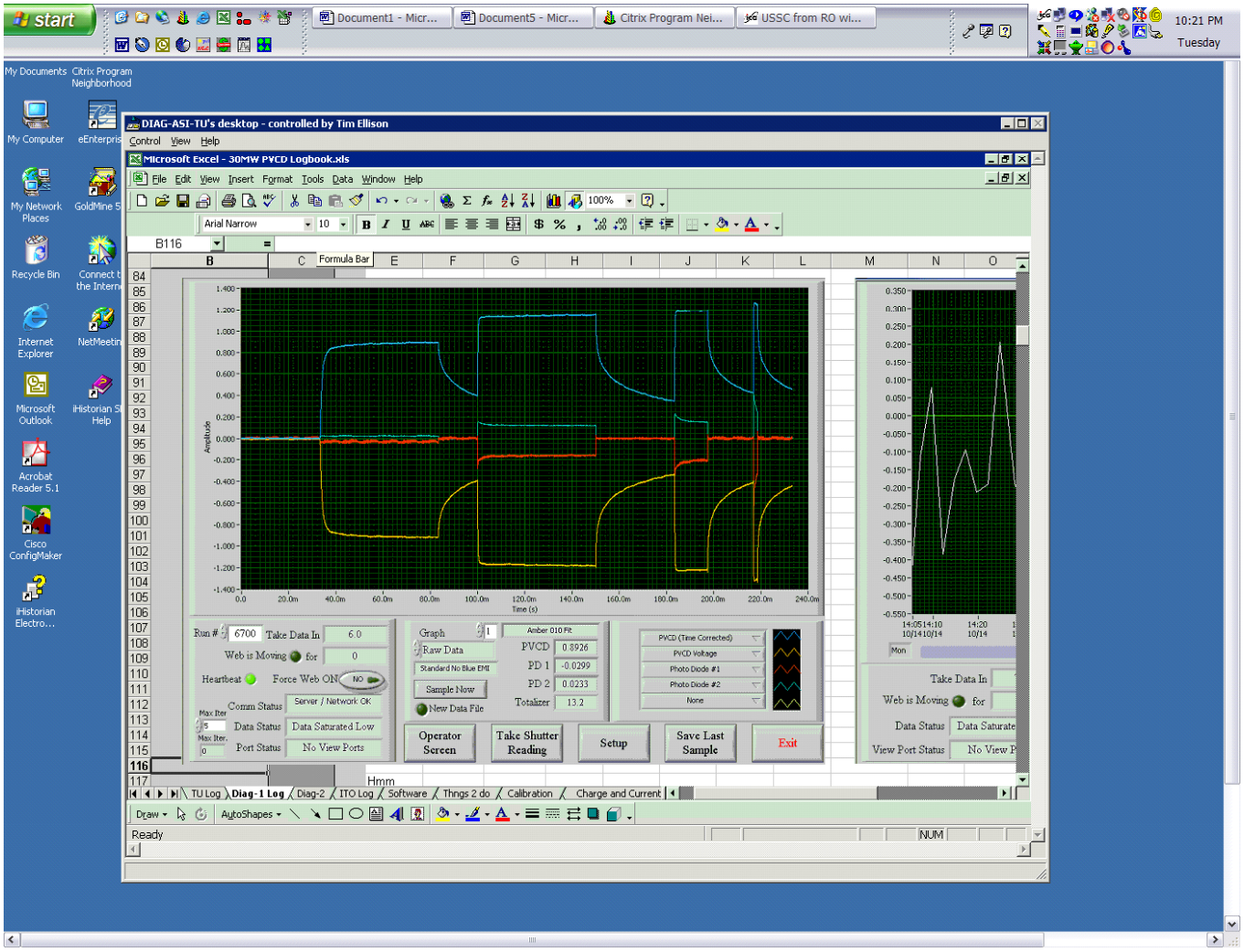

Fig. 2.15. Screen shot of signals from Gen-1 Component Cell PVCD immediately after installation – with deposition chamber heaters and plasmas off. In this "Multi" shot, the SSLS is pulse 4 times with increasing intensity and decreasing pulse-width. The red and green traces are signals from the photo-detectors; the blue and gold signals are the PVCD waveform shown the bottom cell PV device charging up when the SSLS is pulsed, and discharging when the light source is turned off.

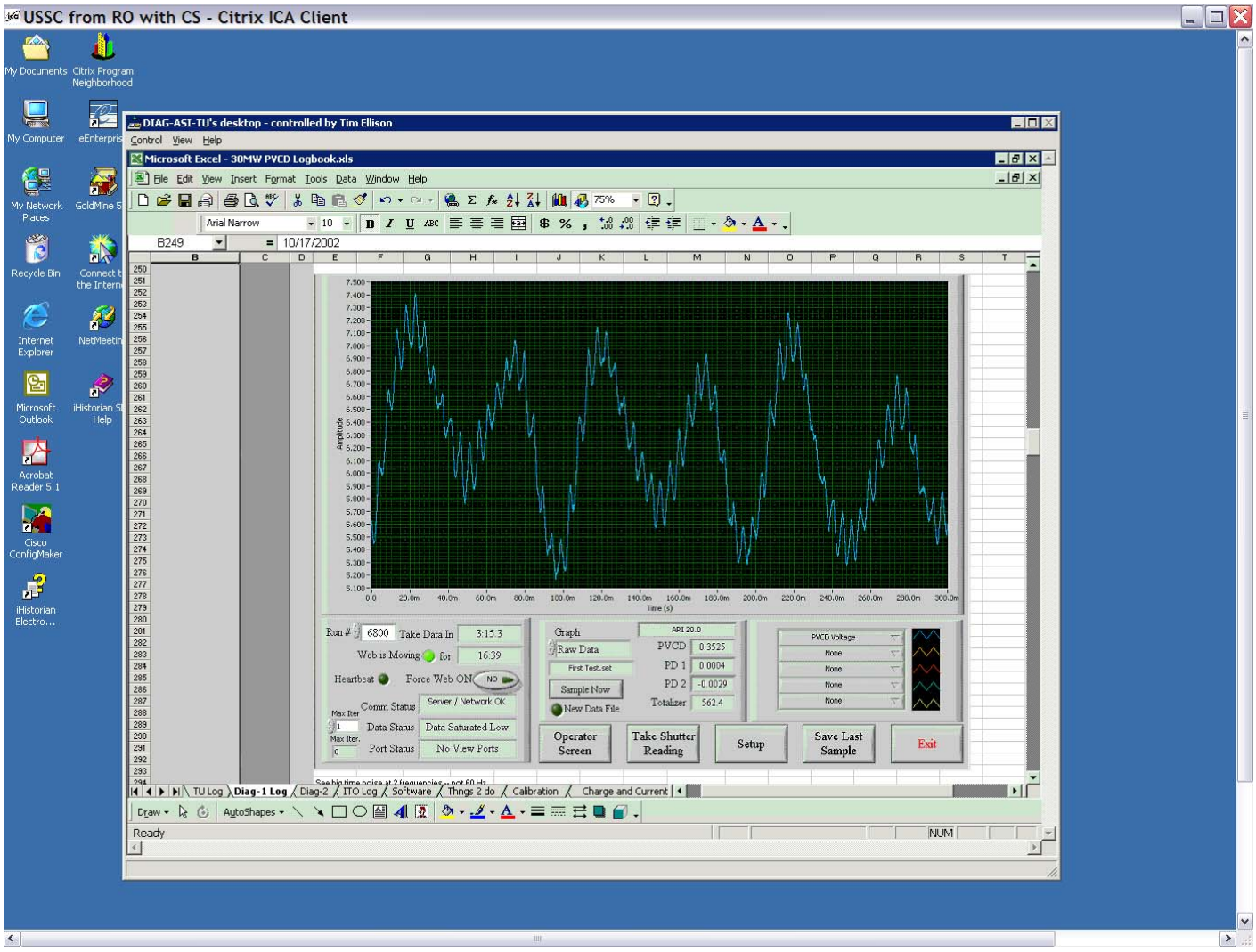

Fig. 2.16. Screen shot showing noise when the plasmas and heaters are turned on – the signal is completely lost in the noise from the plasmas. (This plasma noise may in turn out to be an important diagnostic – we have not yet had the time to investigate this).

In principle, in the absence of this plasma noise, the ultimate S/N ratio for this system should be better than that for the Take-Up (TU) chamber system:

- The PVCD is about 1/3rd the distance to the web, which provides 3 times the signal. The bottom cell V_{OC} is only about ¼ the triple junction device V_{OC}, so the relative signal to noise would be about the same.
- The lower band-gap of the bottom cell enables the cell to discharge much more quickly than the top cell. Consequently measurements can be made an order of magnitude more quickly resulting a factor of 3 in the S/N ratio for signals averaged over the same period of time.

So, while we expected the fundamental S/N limitation for the Component Cell PVCD to about be about a factor of 3 greater than for the TU chamber PVCD, the observed S/N ratio was about a 1000 times worse. There were three principle sources of noise that were identified:

- Small currents flowing between the PV material and the PVCD due to ionized gas in the region of the detector;
- Noise from the long co-axial Teflon cable connecting the PVCD electrode to the amplifier;
- Noise from time-varying electric fields from the plasma; this noise is of the same, or greater, magnitude as the signal and the larges noise source.

We employed all the standard signal processing techniques to pull the signal out of the noise, including:

- Triggering off of the a.c. line;
- Sampling a noise waveform just prior to sampling the signal, and subtracting this noise baseline from the signal;
- Time-averaging the both the signal and noise baselines;
- Using an "Improbability Filter" to remove out-lying waveforms before the averaging process;
- Fitting the resultant averaged waveform to an analytical function; and
- Post-filtering the coefficients from the fit to the analytical function.

With these and other techniques, we were able to finally achieve a V_{OC} S/N ratio of about 30, as shown in Fig. 2.17; the J_{SC}/C signal, however, was still too noisy to be useful.

In Fig. 2.17, the Component Cell PVCD VOC signal highly filter compared to the TU Chamber PVCD. In Fig. 2.18 both VOC signals are shown with the same level of filtering.

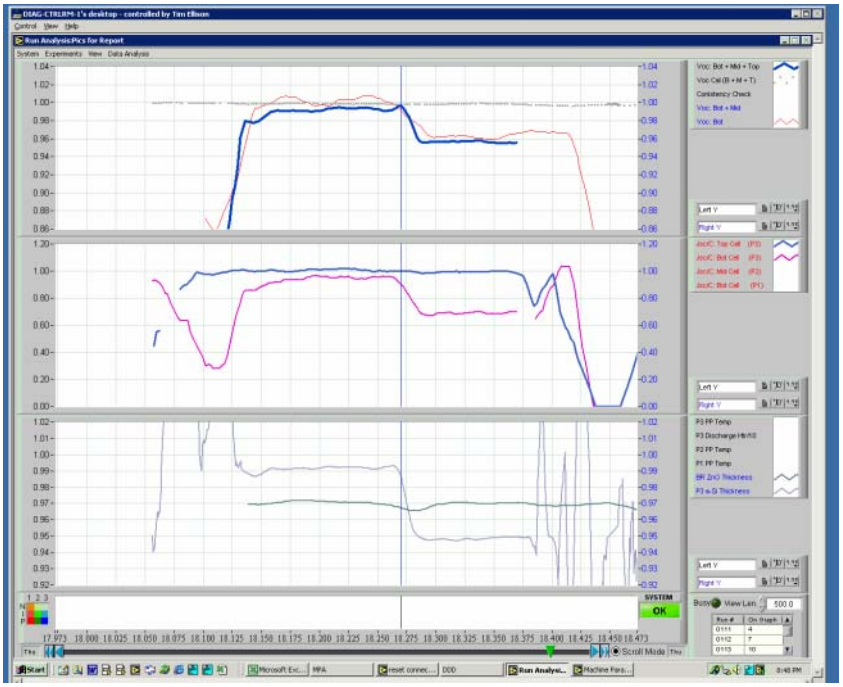

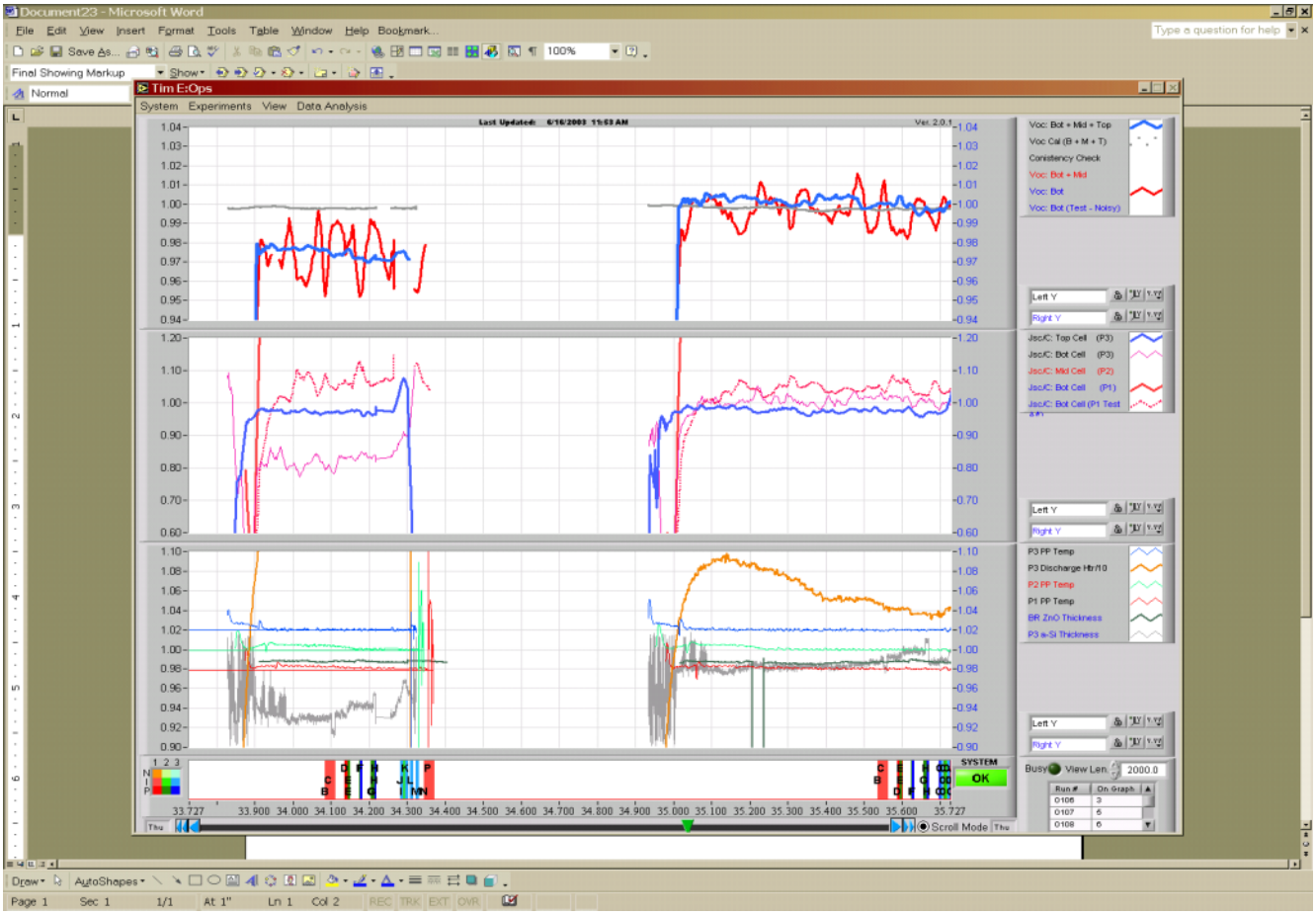

Fig. 2.17. Screen shot from the Control Room Diagnostic Data Display System showing the measured V_{OC} of the bottom cell [First Generation Component Cell PVCD – upper plot, Red] and triple junction device [TU chamber PVCD – upper plot, Blue] from a run in the 30 MW production equipment (2%/div). The middle plot shows the J_{SC}/C for the top [blue] and bottom [purple] cells – both taken using the TU chamber PVCD. The gray curve in the bottom plot shows the device thickness measured by the spectrometer in the TU chamber. In this figure one can begin to see the power of using multiple diagnostic systems: the fact that the bottom cell V_{OC} decreased by the same amount as the complete device V_{OC} tells the operator that the problem was in the bottom cell. The fact that the J_{SC}/C of the bottom cell decreased, while that of the top cell stayed constant, confirms this. One also see a change in cell thickness at the same time. This run was stopped early as a result of these observations. [25 m/div horizontal]. PVCD V_{OC} from the bottom Component Cell PVCD [Red Trace], and complete device, or TU chamber PVCD [Blue Trace]. The Gray Trace is an electronic system calibration signal. [2000 m Full Scale Horizontal Scale]. One can observe in this example that the 2% change in the triple-junction device V_{OC} was probably a consequence of the change in bottom cell V_{OC}; the high level of noise, however, prevents one from seeing small changes, or even large changes over a short period of time.

2.6.2. Improvements in the Component Cell PVCD S/N

As shown in Fig. 2.16, noise from variations in the plasma are on the same order as the signal we are measuring, and averaging soon reaches a point of diminishing returns. One can also observe that this plasma noise to first order can be described as a sum of sinusoids. Consequently, this noise can be measured, fit to a series of sinusoids, and extrapolated in time and subtracted from the signal. This "plasma-noise-killer software" was implemented as shown in Fig. 2.18.

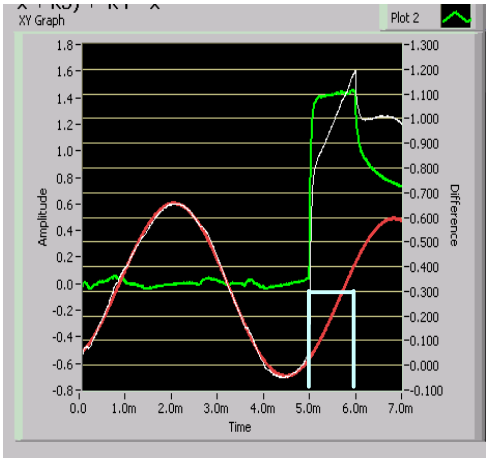

Fig. 2.18. Curves showing the method for plasma noise subtraction. The white curve is the raw data; the blue step square wave shows the time when the LED's are pulsed and the signal is measured. The red curve is a fit to the plasma noise prior to the LED pulse, and the green curve is corrected signal, with the plasma noise fit subtracted.

The signal with the plasma noise subtracted is then averaged, and a high quality signal can then be recorded, and curve-fit, as shown in Fig. 2.19.

Fig. 2.19. PVCD waveform after plasma noise subtraction and averaging, with an analytical fit to the waveform and least-square fit to the initial slope of the waveform.

Figures 2.20 and 2.21 show the difference in the quality of the bottom cell V_{OC} and J_{SC}/C measurements before and after the addition of the "Plasma-Noise-Killer" routine. The peak-peak noise has been reduced from about 4% to about 0.1%.

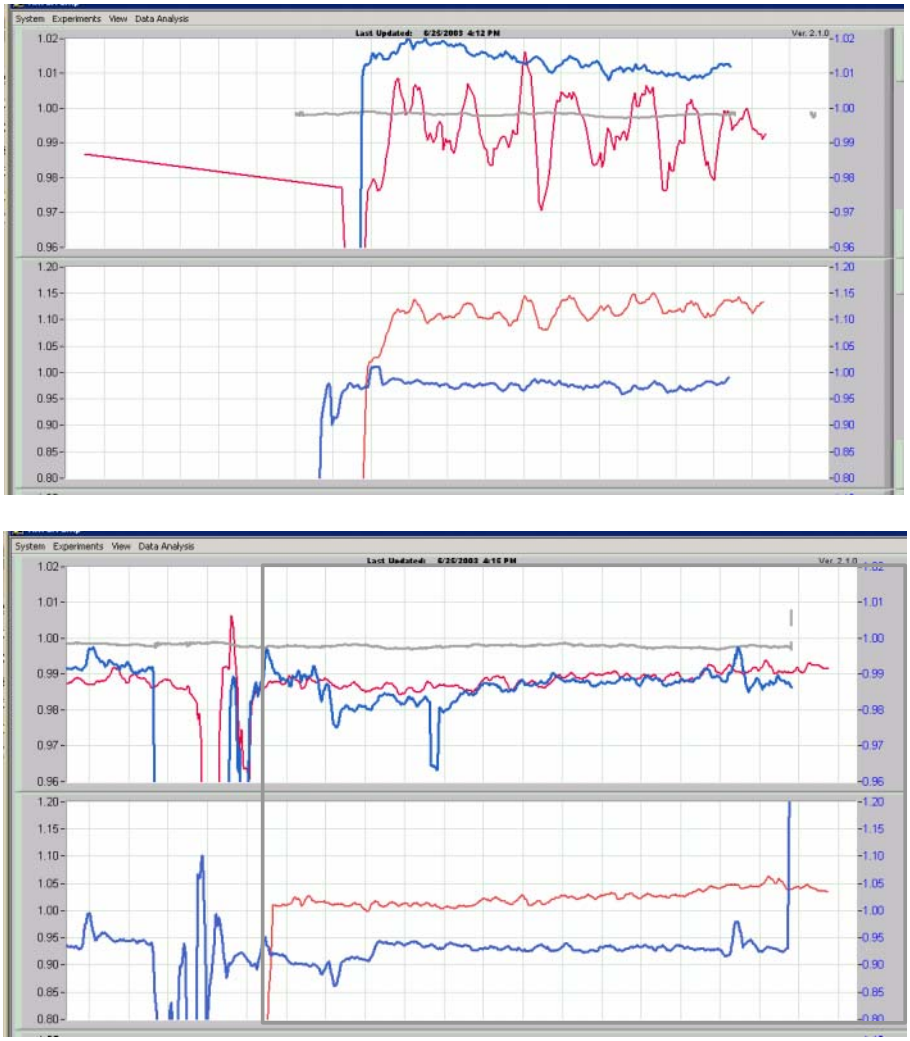

Figs. 2.20 – 21. Normalized Bottom and Triple Cell V_{OC} [upper traces, 1% per division] and J_{SC}/C [lower traces] before [LEFT] and after [RIGHT] implementation of the plasma noise reduction routine. [100 m per division].

2.6.3. Present Operation

After first installation, the signal to noise ratio (S/N) for this system was about 0.1 – it was not clear that the system would work in the presence of the high level of electronic noise generated by near-by high-power plasmas, ionized gas, and high-current heaters. Over the past 10 months we have gradually, through a series of many experiments and improvements in the hardware, electronics, and software signal processing, increased the S/N ratio by about 4 orders of magnitude to about 1000. [See Fig. 2.22]. We believe that we shall be able to rapidly replicate this success in the next Component Cell PVCD in Phase II that will measure the middle cell properties. The next system will also include mechanical design improvements. The high quality signals that we are now obtaining from this device leads us to believe that we shall eventually be able to use these devices to in a program of continuous online optimization – the ultimate goal of this PV Manufacturing R&D Program.

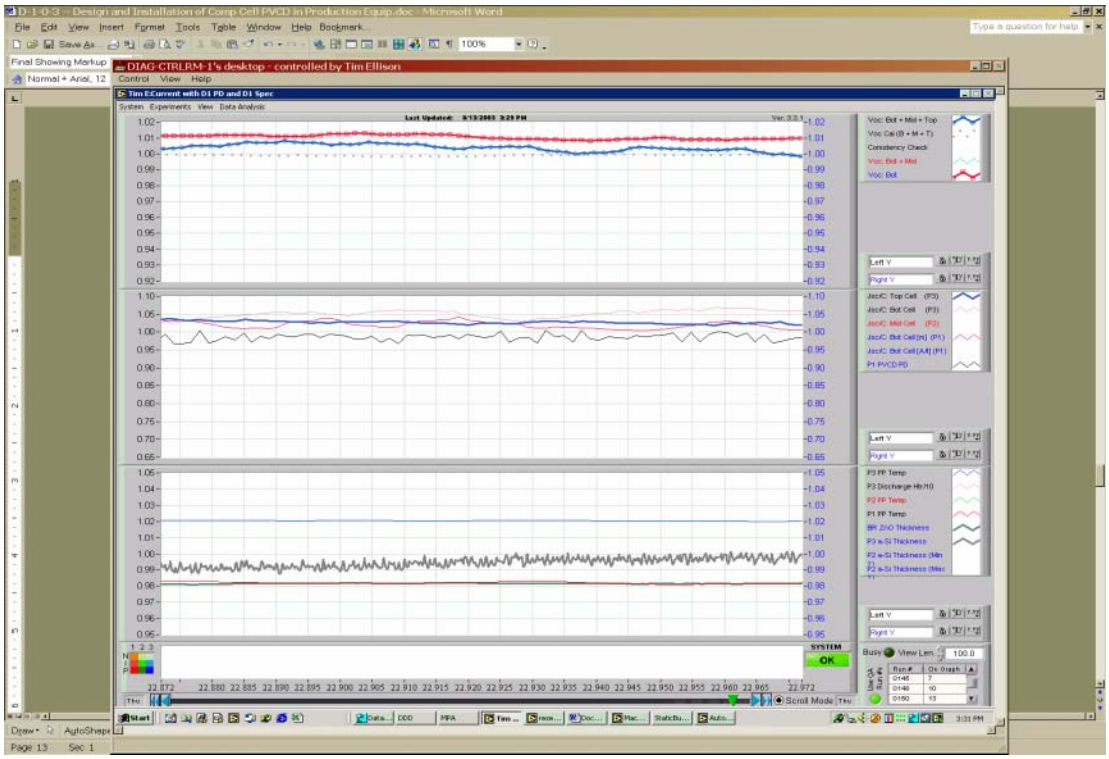

Fig. 2.22. Online display from a recent a-Si production run. The upper plot displays the bottom cell (red line, 7 point running average) V_{OC} from the Component Cell PVCD, and triple junction (blue line, 7 point running average) V_{OC} from the TU chamber PVCD. The vertical scale is 1% per division. The component cell PVCD is now comfortably operating in the 0.1% noise level regime for V_{OC} measurements. The vertical scale is 100 m Full Scale, or 5 m/div. We are presently getting about 1 data point/1.2 m. The data rep rate and S/N ratio can be traded off. The lower plot displays the J_{SC}/C data for the Component Cell PVCD measuring the bottom cell (red line, 11 point running average) and TU chamber PVCD measuring the top cell (blue line, 7 point running average). [5% per division]. These data are noisier than the V_{OC} data – as expected, since they result from a differentiation (the opposite of filtering) of the PVCD waveform.

TASK 3: Plasma Diagnostics

-- **Scott Jones**, Greg DeMaggio, and Tim Laarman (ECD)

Milestones

Complete	**m-1.0.3**	**Initial installation of plasma monitoring sensors in pilot deposition machine.**
Complete	**m-1.1.3.**	**Complete installation of plasma monitoring sensors in pilot deposition machine.**
Complete	**m-1.2.2**	**Initial characterization of plasmas created at 1 Å/s in pilot deposition machine.**
Complete	**m-1.4.3**	**Complete characterization of plasmas created at 1 Å/sec in pilot chamber.**
Complete	**m-1.4.4**	**Complete the Phase I portion of the effort under Task 3.**

Deliverables

~ 1 month	**D-1.4.1**	**Summary report of characterization studies of plasmas at 1 Å/sec in pilot deposition machine**

3.1 Introduction

The initial plan for the program was to install plasma monitoring equipment in the a-Si pilot deposition chamber in order to characterize RF plasmas to be used for the preparation of intrinsic layers for a-Si based solar cells. The plan was to study the chemistry of hydrogen-silane-germane plasmas used in the production of high efficiency cells at ~1 Å/sec rates as a basis to optimize cells using growth rates of 3-5 Å/sec. One goal in this first phase was to initiate the development of sensors for in-process monitoring and control of plasmas during production.

We have completed all but the final milestone in this first phase: the complete characterization of plasmas at 1 Å/sec.

In order to improve the module efficiencies for United Solar's products and ECD module manufacturing lines, an experimental chamber has been built to simulate and study the plasmas generated in the 30 MW machine. The chamber is an exact replica of those used in the 30 MW line. We are initially using an Ocean Optics USB 2000 spectrometer optimized to detect emission in the 200-350 nm range. A schematic of the collection optics used in this first phase is seen in Fig. 3.1. The collection optics are robust enough to take the temperatures within the chamber (~250-270 °C) and their design protected them from being coated over during the run.

Silane, germane, hydrogen and mixed plasmas were initially measured to identify important lines within the spectrometer range. Representative plasma emission lines for H_2, SiH_4:H_2, and GeH_4:H_2 plasmas are shown in Figs. 3.2 and 3.3. In particular, the SiH* and GeH* emission lines from one of the more important deposition species is identified in these spectra.

To characterize the differences in plasmas leading to different deposition rates, we then studied SiH_4+H_2 plasmas with different amounts of hydrogen dilution. Figs. 3.4 and 3.5 display optical emission spectra for plasmas prepared at high and low dilution levels leading to deposition rates of 1 and 3 Å/s, respectively. Comparing the spectra, one can see few differences. Future studies will involve further changes in the hydrogen dilution and variations in the applied power and GeH_4 concentrations in the plasma.

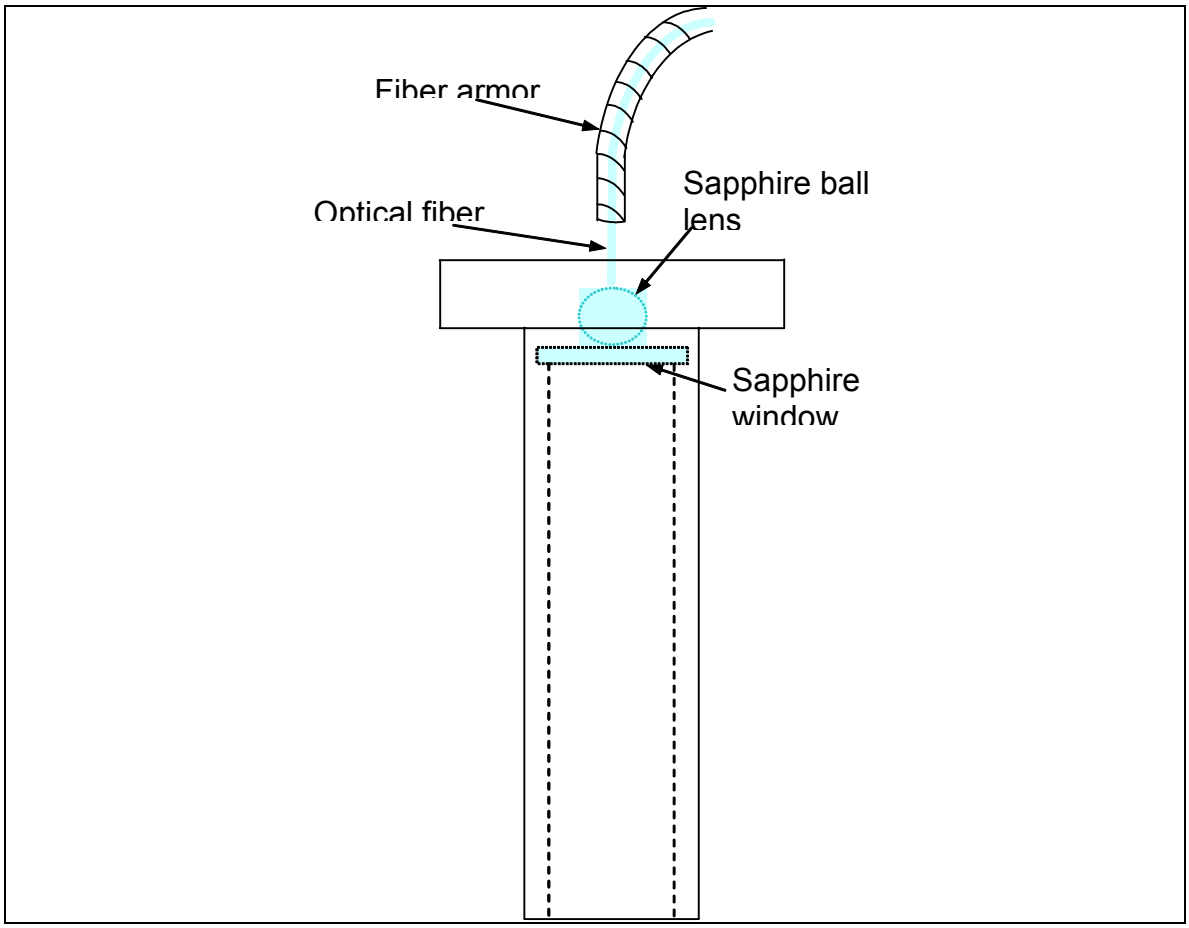

Fig. 3.1. Schematic of plasma emission collection optics.

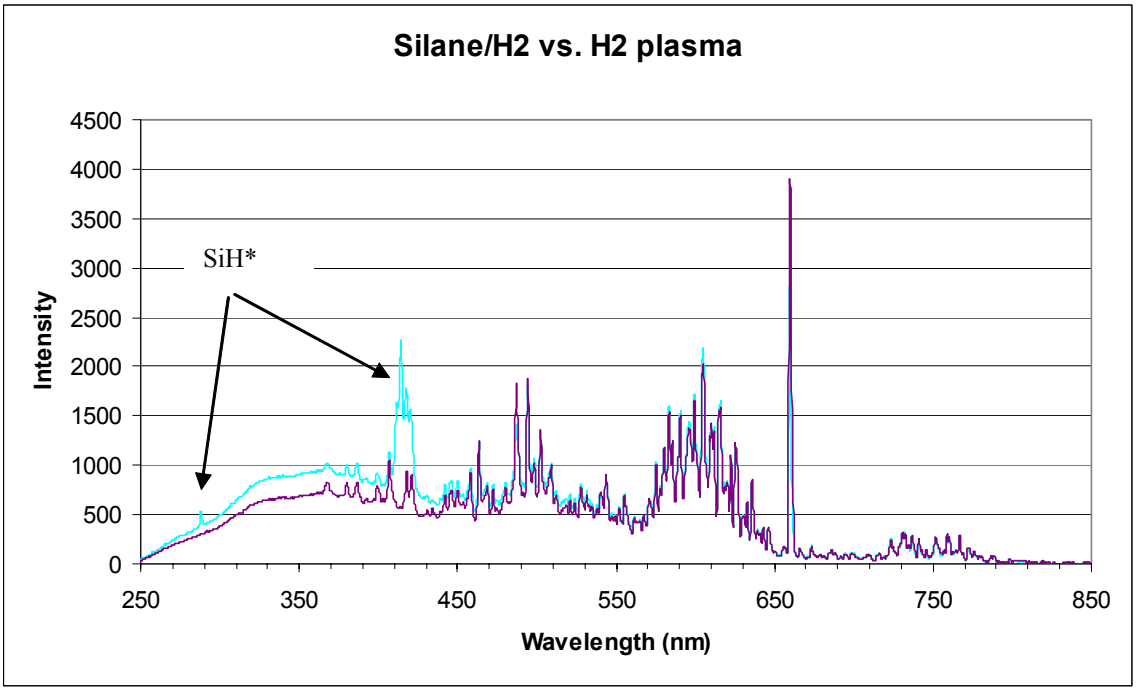

Fig. 3.2. Spectra of silane/H2 versus H2 plasmas

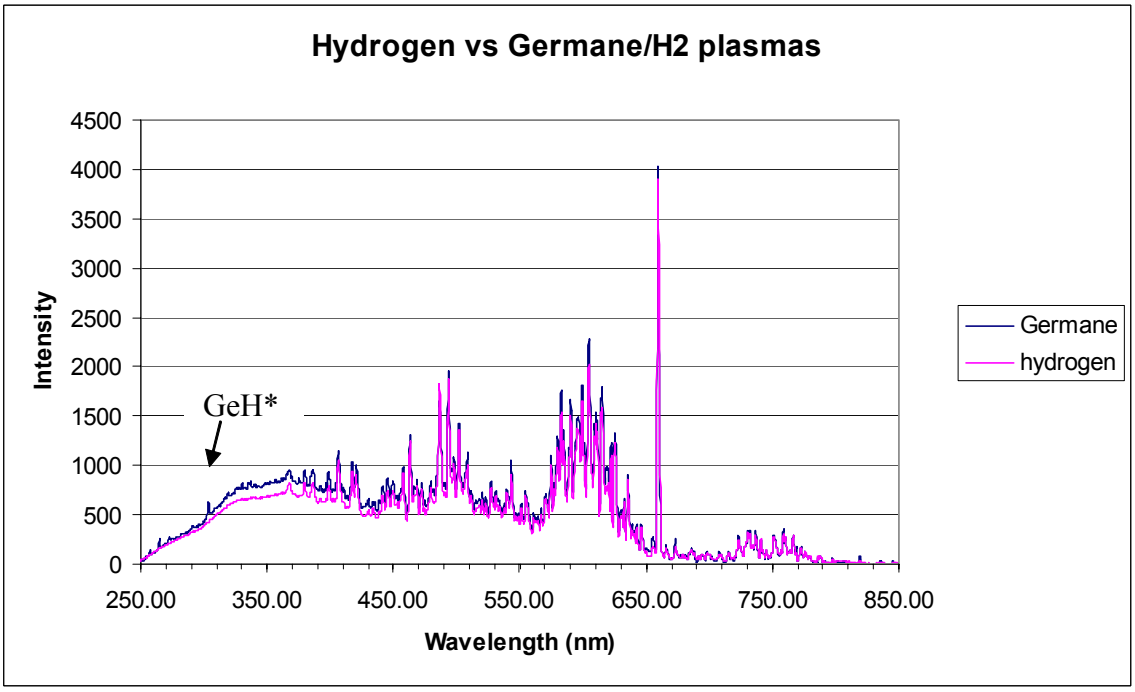

Fig. 3.3. Spectra of germane/H2 versus H2 plasmas

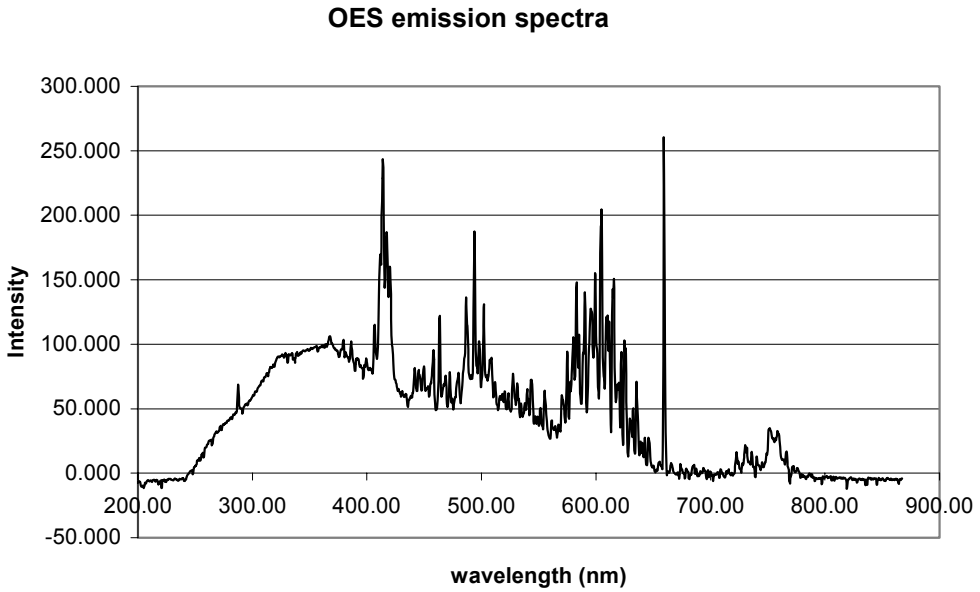

Fig. 3.4. Silane/H2 plasma at high emission

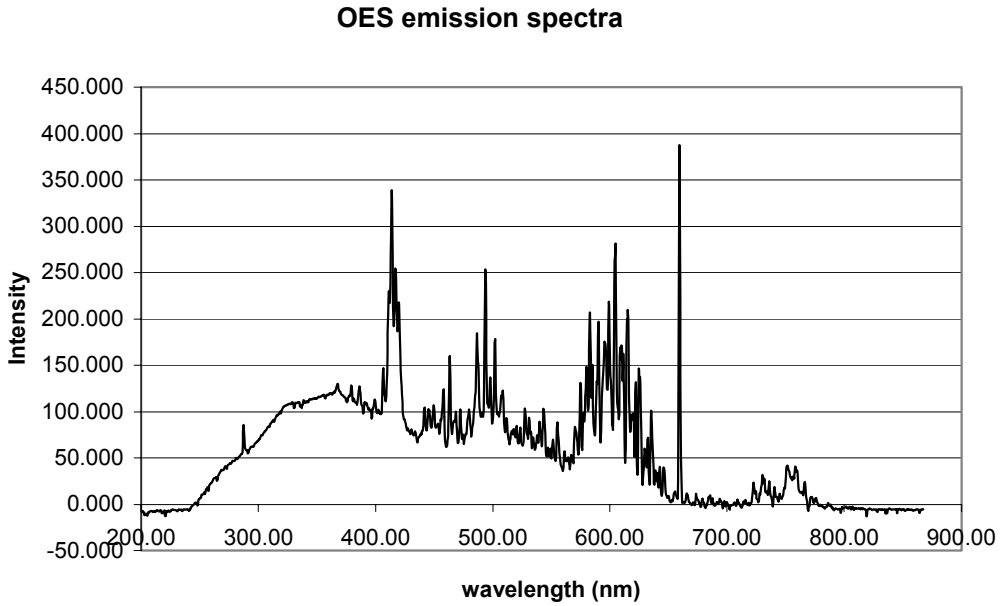

Fig. 3.5. Silane/H_2 plasma at low dilution

Our initial investigations concluded thus far with an observation that the first design of light collection optics is rather poor, the light transmission to the spectrometer is down by a factor of ~200-300 especially at the 250 nm end where we need it the most, and we detected some variation between different optics placed in different positions. This made it difficult to compare the relative intensities of plasma species at various points around the cathode, and therefore make a quantitative evaluation of the differences

between high and low rate depositions very difficult. We are redesigning the optics to improve this situation.

3.2 Powder Formation Measurements

Another area of plasma diagnostics which is important to growth rate studies is the measurement of powder formation within the plasma. Powder formation is known to reduce film deposition rates.

We have made progress with the monitor for powder formation during film deposition. The setup has undergone several modifications to improve sensitivity and stability during the deposition: protection from overcoating the optics with dust and deposited Si, and designing internal optical supports that maximize stability during the chamber heating. The laser and chopper are mounted on an adjustable platform, shown in Fig. 3.6, and an optical fiber and mirror arrangement to carry the transmitted light to a detector outside of the chamber is mounted to the chamber wall beyond the box that confines the plasma.

Fig. 3.6. Laser and chopper mount on test chamber

Fig. 3.7. Mirror and fiber optic mounting at exit of plasma chamber

First tests of the detection system did show a small response to formation excessive powder formation within the plasma. There are a few improvements we have identified to further increase the sensitivity and stability. This work has temporarily stopped in order to make changes to the test chamber as outlined below.

3.3 Modification to Install "P" Cathodes

In parallel with this work, we began the modifications, described last month, in the test chamber that will enable us to study the high intensity p-chamber plasmas as well as the intrinsic deposition plasmas. The installed P cathodes can be seen in the test chamber in Fig. 3.8.

Fig. 3.8. View of P cathodes mounted in test chamber

Installation should be completed by end of August with first plasma tests completed by 2nd week in September.

TASK 4: Yield Improvement: Substrate Cleaning and Monitoring

Greg DeMaggio (ECD), Gary Di Dio, Peter Nam, Wai Kei Chan (United Solar)

Milestones

Complete	**m-1.0.4**	**Complete setup of OSEE Surface Quality Monitor on United Solar wash line.**
Complete	**m-1.1.4**	**Complete initial baseline characterization of surface monitor. Correlation with substrate cleaning parameters.**
Complete	**m-1.2.3**	**Complete initial investigation of plasma cleaning parameters and correlation with QA/QC data.**
Complete	**m-1.4.5**	**Complete evaluation of effectiveness of plasma cleaning vs. chemical cleaning.**
In Progress	**m-1.4.6**	**Complete evaluation of on-line techniques for measuring substrate cleanliness.**
Complete	**m-1.4.7**	**Complete the Phase I portion of the effort under Task 4.**

Deliverables

Complete	**D-1.0.2**	**Report describing surface quality monitor on substrate wash line.**
~month	***D-1.4.2***	***Report summarizing of plasma vs. chemical cleaning, and correlation with offline QA/QC***
~monty	***D-1.4.3***	***Report summarizing data from cleanliness monitoring and correlation with offline QA/QC***

4.1 Introduction

We have accomplished all but the last of the milestones planned for this first phase of the program. Characterization of the effectiveness of plasma cleaning has just begun and we do conclude that this method should be more effective both from a cost savings as well as preparing a better surface for the back reflector. Whether we can find the best cleaning parameters that would be amenable for use within the 30 MW production process will be determined during the next phase of work.

4.2 Installation of Surface Quality Monitoring Equipment

Based on earlier tests on stainless steel substrates with various contamination levels and subsequent wash conditions, it was determined that the Optical Stimulated Electron Emission (OSEE) Surface Quality Monitor had the potential as both a quality control monitor for production during substrate cleaning, the first step in the PV production process, and as a tool for optimizing the wash machine parameters. The OSEE uses ultra-violet light from a mercury discharge lamp to photo-emit electrons from the surface under study. A biased grid collects these electrons across the air gap, and the total current is displayed. Presumably, a higher level of emitted electrons should signal a cleaner surface, but it is not clear that the device is only sensitive to surface quality, as will be described in this report.

As the device is very sensitive to substrate-to-sensor distance (the photo-emitted electron current decays exponentially with distance from the surface in air), the best mounting location was determined to be on the steering roller platform (see Figs. 4.1 and 4.2.) This allowed enough room for the sensor head and maintained a constant substrate-to-sensor distance. The output from the electronics was input to a computer

(with LabView) for monitoring and data logging during each wash. The UV lamp intensity degrades over time (~5500 hour half-life), and so over time the lamp output was measured using a calibrated photometer. The lamp intensity can be input into the LabView program so that a run-to-run quality comparison could be maintained.

Fig. 4.1. Position of OSEE sensor head (at lower left corner) within wash line take-up chamber

Fig. 4.2. Close-up of OSEE sensor on steering roller platform

4.3 Measurements on Different Stainless Substrates

The wash parameters that can be easily varied in these studies are web speed, detergent concentration, wash temperature, and rinse temperature. We decided to limit the early tests to the first two parameters, so that tests can be made in between or during production runs. While making initial measurements, we began to notice that the substrate type determined the absolute magnitude of the OSEE output. Substrate from three different suppliers was tested, referred to as "A", "B", and "C", although "C" has not been qualified for use as substrate for PV production. Fig. 4.3 displays some OSEE readings on pre-cleaned surfaces of these three steel supplier substrates.

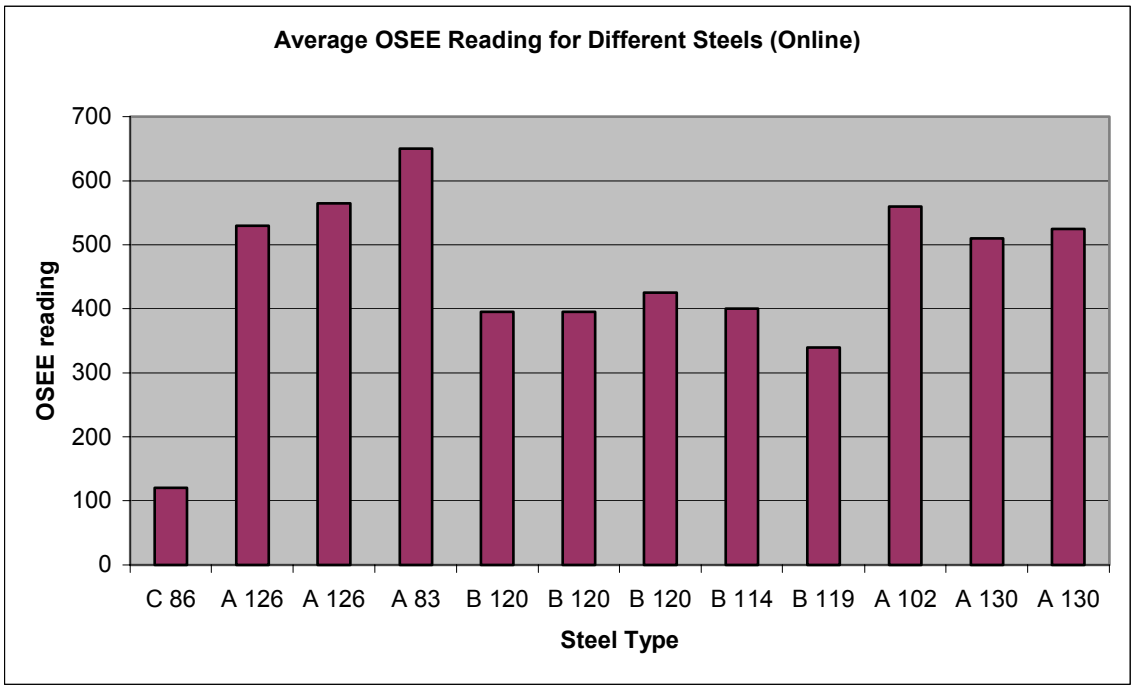

Fig. 4.3. Average readings from OSEE for different coil numbers and manufacturers

At present, the only measurable differences between supplier steels is the surface finish, although the manufacturer of the OSEE states that surface finish should not influence the measurements. Supplier "A" provides the best surface finish (R_a ~ 0.007 μm), "B" is slightly poorer (R_a ~ 0.025 μm), and "C" steel has the poorest and most inconsistent (R_a ~ 0.040 μm).

4.4 Experiments Varying Wash Conditions

Early OSEE measurements also display an influence of detergent (oakite) level and web speed; an example of this can be seen in Fig. 4.4. The increase in reading with the addition of detergent was expected, however the increase in reading with web speed seems counter intuitive. If the detergent is providing a cleaner surface and hence, giving rise to a higher OSEE reading, then increasing the web speed should

decrease the OSEE reading as the residence time for the detergent to act on the surface should be reduced.

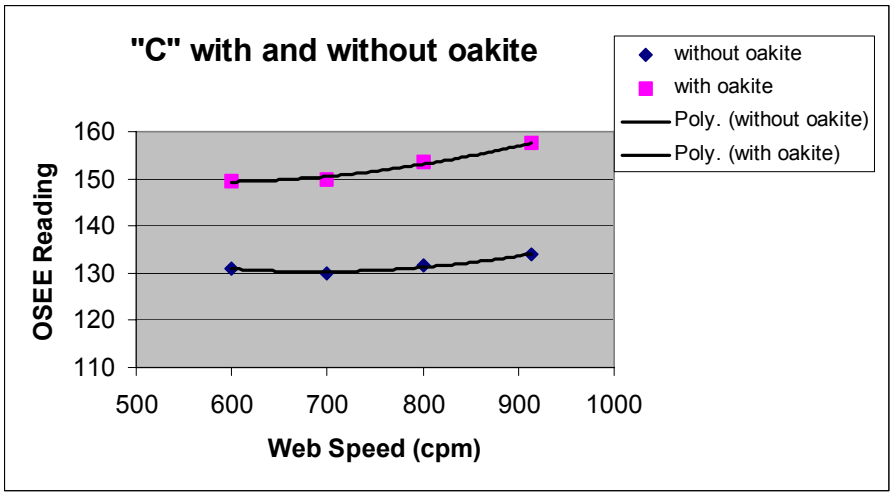

Fig. 4.4. OSEE readings (along with a fitted trendline) for C substrate vs. washer web speed and detergent level

At this point, we considered that the variability of the substrate surface condition needs to be eliminated from the analysis, and the difference in OSEE readings between the web as-received (from the pay-off end of the wash) and post wash (at the take-up) should be monitored as a function of wash parameters. So a second OSEE was placed at the pay-off end and the data monitor was set up to shift these two readings by the time difference in the machine, so that the OSEE reading for the same section of web can be viewed before and after wash.

A full set of experiments varying speed and detergent level (monitored by pH) can be seen in Table 4.1 below. These experiments were run on “A” substrate and this coil was then used in PV production in order to correlate wash parameters, OSEE readings, and cell yield data after processing.

Table 4.1.

Test #	PH	Speed	OSEE reading		Difference
			PO	TU	
1	pH 8.5	600cm/min	352.7	434.8	23.3%
2		750cm/min	368.7	441.2	19.7%
3		914cm/min	370.0	433.9	17.3%
4	pH 10	600cm/min	375.5	488.3	30.0%
5		750cm/min	384.3	475.9	23.8%
6		914cm/min	391.1	475.0	21.5%
7	pH 12.3	600cm/min	397.7	665.5	67.4%
8		750cm/min	399.4	630.6	57.9%
9		914cm/min	407.1	609.2	49.6%

The detergent tank was cleaned prior to this experiment. Tests 1-3 were run without detergent; the 8.5 pH reading was due to tank residues that were impossible to totally clear out. In this case, the OSEE readings at the pay-off end are still slightly sensitive to web speed, slightly increasing with speed. The difference in the readings increases as the detergent increases, but the difference drops as web speed increases. This appeared to make sense now from the above argument about wash residence time, and the increase in readings with increasing detergent level displays some influence the detergent has on the surface.

After this coil was processed in the PV line and QA data taken, the results were somewhat surprising. The graph below (Fig. 4.5) displays the open circuit voltage at low light levels (V_{LL}) vs. slab number over the full length. The different experiments within the run are identified using different symbols.

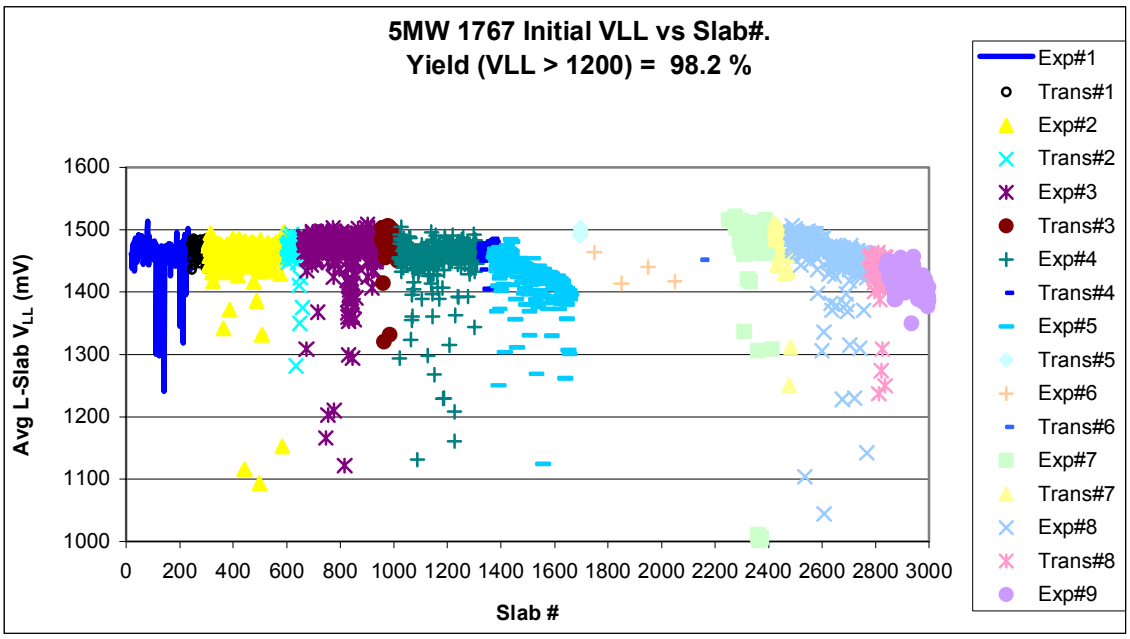

Fig. 4.5. Summary of average VLL for each slab (section of entire length of coil) identified by experiment number.

The V_{LL} is a measure of the density of shorts or shunts present in each cell; higher values are associated with higher quality devices. From experience, this appears to be a good measure not only of immediate performance, but also an indicator of post deposition process yield and even device lifetime.

Comparing the above data with the information from table I we see a couple of trends:

1) In the "no detergent" experiments (1-3), an increase in web speed does not influence V_{LL} to any great extent.
2) Although we only have a few points for experiment 6, once detergent is added, there is a repeated trend to decreased V_{LL} with increasing web speed. This drop

correlates with the decreasing difference in OSEE take-up to pay-off readings with increased speed.

Experiment 7 with slabs having some of the highest measured V_{LL}, also has the highest difference in OSEE readings. Despite this one point, there are no other significant trends in concentration or speed that suggest the addition of detergent yields a dramatic improvement. What this does suggest is that the addition of detergent modifies the surface to enhance the OSEE signal, but raises the question as to whether the surface is actually *cleaner*. It is obvious that as the web speed increases, the rinse section does not do an adequate job of removing detergent residue and so both OSEE reading and V_{LL} drop.

One caveat here is that while we did not discover any process variations in this run that could influence V_{LL}, it's possible that *unintentional and unmeasured* effects occurred during production stages.

4.5. Further Experiments

For production, the target is to run the wash machine at its highest (design) speed, which would be ~900 cm/min. So, these next experiments took a simpler approach, maintained a constant web speed at 914 cm/min. and varied detergent concentration in two levels: between 0 and enough to give a pH~11-12.

Substrate from the "B" supplier (as mentioned above has slightly poorer, although acceptable, surface finish than "A") was used for the next experiment. Table 4.2 summarizes the test conditions, OSEE readings, and overall average V_{LL}.

Table 4.2. Experiment matrix, OSEE, and V_{LL} result

Test #	PH	Speed	OSEE reading		Difference	Average
			PO	TU	OSEE	V_{LL}
1	6.22	914cm/min	332.00	355.00	23.00	1.48
4	7.50	914cm/min	327.00	337.00	10.00	1.45
2	11.38	914cm/min	329.00	454.00	125.00	1.52
3	11.94	914cm/min	327.00	498.00	171.00	1.49

Again, the OSEE reading at the take-up end read higher in response to the use of detergent, although there was not any dramatic improvement to the average V_{LL}. A more detailed plot of average V_{LL} over the entire coil is only slightly more helpful (Fig. 4.6.)

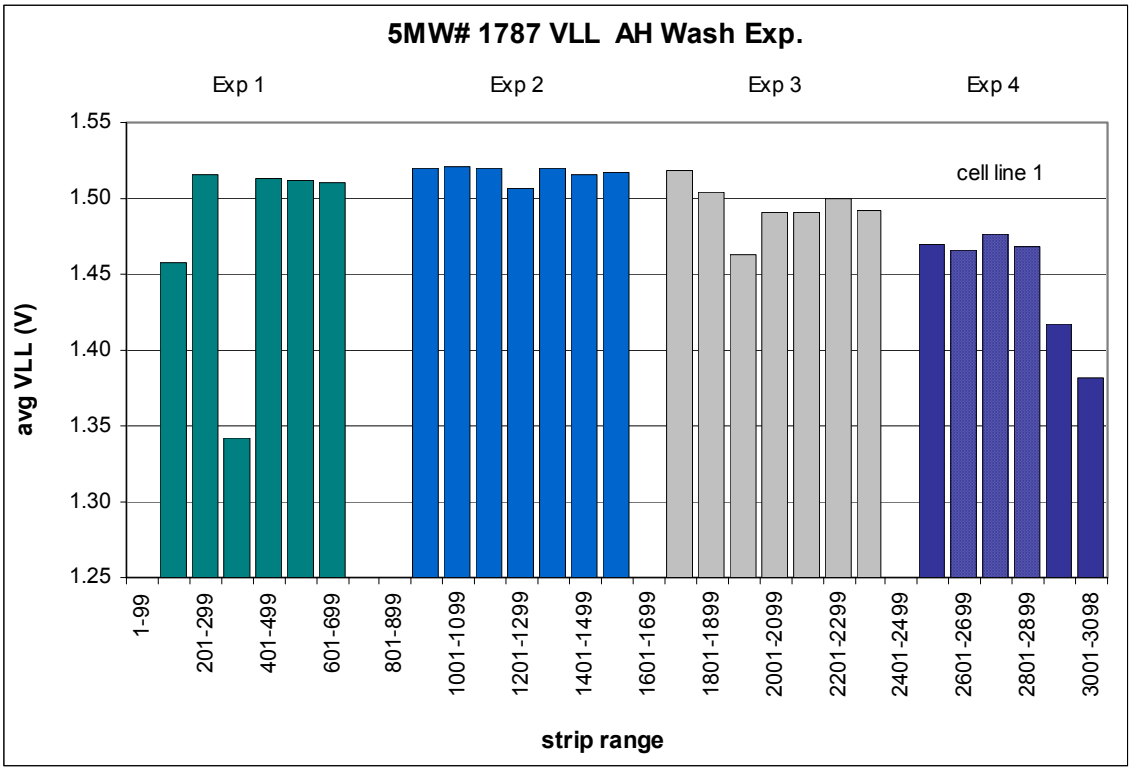

Fig. 4.6. VLL averaged over a number of slabs within strip ranges, separated with respect to experiment numbers

It appears from the graph that experiments 2 and 3, in which detergent was added, contain a higher number of cells with higher average V_{LL} than the sections without detergent. However, the fact that within experiment 1 alone we find strip ranges with high average V_{LL} numbers suggests that there may be other (in this case undetermined) reasons for reduced yield.

The last set of experiments repeats the above conditions this time with supplier "A" substrate. Table 4.3 displays the conditions, OSEE readings, and average V_{LL}.

Table 4.3. Experiment matrix, OSEE and V_{LL} result

Test #	Meter Mark (m)	pH	Speed	OSEE reading		Difference OSEE	Average V_{LL}
				PO	TU		
1	200	6-7	914cm/min	288	329	41	1.25
2	400	11-12	914cm/min	363	483	120	1.22
3	600	6-7	914cm/min	426	465	39	1.27
4	685	11-12	914cm/min	382	591	209	-

In this case, the V_{LL} was very low overall for some unknown reason, and an entire section (experiment 4) of coil was unavailable for testing. So only section 2 had added detergent, but we observe no significant affect (Fig. 4.7) from this.

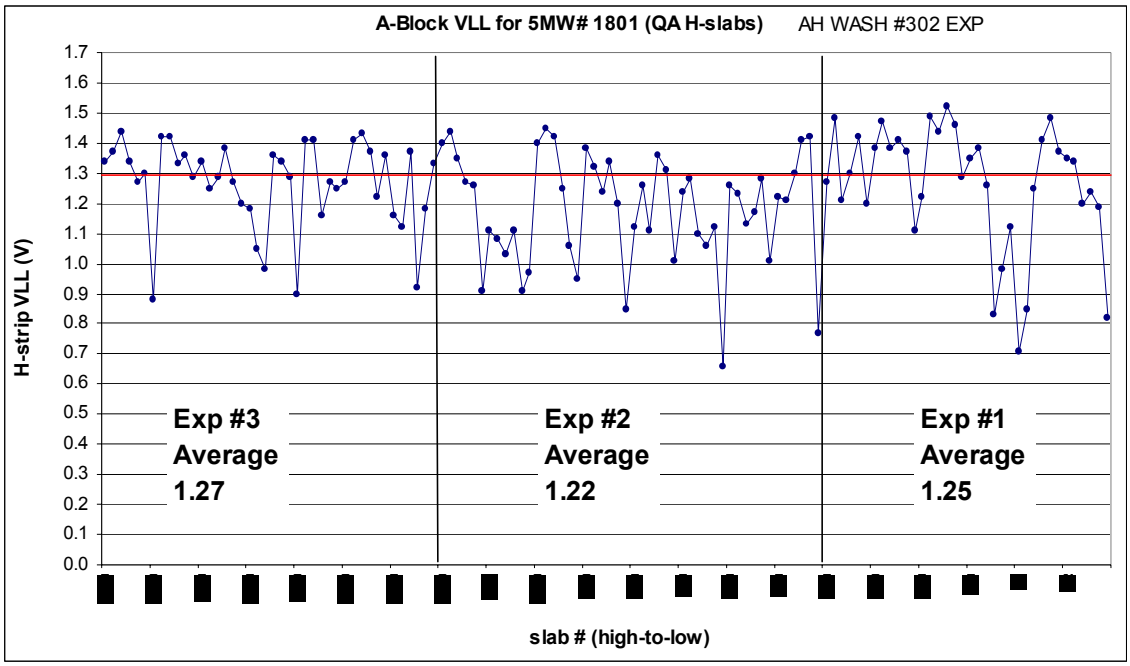

Fig. 4.7. Average VLL vs. slab numbers indicating experimental divisions.

4.6. Discussion and Conclusions

In the first set of experiments, both detergent concentration and web speed were varied, and a reduction in V_{LL} was observed with web speeds at and above 750 cm/min. The fact that we did not see a reduction vs. speed for the experiments without detergent suggests that the detergent plays a role in this reduction. At higher speeds, the rinse section of the wash line appears to be less effective in removing the detergent residue. The OSEE readings confirm this as we noted from the drop in difference readings with increasing web speed. Some of the highest V_{LL} numbers were observed for the highest detergent concentration at the slowest speed (experiment 7). Again, the OSEE confirms this.

The experiments that followed were set up to run at the highest web speed, for which the rinse section of the wash line appears to be less effective. This could be one reason that the data obtained was more inconclusive. It is also possible that the substrate is generally clean as received, which means that the wash line is unnecessary for the most part, and could accidentally add unintended contamination. Accidental contamination of the substrate by the supplier would more likely be at edges during slitting operation. Since the OSEE was set up to monitor the center of the web, we would have missed detecting this.

The efficiency of the rinse line in the wash system should also be studied to determine the amount of detergent residue remains on the substrate following the rinse.

4.7 Initial Tests of Plasma Cleaning

The next proposed task under this program is to evaluate the effectiveness of plasma cleaning, either as a means of improving yield or if possible to simplify production by eliminating the wet chemical cleaning process step. The reason for this comes from the high V_{LL} level seen for substrate washed with no detergent. We will begin by collecting Auger surface analysis data to determine the consistency of incoming substrate surface cleanliness. Once some confidence in substrate consistency is developed, a set of experiments varying plasma conditions will be run and the V_{LL} compared.

Initial experiments are being conducted in the small vacuum system shown in Fig. 4.8 below.

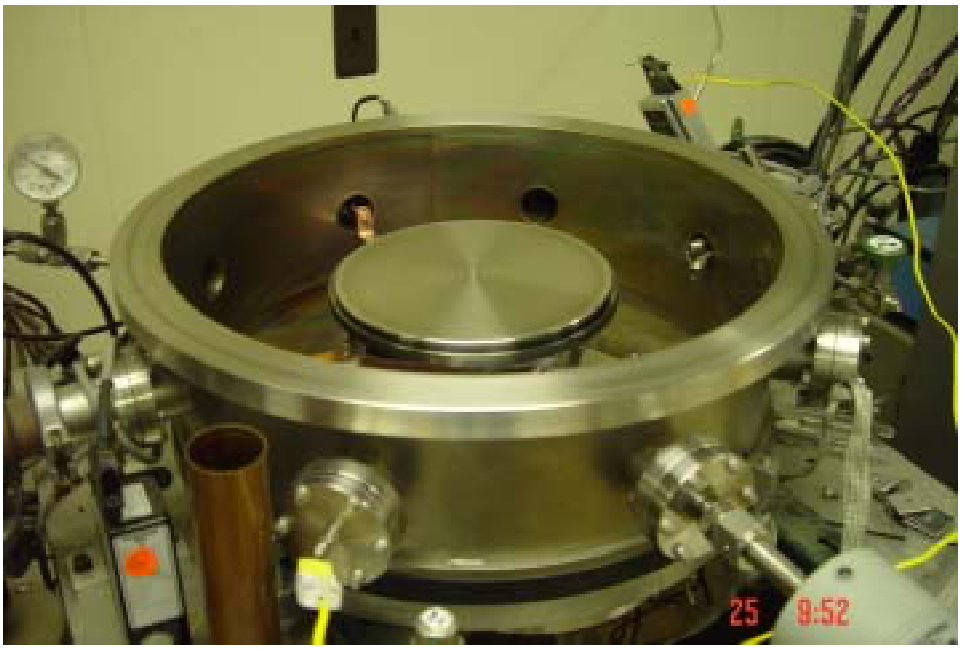

Fig. 4.8. View inside small chamber to conduct initial studies of plasma cleaning stainless steel substrate.

This chamber has an 8" diameter stainless steel electrode, biased positively, approximately 1.5" from the grounded substrate attached to the lid of the chamber. The lid has an integral heater behind the substrate and a thin foil thermocouple is placed under the substrate to monitor temperature.

The chamber pressure during plasma cleaning was fixed at 40 mTorr, 100% Ar, (this would be a typical pressure in the plasma chamber in the 30 MW back reflector system) and the temperatures were 130 °C. The chamber background was typically 2-4 x 10^{-6} Torr prior to the tests. In the first set of experiments, the bias voltage was varied from 300 to 400 V while holding the time constant at ~10 seconds. This time would be equivalent to the time the stainless steel substrate is exposed to the plasma in the cleaning chamber in the back reflector machine in production. In the second series of tests, the voltage is fixed at 300 or 350 V and the plasma time is varied from 30

seconds to 150 seconds. Following each set of runs, the samples are placed in a clean vacuum desiccator and then sent for Auger analysis.

Fig. 4.9 displays the levels of contaminants observed by Auger on the surface of the samples versus the plasma cleaning parameters.

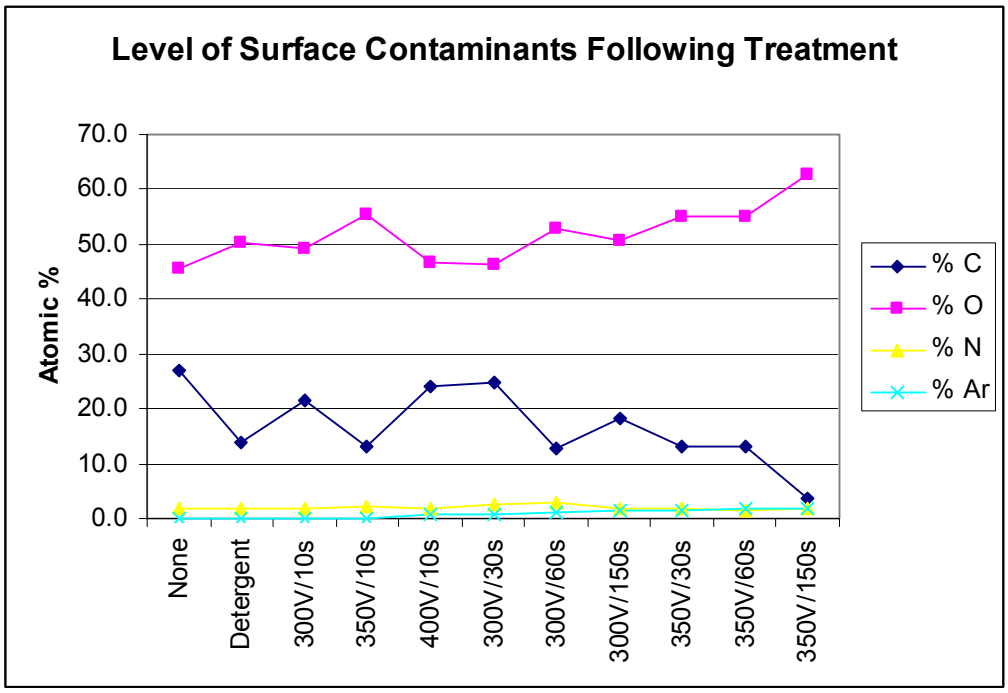

Fig. 4.9. Surface contaminant levels versus plasma cleaning parameters.

We observe no change in surface levels for the shortest times independent of plasma voltage, but begin to see reduction of surface carbon at and beyond 60 seconds. At 150 seconds, the amount of carbon was reduced below that for a detergent wash followed by a deionized water rinse. The amount of oxide increased, however, and will be commented on in the summary.

Fig. 4.10 shows a blowup of the vertical scale showing an increase in Ar content of the surface. This shows that there is some shallow implantation of Ar and indicates that we are sputter etching the surface during the plasma process at the higher energies and longer times.

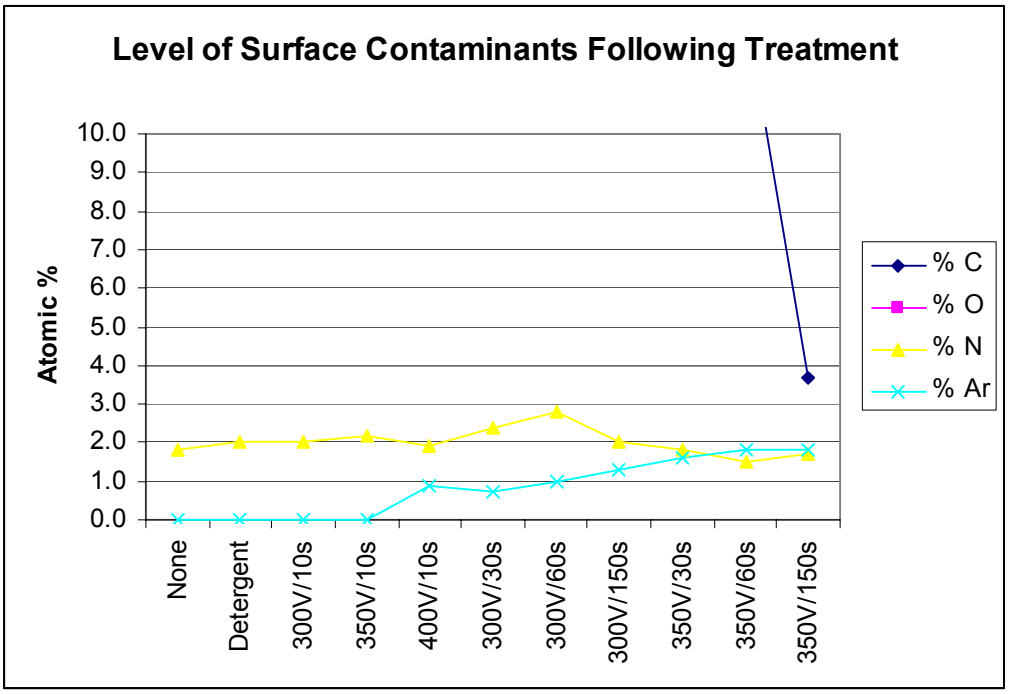

Fig. 4.10. Expansion of the vertical scale in figure 9 showing the N and Ar levels.

In Fig. 4.11 is displayed the thickness of the surface oxide following treatment. This appears to go along with the increase in oxygen on the surface and appears to contradict the effectiveness of plasma cleaning seen through the removal of carbon. It is well known that sputter cleaning the surface can leave it in a very reactive state, especially a clean chromium surface, which is effectively what this stainless steel has.

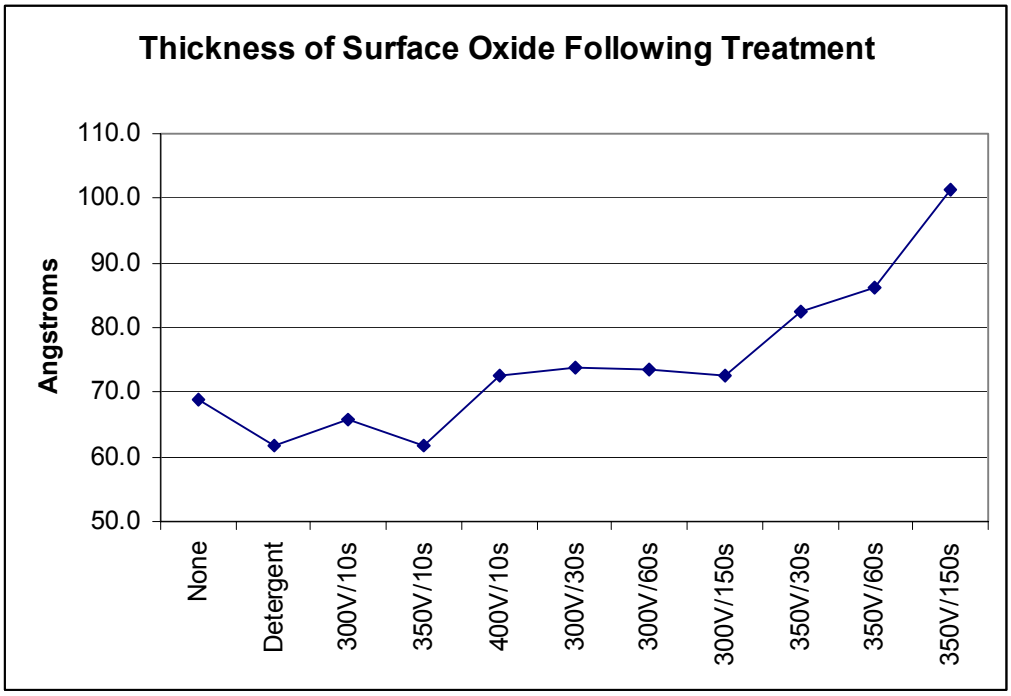

Fig. 4.11. Surface oxide thickness versus plasma treatment.

4.8 Conclusions and Further Work

With the data thus far we conclude that plasma cleaning could be an effective means of removing surface contaminants and would leave a much cleaner surface than wet chemical cleaning. One other test we will run shortly is to see how effective the plasma cleaning is in removing a thin layer of oil. This is probably the most common contaminant causing adhesion failure. The problem then would be to determine if we can find a set of parameters that can accomplish the cleaning in a shorter time. Higher bias voltages are more effective and the addition of a chemically reactive gas (hydrogen, for instance) may enhance this. These are planned for the next series of experiments within the small chamber. If these show promise that we can be within the parameters accessible in the 30MW back reflector system, we will plan experiments looking at the yield from substrate that is run through the system without first going through the wash.

REPORT DOCUMENTATION PAGE

Form Approved
OMB No. 0704-0188

PLEASE DO NOT RETURN YOUR FORM TO THE ABOVE ORGANIZATION.

1. REPORT DATE *(DD-MM-YYYY)*	2. REPORT TYPE	3. DATES COVERED *(From - To)*
August 2004	Phase I Annual Report	23 April 2003–31 August 2003

4. TITLE AND SUBTITLE
Implementation of a Comprehensive On-Line Closed-Loop Diagnostic System for Roll-to-Roll Amorphous Silicon Solar Cell Production: Phase I Annual Report, 23 April 2003–31 August 2003

5a. CONTRACT NUMBER
DE-AC36-99-GO10337

5b. GRANT NUMBER

5c. PROGRAM ELEMENT NUMBER
NREL/SR-520-36610

6. AUTHOR(S)
T. Ellison

5d. PROJECT NUMBER

5e. TASK NUMBER
PVP46101

5f. WORK UNIT NUMBER

7. PERFORMING ORGANIZATION NAME(S) AND ADDRESS(ES)
Energy Conversion Devices, Inc.
1621 Northwood
Troy, Michigan 48084

8. PERFORMING ORGANIZATION REPORT NUMBER
ZDO-3-30628-11

9. SPONSORING/MONITORING AGENCY NAME(S) AND ADDRESS(ES)
National Renewable Energy Laboratory
1617 Cole Blvd.
Golden, CO 80401-3393

10. SPONSOR/MONITOR'S ACRONYM(S)
NREL

11. SPONSORING/MONITORING AGENCY REPORT NUMBER
NREL/SR-520-36610

12. DISTRIBUTION AVAILABILITY STATEMENT
National Technical Information Service
U.S. Department of Commerce
5285 Port Royal Road
Springfield, VA 22161

13. SUPPLEMENTARY NOTES
NREL Technical Monitor: R. Mitchell

14. ABSTRACT *(Maximum 200 Words)*

This subcontract report describes how Energy Conversion Devices, Inc., has developed and built 7 generations of roll-to-roll amorphous silicon PV production equipment. In the ECD/United Solar production process, we deposit about a 1-μm-thick, 12-layer coating consisting of a metal/oxide backreflector, a 9-layer a-Si/a-SiGe alloy triple-junction solar cell, and top transparent conductive oxide coating onto 125-μm-thick, 35.5-cm-wide stainless-steel webs in a series of three roll-to-roll deposition machines. In the PV Manufacturing R&D 6 program, ECD is building upon these accomplishments to enhance the operation of the present production machine, and lay the foundation for improvements in the next-generation machine. ECD has completed the Phase I work for the first two Tasks, and will complete the Phase I work for the second two tasks within the next two months. In the following report, we summarize the Phase I work in each of these tasks. We have involved United Solar production personnel in each of these Tasks. This is important for two reasons: First, the collaboration of ECD and United Solar personnel keeps the projects responsive to the developing needs at United Solar; and most of the tasks affect operations and consequently need the support of United Solar production and QA/QC managers. In the process we have developed a good working relationship between the production personnel, whose mantra is “change nothing,” and the R&D personnel, who mantra is “change everything.”

15. SUBJECT TERMS
PV; on-line closed-loop diagnostic system; roll-to-roll amorphous silicon; manufacturing; device; backreflector; solar cells; thin film; triple-junction; a-Si deposition; electrical property;

16. SECURITY CLASSIFICATION OF:			17. LIMITATION OF ABSTRACT	18. NUMBER OF PAGES	19a. NAME OF RESPONSIBLE PERSON
a. REPORT	b. ABSTRACT	c. THIS PAGE			
Unclassified	Unclassified	Unclassified	UL		19b. TELEPONE NUMBER (*Include area code)*

Standard Form 298 (Rev. 8/98)
Prescribed by ANSI Std. Z39.18